The University Of Sheffield.

Polymer Brush Microsystem for Analysis of Membrane Transport

By

Nasiru Liman Usman

A thesis submitted in partial fulfilment of the requirements for the degree of
Doctor of Philosophy

The University of Sheffield
Faculty of Science
Department of Chemistry

Submission Date:

14th January 2023

Declaration

This thesis is submitted in partial fulfilment of the requirement of the degree of Doctor of Philosophy at the university of Sheffield. The work described in this thesis was undertaken between June 2018 and January 2023 under the supervision of Professor Graham Leggett. Unless otherwise stated, it is the work of the author and has not been submitted in whole or in part for any other degree at this or other universities or institutions.

Jan. 2023

Signed: ……

Name: ……

Department of Chemistry,

Dainton Building,

The University of Sheffield,

Brook Hill,

S3 7HF,

Sheffield,

United Kingdom.

Acknowledgments

All through the duration of my PhD program I have had the fortune and privilege of working with a team of very talented and most importantly friendly people. I would like to utilize this opportunity to say thank you to all these distinguishing people who have made my experience bearable.

I would like to thank Professor Graham J. Leggett for giving me the unique opportunity to work in his research group and for his advice and guidance throughout this project. In addition, I want to specially thank and appreciate him for the fatherly care and advice, including a 6-month scholarship which he granted me, when my funding was long-delayed by my sponsors. I would also like to thank Dr. Barbara Ciani (my independent adviser).

I would like to thank the University of Sheffield for the chance to study in this great institution as well as, granting my children and I reliefs from the Student Hardship Support Fund in 2021 and 2022 to help cushion the financial distress brought about by the long-delayed fund remittance by my sponsors.

I would like to thank the Chemistry department and its staff for enabling my research, as well as for being there for me and making it worth the while. I would also like to extend my gratitude and appreciation to our esteemed research group members: Dr. Deborah Hammond (my caring Angel), Dr. Anna Lishchuk, Dr. Edwin Johnson, Dr. Demetris Bates and Sami Alalawi including, Jabrah Alkorbi, Ibrahim Alatawi, Evelin Csanyi, Abdullah Sari, Bayan Samman and Sharifah Alharthi as well as, Munirah Alfarhan, Camary Ma, Aysha Mehter, Owen Gardner and Devy Pramudyah Wardani. Including former group members Dr. Martin Munz, Dr. Ben Bower, Dr. Wassie Takele, Dr. David Owen, including Brice Darroch, Max Chambers, and Charlie Smith.

I would also want to thank my sponsors: Isa Mustapha Agwai 1 Polytechnic, Lafia-Nigeria and Tertiary Education Trust Fund (TETfund) Nigeria, for finding me worthy and granting the scholarship that enabled me to embark on this PhD research.

Most importantly, I want to specially thank my family members: My late father Alhaji Usman Liman, my mother Hajiya Salamatu Liman and my stepmother Hajiya Salamatu Liman Egba for giving me a good foundation and the necessary start in life. My lovely brothers and sisters and my loving wife Hajiya Maryam Haruna as well as my adorable children; Usman Nasiru, Safiya Nasiru, Hauwa Nasiru and little Ahmad Nasiru for their love, support and enduring with me all through. Finally, I am grateful to God Almighty for enabling me to accomplish this PhD program.

Contents

Abbreviations

ADP	Adenosine Triphosphate
AFM	Atomic Force Microscopy
Amu	Atomic Mass Unit
APTES	3-Aminopropyltriethoxy Silane
ARGET	Activator Re-Generated by Electron Transfer
ATP	Adenosine Diphosphate
ATRP	Atom Transfer Radical Polymerization
BIBB	2-Bromoisobutyryl bromide
BIBB-APTES	Bromoisobutyrylamidotriethoxysilane
Bipy	2,2-Bipyridyl
BnB	Benzoyl Bromide
C.A	Contact Angle
CMPTS	4-(Chloromethyl) phenyl trichloro silane
^{13}C-NMR	Carbon Nuclear Magnetic Resonance
CuAAC	Copper-Catalyzed Azide Alkyne Cycloaddition
CysMA	Cysteine methacrylate
DCM	Dichloromethane
DMF	Dimethylformamide

DMPP	Dimethyl phenyl phosphine
DSS	Disuccinimidyl Suberate
FAD	Flavin Adenine Dinucleotide
FRAP	Fluorescent Recovery After Photobleaching
^{1}H-NMR	Proton Nuclear Magnetic Resonance
HPLC	High-performance Liquid Chromatography
LP	Laser Power
MSE	Mean Squared Error
NAD	Nicotinamide Adenine Dinucleotide
NB	Amine-modified Nile Blue
NBC	Nile Blue 2-(methacryloyloxy) ethyl carbamate
OEGMA	Oligo ethylene glycol methyl ether methacrylate
PCysMA	Poly (Cysteine methacrylate)
POEGMA	Poly (Oligo ethylene glycol methyl ether methacrylate)
PPE	Personal Protection Equipment
R*	Alkyl Radical
RX	Alkyl Halide
SAMs	Self-Assembled Monolayers

SE	Spectroscopic Ellipsometry
SI-ATRP	Surface-Initiated Atom Transfer Radical Polymerization
SSAC	Sheffield Surface Analysis Centre
TEA	Triethylamine
TFEA	2,2,2-Trifluoroethylamine
UV	Ultraviolet
XPS	X-ray Photoelectron Spectroscopy

List of Figures

List of Tables

Abstract

The growing interest for microsystems that enable us to address fundamental questions in biology, has necessitated this work as well as the need to develop sensors and other functional devices for the analysis of small analytes. It entails the development of supporting lipid bilayers (SLBs). These SLBs are accommodated on cushions of water but cannot typicality incorporate fundamental proteins. The first goal of this work is to develop model microsystem to enable lipid bilayer to be supported within a two-dimensional compartment of polymer brushes cushion (with the aim of supporting membrane diffusion). Transmembrane proton gradient drives many biological processes as proton motive force is arguably the basis for life existing on earth.

A key concept in our microsystem is the introduction of pH-sensitive reporters to measure transmembrane proton transport. Polymer brushes offer a variety of advantages such as control of thickness, copolymer formation capability and ease of derivatization. However, polymer patterning is more complicated, particularly where it is necessary to organize multiple components. In order to design systems for biological applicability, biofouling control is pertinent. Thus, we picked POEGMA which is extensively used in literatures and PCysMA a new polymer that seems to display an even better fouling resistance compared to POEGMA.

The ability to assess pH changes in a host of media including biological environments is essential. The concept of utilizing *ratiomeric* reporters for simple optical readouts in situ could have vast applicability. Nile blue as one such *ratiomeric* reporter is important in this regard owing to its ability to fluorescence and have high quantum yield, possessing an absorbance and emission maxima which strongly depends on pH, including being a

photostable dye. It can be used with a live or fixed cell. It has an excellent environmental sensitivity as well as impacting a blue colouration to cell nuclei. The chemistry of binding of Nile blue to brushes will be examined to ascertain the most effective method of introducing a pH reporter into surface grafted polymers.

Three main approaches will be employed to determine how to optimize the binding of Nile blue dye to POEGMA and PCysMA. Firstly, a dye-labeled acrylic monomer Nile blue 2-methacryloyloxy ethyl carbamate will be added to the reaction solution along with the catalyst and monomer solution to achieve incorporation into the brushes. The second approach involves the end-capping of the polymer end with NBC acting as chain terminator. While the third method involves the covalent attachment of the dye to the polymer which is achieved through derivatization.

Thus, we have been able to develop new methods for binding dyes to PCysMA brushes. NBC dye, a *ratiomeric* reporter was successfully incorporated into POEGMA brushes with noticeable absorbance peak intensities as well as showing a positive response to changes in pH environments. On the other hand, amine-modified Nile blue dye in PCysMA brushes showed prominent absorbance peak intensities even at very low concentrations. A two-component brush system of POEGMA and PCysMA brushes has been successfully fabricated incorporating NBC dye. Although, due to constraints of time, we were not able to carry out studies of membrane processes. However, the methodologies developed in this research could be useful for future researchers to continue in this direction.

CHAPTER 1: INTRODUCTION

This work has been motivated by the need to develop microsystems to enable us to address fundamental questions in biology and to develop sensors and other functional devices for the analysis of small volumes of analyte. In most studies, membrane free protocells or membraneless organelles formed from liquid-liquid phase separated microdroplets have widely been used to gain insights about the physicochemical properties of cells.[1-3] However, these attempts have witnessed limitations brought about by the lack of a discrete membrane-like boundary system or compartment in the configuration of micro models that mimic the basic functions of a cell.[4-6]

Compartmentalization is important in biological systems. Cells are contained in membranes, and within cells organelles are also enclosed within membrane systems. Cells represent fundamental functional unit for the existence of all living organisms. The location of important functional components of cells are in membranes.[4] A high fraction of the targets of antibiotics are bound by membrane structures. In recent years microfabrication of miniaturized study platforms or microsystems are being investigated via incorporation of polymer brushes and Supported lipid bilayers (SLBs) for the application of several cellular processes.[4,6]

SLBs were developed as models for biological membranes owing to their ability to mimic a natural environment for protein incorporation on substrate surfaces.[4,7] They have enabled the biofunctionalization of inorganic solid materials such as gold coated surfaces, polymeric material surfaces and semi-conductors for applications in surface plasmon spectroscopy, ellipsometry and micro interferometry. These SLBs rest on cushions of nanometer-thick layers of water or on ultrathin layers of soft polymer brush films.[8,9]

The first goal of this work is to develop model microsystems to enable lipid bilayers to be supported within two-dimensional compartments on polymer brush cushions, with the aim of supporting membrane diffusion of protons. The proton motive force is arguably the basis for life on earth.[10] It is essentially the cells driving force responsible for the exchange of chemical substances required to sustain life. Transmembrane proton gradients drive many biological processes such as ATP production and energy transduction. A key concept in our microsystems is the introduction of pH-sensitive reporters to measure transmembrane proton transport. Chip-based sensors are important in many areas of technology, including medicine, aerospace, automotive, defense and industrial applications. Chip-based sensors require precise control of surface chemistry. Organic monolayers have been widely used, but polymer brushes less so utilized.[6,11-14]

Polymer brushes offer a variety of advantages such as control of brush thickness, capacity for formation of copolymers and the ease of derivatization and coupling to other reactive groups. However, polymer patterning is more complicated, particularly where it is necessary to organize multiple components. For systems designed for biological applications, control of biofouling is important.[15,16] In this study POEGMA and PCysMA will be deployed for their excellent biofouling resistance properties. Although POEGMA will additionally provide and inert environment however, PCysMA is a newer polymer that seems to display even better fouling resistance than POEGMA.[8]

Local measurement of pH is important in many areas besides membrane biology. The basic concept of using a *ratiomeric* reporter for simple optical readout in situ could have wide applicability. Nile Blue is one such reporter and has been selected because its absorption and emission are strongly dependent on pH, its fluorescence appear at longer

wavelengths, and it can be used as a probe for environment polarity as well as it impacts blue colour to cell nuclei.[17,18] In *ratiomeric* sensors, the pH change is detected by a shift in the emission spectrum rather than by a change in the fluorescence intensity.[19,20] The chemistry of binding of Nile Blue to brushes will be studied to determine the most effective method of introducing pH reporters into surface-grafted polymers. Three methods are to be employed for the incorporation of Nile blue dye into polymer brushes: The first method involves introducing the dye solution along with the reacting catalyst and monomer solution in order to achieve copolymerization of the Nile blue dye along the polymer brush structure. The second method involves end-capping of the dye molecules to the terminal end of the polymer. While the third method involves the coupling of an amine-modified version of Nile blue dye (acquired from Demetris Bates, a senior research group member) to PCysMA.

The main experimental findings in this study include: the achievement of significant polymer brush growth control, successful patterning and fabrication of POEGMA and PCysMA two-component brush system and significant incorporation of Nile blue dye into these brushes, as well as establishing considerable pH responsiveness in POEGMA brushes. Although, because of constraints due to time, we were not able to carry out studies of membrane processes however, the methodologies developed in this research could be useful for future researchers to continue in this direction.

CHAPTER 2: LITERATURE REVIEW

2.1 Introduction

The last two decades have seen an explosion of interest in nanoscience and nanotechnology and their use to address fundamental and scientific questions. This has led to great developments that have unveiled novelties in nanoscale manipulations and applications. Microsystem fabrications on surfaces have been exemplified through constructions of multi-component brush structures. These can take the form of a combination of charge neutral polymer and zwitterionic polymer as well as an amphoteric polymer to enhance the functioning ability of the device.[21]

To answer many fundamental questions in biomedical sciences, it is necessary to create model systems in which components can be localized at specific regions. To measure membrane transport processes. It is additionally necessary to be able to incorporate into the system a means to measure the rates of membrane transport processes such as proton transfer. The ability to assemble a microsystem as an experimental platform would provide a viable tool, [21-24] for the *in-situ* interrogation of membrane transport system owing to the behavior of membrane proteins.[21] This group of proteins is specialized and plays a vital role in the cell membrane.[22] The development of new methods to study membrane processes in situ would lead to new opportunities in biomedical sciences, such as the study of diseases[21,22] and pH-changes which is associated with the performance of certain microorganisms.[21,23,25]

Miniaturization has driven technological advancement during the last century. Most obviously, this has been seen in the relentless advances in capability of microprocessors, leading to the rapid growth of computing capabilities. However, miniaturization has had a

revolutionary impact on molecular sciences following the emergence of self-assembled monolayers (SAMs - see chapter 2 section 6 below for a more detailed discussion). Whitesides and co-workers developed a suite of approaches which they termed "soft lithography" to produce microstructured materials and devices for exploring a diversity of phenomena including cellular adhesion, and for the development of inexpensive paper-based diagnostic systems. Central to this work was the development of microfluidics. This has had huge impact in biomedical diagnostics such as dipstick for urine tests, strips for glucose level monitoring in blood as well as test-kits for pregnancy detection.[15] Technologies for microscale engineering have also enabled the development of microchips[26], including microfabrication of models of blood vessels,[27] bones,[28] muscles[29] and respiratory airways of the lungs[30].

This has led in turn to the concept of a lab on a chip, in which Wu and co-workers fabricated a 3D microwell array chip for detecting single-cell antimicrobial susceptibility.[31] Similarly, it paved way for the unveiling of a microsystem with cellular temperature measuring capability.[32] As well as, hyaluronic acid microneedles made from encapsulated triple layered liraglutide for the treatment of obesity.[33] Furthermore, titanium micro-ring (TMR) with an excellently efficient capacity to deliver either very large or small therapeutic biomolecules into different cell types was successfully developed by Shinde and co-workers.[34] The ease of assisted reproduction procedures also got a booster with the introduction of a microfluidic chip with an ability to detect and separate highly motile sperm cells from less motile ones to enhance the success rates.[35]

The emergence of micro and nanofabrication methods has opened the way to investigation of problems that previously remained intractable. The specific focus of this

thesis is the development of microsystems to enable the investigation of cell membrane processes. Compartmentalization is important in biological systems (eg cells are contained in membranes, and within cells organelles are also enclosed within membrane systems). Important functional components of cells are located in membranes (a high fraction of the targets of antibiotics are located in membranes). A key element of the way that biological membrane function is the creation and maintenance of transmembrane gradients, for example gradients of pH and/or ion concentrations.[4,8]

To understand how these phenomena are regulated in compartmentalized systems within cells (e.g., organelles or whole cells) it is desirable to be able to design model systems that enable the controlled fabrication of compartmentalized model membranes. Such approaches promise to enable the investigation of wide range of phenomena. DeMond and co-workers are of the view that cell cluster formation is unperturbed by micropattern compartment confinements. In order to address this issue of biological relevance associated with model synthetic systems, studies were performed into membrane bound mobility of mucin mimetics deploying fluorescent recovery technique after photobleaching over several minutes of monitoring with a significant diffusion coefficient yield observed.[4]

Groves in his recent studies, reviewed an array of experiments that investigated membrane bending-mediated interactions together with recent model membrane topographical imaging and it was revealed to exhibit unhindered fluidity. However, the ease with which the supported membrane bends away from the supporting substrate was highly restricted owing to the strong Van der Waals attractive forces. Thus, enabling the stable establishment of a second membrane on top of the initially preformed membrane.[2]

In this review, we begin by characterizing biological membranes and then explore how it is possible to model their biophysics using supported lipid bilayers.

2.2 Biological Membranes

A membrane is a selectively active barrier between all the necessary components of a cell and its external environment.

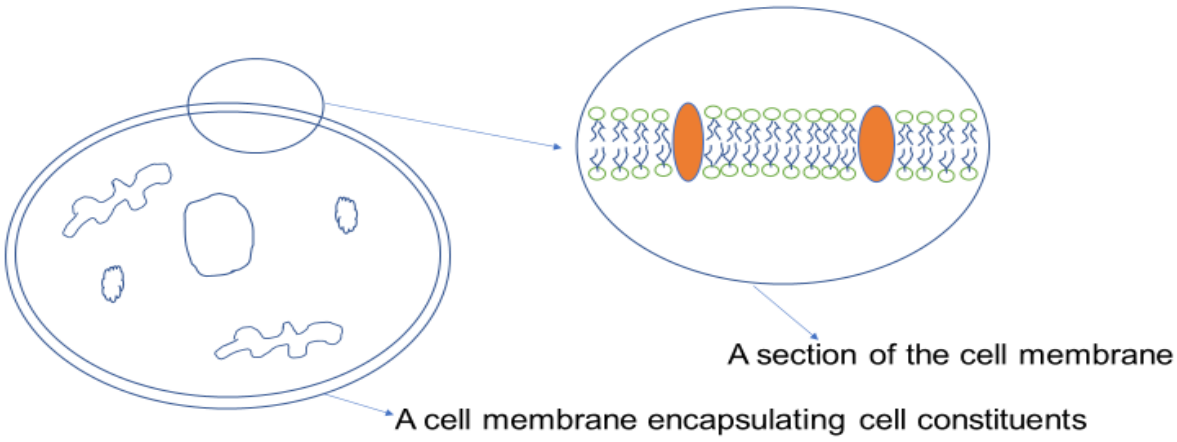

Figure 2-1: A representation of a membrane bilayer in a cell

The cell membrane provides an enabling environment for passive, facilitated or active communication and diffusion of substances in cells.

Cell membranes are made up of amphipathic lipid molecules, arranged in the form of double-layered sheets or bilayers, membrane proteins and polysaccharides. The hydrophobic regions of the lipid molecules cluster inside the bilayers. whilst the

hydrophilic parts of the lipids freely associate with the surrounding aqueous medium.[22] Parikh et al, elucidated that the ease of arrangement of lipid molecules into these bilayers is achievable owing to hydrophobic effects of lipids in aqueous phases.[23]

Membrane proteins can be integral to the membrane, fixed in place and spanning both layers of the lipid bilayer, or can be peripheral to the cell membrane and only weakly attached to one layer. The membrane structure controls what goes into and out of a cell. Small hydrophobic molecules can cross the bilayer by simple diffusion, but the exchange of specific molecules, metabolic products and ions necessary for cellular activity can only occur through the integral membrane proteins acting as channels.[21] This, restriction on the passage of ions into the cell except through specific openings referred to as ion channels ensures that the desired internal and external chemical concentration of a cell is maintained.[24] This phenomenon can create a proton gradient which is exploited as an energy generator. Ion channels in cells have been singled out by pharmaceutical companies as the main targets for drug delivery. This is largely because these drugs consist of chemical substances in ionic forms that may not have access through the hydrophobic regions of the cell membrane.[36]

Membrane processes make up the driving force which facilitates life. As molecules such as glucose are metabolized within cells, electrons released by this process are used to reduce carrier molecules such as nicotinamide adenine dinucleotide (NAD) and flavin adenine dinucleotide (FAD). The carrier molecules pass the electron to a protein within the membrane wall with a loss of energy that is used to pump a proton through the protein to outside of the cell. The electron is then transferred to the next protein, and a next, and a next, as it makes its way through a sequence of proteins called the “electron transfer

chain" (see figure 2-2). At each protein, energy is released which is used to drive a further proton through the protein to outside of the cell.[37,38.] The last step for the electron is to be transferred to molecular oxygen where, with excess protons, water is formed. This pumping of protons across the cell membrane through these integral proteins causes a charge separation, or a chemical gradient, and is a potential of stored electrochemical energy. It is the proton motive force. The protons can travel back into the cell through another integral protein, which is the enzyme ATP Synthase. By travelling across the chemical gradient, the protons give up enough energy to enable ATP Synthase to regenerate ATP by combining ADP with inorganic phosphate. ATP can then travel round the body to where this energy is needed. This conversion of food, or sunlight, into stored energy and then a means of dispersing it to where it is required means membrane processes and the proton motive force are essential for all life, both animal and plant.[39,40,41]

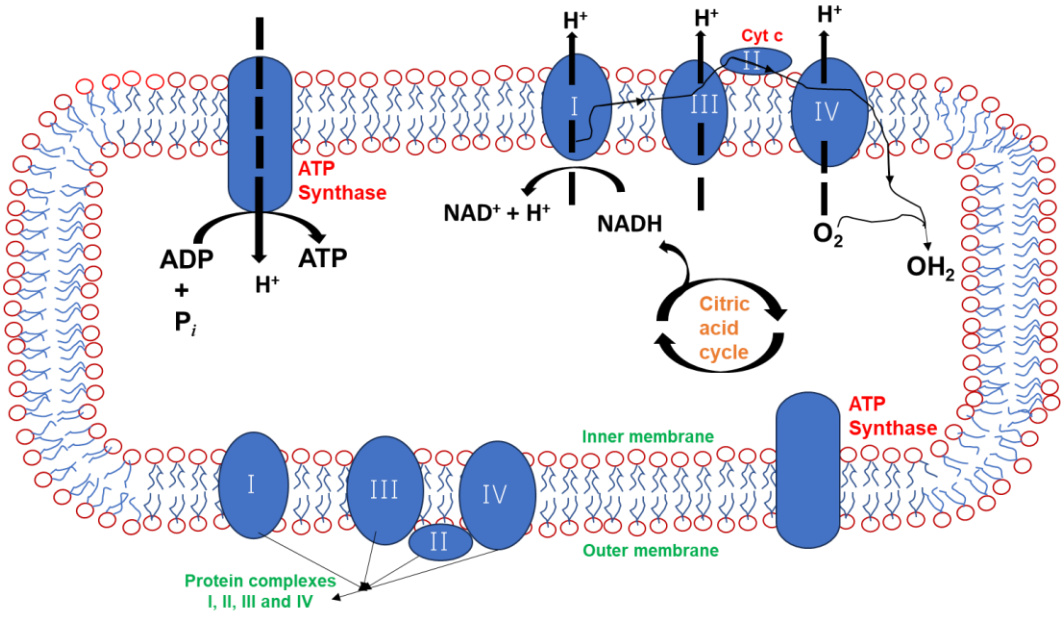

Figure 2-2: Membrane system showing electron transfer chain and proton build-up within and outside a cell membrane

2.3 The Membrane Structure

The membrane system has been represented as a floating collection of individual objects packed together forming a massive mosaic.

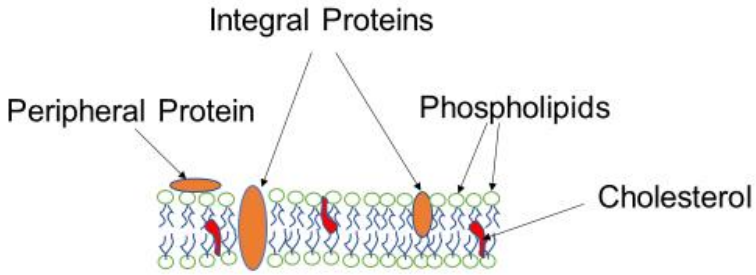

Figure 2-3: A representation of cholesterol and membrane proteins in lipid bilayer

It is a random and partially free fluidic arrangement of different molecules which include lipids, proteins and cholesterols. The fluidity in membrane system is determined by the weakly intermolecular, noncovalent bonds that exist between these molecules. It is also determined by the presence of cholesterol molecules which help to regulate the optimum fluidity of the membrane in hotter or cooler conditions, making it not too loose or too rigidly packed. The amphipathic lipid configuration and the presence of proteins serving as channels enable the selective permeability found in the plasma membrane system. There

are three main classes of lipids found in membranes. These include phospholipids, glycolipids and cholesterols.[42-45]

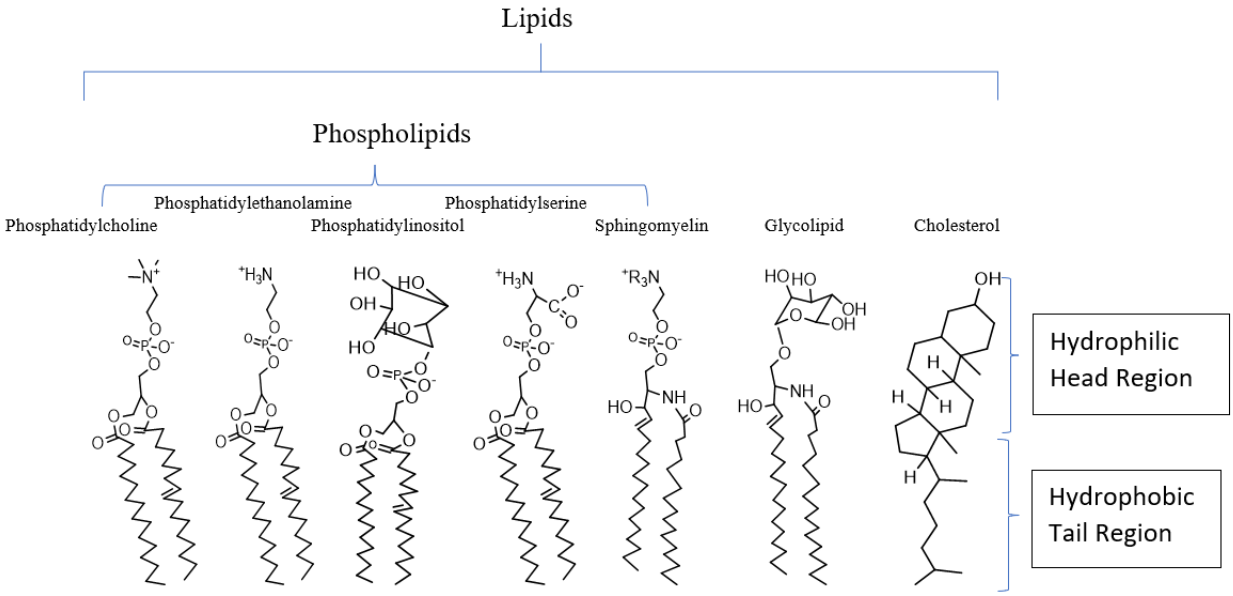

Figure 2-4: The Three Main Classes of Lipids

The most commonly occurring of the lipid molecules in bulk membranes are the amphipathic or amphiphilic phospholipids (comprising phosphatidylcholine, phophatidylethanolamine, phosphatidylinositol, phosphatidylserine and sphingomyelin, which possess both hydrophobic and hydrophilic regions.[45,46] The hydrophobic tail regions of the lipid bilayers are oriented towards each other while the hydrophilic head regions point outwards towards an aqueous media. The lipid membrane plays a vital role in compartmentalizing cellular systems.[46-49]

Lipid bilayers serve as vital structures which maintain several biological and physical properties in cell membranes, including fluidity, proton transport control and facilitating

transmembrane proton gradients which incidentally is an indispensable aspect of proton motive forces that chiefly drive life in living organisms.[50]

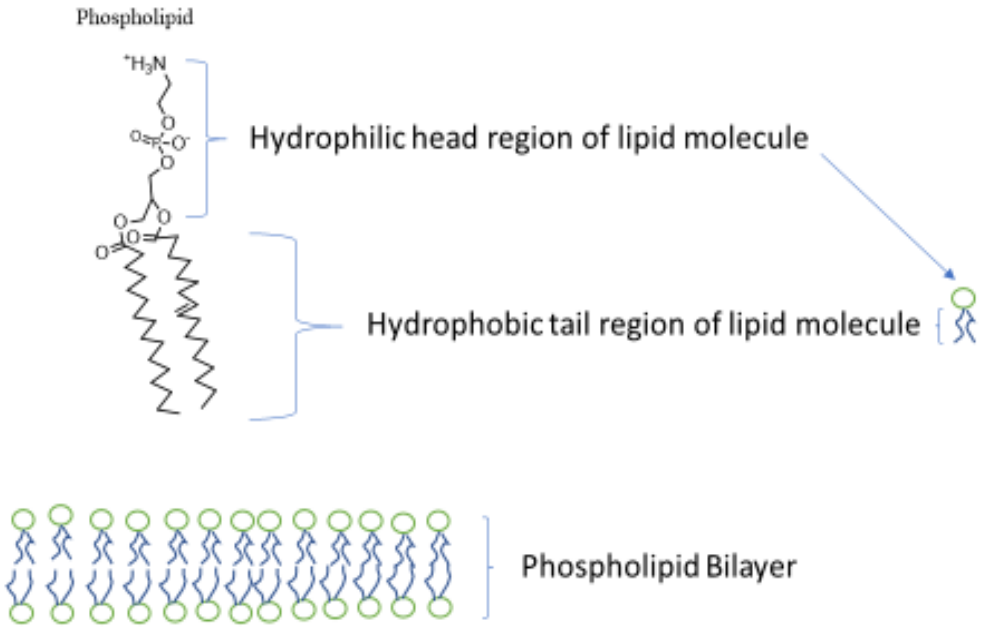

Figure 2-5: A representation of lipid bilayer

Membrane proteins play key roles in numerous biological processes like transduction of signals, energy and solute transportation. However, there exist some impediments in studying membrane proteins. It is difficult to ensure their stability and preservation of activity *in vitro*.[51,52] This is predominantly because membrane protein activity is often compromised following reconstitution, since the resulting composition of the model phospholipid bilayer membrane differs from those of the native cell phospholipid membrane. Although solubilization destroys the membrane structure it can however be achieved via detergent micelles exploitation with amphipathic polymers designed to bind to the membrane protein in an irreversible way.

However, amphipathic polymers also allow folding of membrane proteins into their native form in detergent-free solutions: they can complex with membrane proteins enabling increased stability compared to those in detergent.[53,54]

There has been an upsurge in research aimed at assembling model membrane microsystems in recent years.[55,56] This is in line with the need to unravel basic membrane processes and understanding lipid mobility.[57] Some examples of these model microsystems are supported lipid bilayers,[58] hybrid bilayers[59] and supported vesicle bilayers.[60]

2.4 Supported Lipid Bilayers as Model Membrane System

To understand the role of the lipid membrane, it is desirable to be able to prepare model systems that replicate key features of the functions of biological membranes, such as the semi-permeable tubing used in kidney dialysis machines.[47] Mimicking the surface of cells and tissues via supported lipid membranes by researchers has assumed center stage owing to the numerous applications as an instrument of interrogation and unveiling their inherent potentials. Some of these applications have been useful in biodegradable polymer capsules, silica beads and biosensors.[48,49,61-64]

A supported lipid bilayer is a very important component of a model microsystem which takes the form of a two-dimensional film consisting of lipid molecules kept in place due to hydrophilic interactions that result in a uniform self-assembled monolayer in aqueous solution. They are referred to as supported lipid bilayers (SLBs) because of their confinement on solid substrates like glass, silicon or mica. Biological membrane reconstitution on solid surfaces undoubtedly holds the potential not only for exploring the basic processes occurring in cell membranes but also can usher in a new era of

applications in biotechnology.[61] An important aspect of supported lipid bilayers system is that it enables the utilization of a host of optical techniques for characterization such as fluorescence recovery after photobleaching and total internal reflection fluorescence. These methods of characterizations often require pre-synthesized lipid bilayers to be transferred on to solid surfaces.[62,65,66] There are three documented approaches based on the Langmuir Film Balance for the transfer of lipid bilayers on to substrates.[63] These include the Langmuir-Blodgett, Langmuir-Schafer and the lipid vesicle rupture methods. All these methods require a polymer brush layer to be deposited first in order to support the lipid bilayer.

2.4.1 The Langmuir-Blodgett Method

This involves a protocol where the monolayer of lipids is assembled by the adjustment of surface pressure between air-water interface. In this approach the substrate is submerged vertically through the solution-monolayer lipid interface enabling the deposition of a monolayer of lipid on to the surface of the substrate. The subsequent step requires that the substrate be withdrawn from its submerged state to allow a second monolayer of lipid deposition on top of the first layer forming a bilayer.[64,65,67]

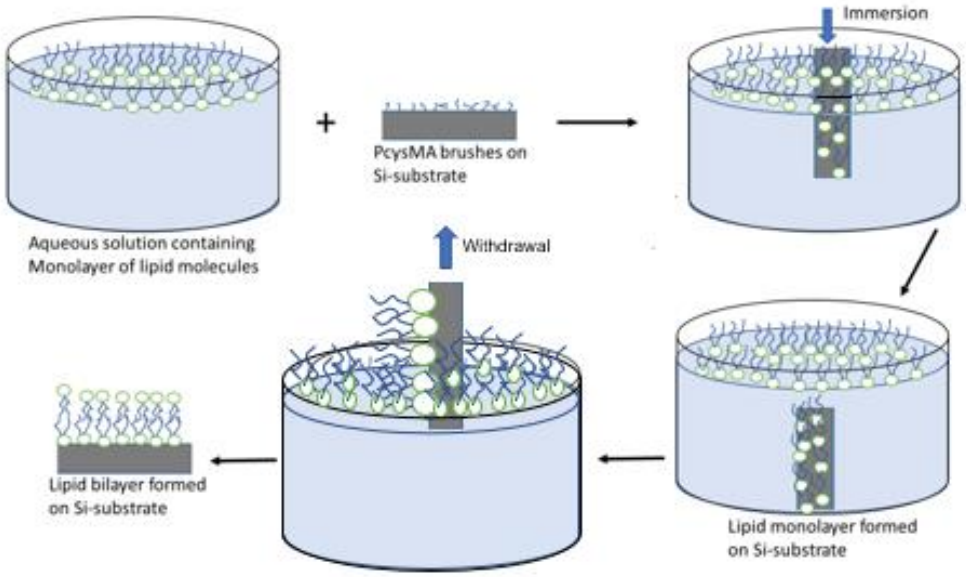

Figure 2-6: A schematic representation of Langmuir-Blodgett method of lipid bilayer formation

2.4.2 The Langmuir-Schafer Method

This approach is the second method of lipid monolayer confinement on surfaces. It requires the initial immobilization of lipid monolayers using a Langmuir trough, but the second lipid monolayer deposition was achieved differently by moving the substrate horizontally across the dispersed monolayer lipid molecules within the interface yielding higher quality supporting lipid bilayers devoid of pressure adjustment.[66.68,69]

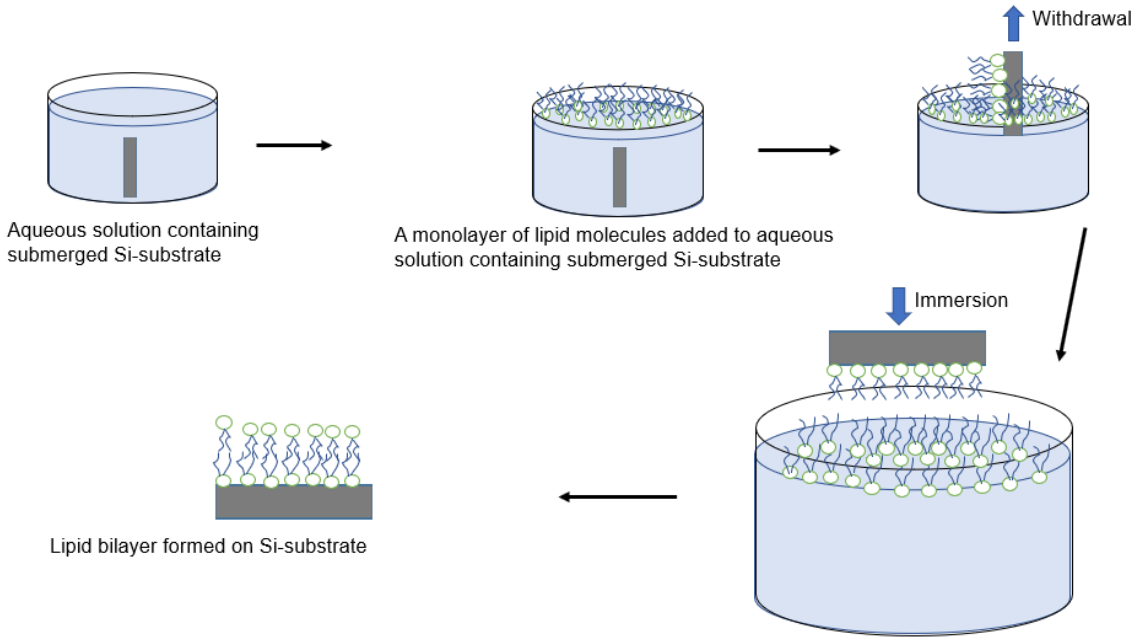

Figure 2-7: A schematic representation of Langmuir-Schafer method of lipid bilayer formation

2.4.3 The Lipid Vesicle Rupture Method

This third approach is considered the most convenient for the formation SLBs. It involves adsorption, fusion and vesicle rupture from solution. This technique is initiated by the transfer of lipid vesicles onto substrates in an increasing manner reaching optimum density before being absorbed on the surface. Thus, enabling fusion and subsequent rupture of the lipid vesicle resulting in the formation of a uniform lipid bilayers.[67,70-74]

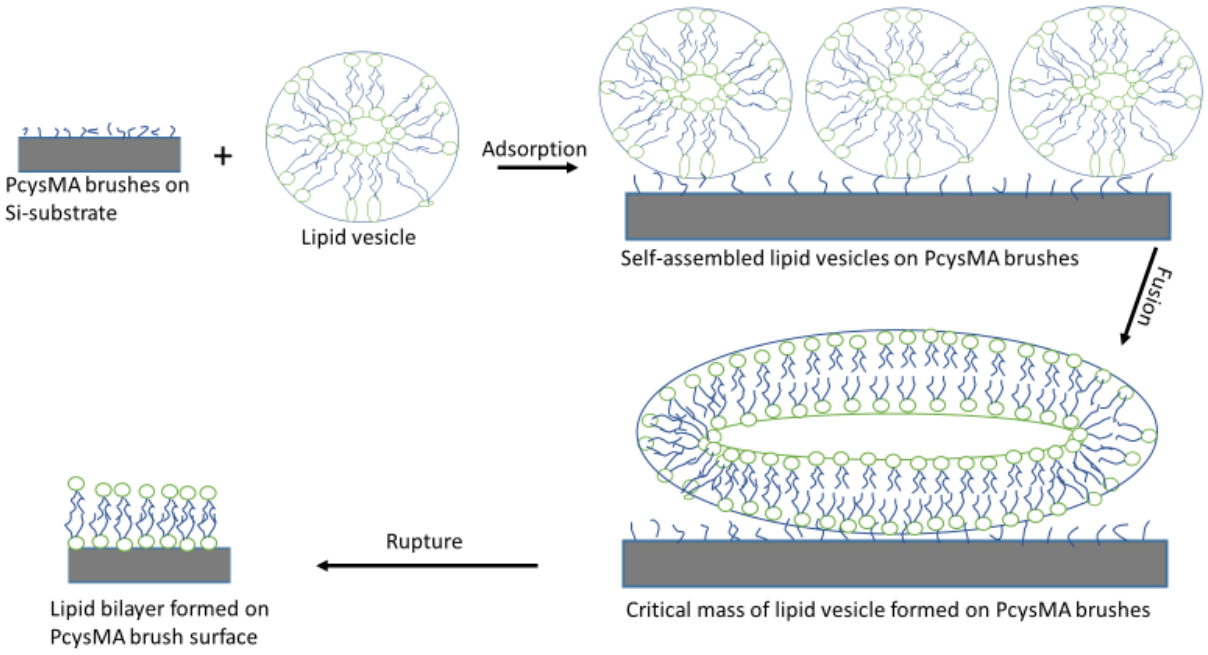

Figure 2-8: A Schematic Representation of Lipid Vesicle Rupture forming Lipid Bilayer

2.5 Techniques for Measurement of Membrane Properties

Within a phospholipid bilayer membrane system, the phospholipid and protein molecules are in a constant state of lateral motion. The movement is free, flexible and random. Consequently, the membrane may be described using the fluidic mosaic model that is seemingly non-static and possessing fluidity and elasticity. It is this membrane fluidity that allows molecules to diffuse through the plasma membrane in order to facilitate cellular activities.[75,76,77]

Diffusion of molecules in membrane systems has been studied with the aid of fluorescence microscopy techniques such as fluorescence recovery after photobleaching (FRAP). In this technique, a small portion of the lipids (or proteins) in the phospholipid membrane are labelled with a fluorescent dye.[78,79,80] A region of interest within the membrane is exposed to an intense confocal laser light source, causing bleaching of the

dyes in that region. If the membrane lipids are mobile, then diffusional transport will lead to the replacement of bleached dyes by dyes that were not exposed to the laser spot. The recovery of fluorescence in the region of interest is monitored under reduced intensity illumination as the photobleached and unbleached phospholipid molecules laterally move freely in all directions thus restoring fluorescence in the photobleached region of interest. A recovery curve can be measured.[81-84] By modelling the recovery curve, the diffusion coefficients, binding rates or turnover rates of lipids in the bleached region can be determined. The steeper the recovery curve is, the faster the molecules can diffuse through lipid membrane systems. Measurements of diffusion coefficients (D) in this technique is arrived at through the stokes-Einstein relationship for spherical molecules.[43,85]

2.6 Self-Assembled Monolayers (SAMs)

Investigations about the effects of thin organic material film on surfaces started some two centuries ago, when in 1774 Benjamin Franklin noticed a seemingly calming effect brought about by an oil film on the surface of agitated water.[65,90] Agnes Pockels developed the first surface balance, later developed by Irving Langmuir into what is now called a "Langmuir trough" and used to form organized assemblies of organic molecules at the air-water interface. Katherine Blodgett discovered how to transfer these Langmuir films to solid surfaces, structures that are now referred to as Langmuir-Blodgett films.

Self-assembled monolayers (SAMs), formed by the adsorption of amphiphiles onto solid surfaces to form ordered, close-packed monomolecular films have been widely used for the control of surface chemistry.[59,60,86,87] Self-assembled monolayers are two-dimensional analogues of Langmuir-Blodgett films that are formed by the spontaneous adsorption of

active surfactants from an organic solvent onto the surface of a suitable substrate.[61-63,88,89] SAMs (Fig. 2-9) can be formed via either their gaseous or solution phase processes.[61,62,64]

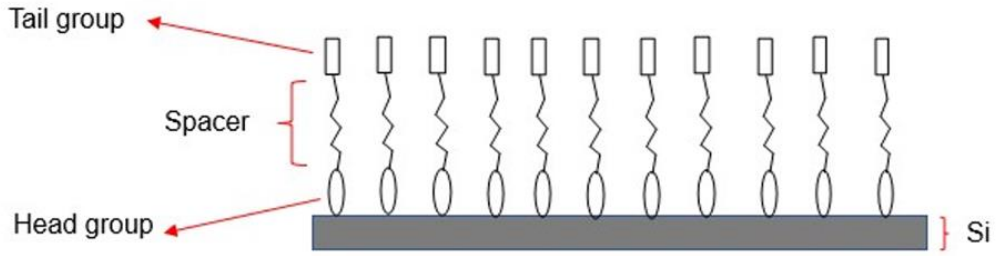

Figure 2-9: Diagram of Self Assembled Monolayer Molecules on the Surface of Silicon

To form a SAM, it is necessary that the head group has a suitably strong interaction with the substrate surface. In the most widely studied systems, formed by the adsorption of alkylthiols onto gold surfaces and by the adsorption of alkylsilanes onto silica surfaces, the adsorbate-substrated interaction bond is covalent, although in other systems (e.g., carboxylic acids on oxide surfaces) the interaction is physical in nature. Attached to the head group is the spacer or backbone.[91-94]

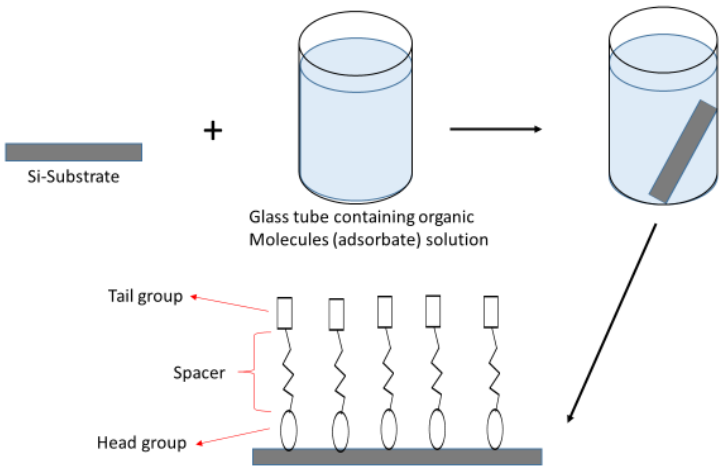

Figure 2-10: Diagram Depicting Schematic Formation of Self-Assembled Monolayer Molecules on Silicon Substrate's Surface

The spacer is made up of alkyl chain that is connected to the tail functional group which effectively facilitates the functionality of the monolayer surface. Some common head groups include thiols, silanes and phosphonates. They easily can be adsorbed onto substrates because of their ability to lower the surface-free energy of the substrates.[61]

2.6.1 Kinetics of Formation of Self-Assembled Monolayers

Long chain alkanethiols have been known to spontaneously assembly together forming a chemisorbed semi-crystalline or crystalline two-dimensional layer on either gold or other metal substrate's surfaces.[66,67] This could be attributed to the occurrence of an aggregated dipole moment, where there is a dynamism between affinity for electrons and the work function.[59,68] Recently there has been improved comprehension of the processes leading to the self-arrangement of monolayers on surfaces. These processes include: the diffusion of molecules from bulk solution to the surface of the substrates, followed by the process of adsorption which is facilitated by the nature of surface functional groups in relation to that of the monolayer molecule head-group, culminating in the alignment of the adsorbed molecules on the surface of the substrates forming self-assembled monolayers.[67,95-98]

Improvements made on the surfaces of silicon substrates using organic molecules that exhibit photoresponsivity have enabled the incorporation of more control in the manipulations of their functional surface's electronic capabilities.[59,69,99,100] Focusing on the relationship between inorganic surfaces and biological materials is critical in enabling the success of integrating biomolecules into non-biological environments. However, the ability to influence interactions at the interface between biological and non-biological surfaces has been a major source for concern, owing to electrostatic, chemical and

structural disposition of these inorganic surfaces compared to dilute buffer solutions where biomolecules have most often been investigated.[70,101-104]

Alkyl silanes are also extensively used in making microelectronics, biomaterials, composites and functional materials. They are essentially a group of saturated compounds made of one or more atoms of silicon attached to each other or to other elements. Metal surface functionalization via molecular adsorption have been utilized to change their wettability, lubrication, adhesion and corrosion properties.[71] Self-assembled monolayers made up of alkanethiols on the surfaces of gold substrates have been interrogated with the aim of unraveling their potentials. Consequently, varying the length of their alkane chains and end groups has promoted greater perception of surface chemistry of substrates.[62,72] Self-assembled monolayers comprising varying functional groups have been extensively fabricated from organosilane molecules.[73] The considerable ease of reactivity of the organosilane head group enables effective covalent interaction to occur between the hydroxyl (OH) surface functional groups and the silanols thus, silane monolayer molecules are favourably chemisorbed onto the metal surface.[71,73,105,106]

2.7 Polymer Brushes

Polymer brushes are tethered linear or branched chains of polymers that have been grafted from or to surfaces of substrates at one end of the chain. The conformation of the surface-grafted polymer depends on the grafting density, solvent and other parameters. There are three broad structural regimes, which include the mushroom, pancake and brush conformations.[107] At low grafting densities, surface-grafted polymers do not interact with each other, and the chains adopt a collapsed morphology. The dimensions of the

polymer are, under these conditions, determined by the radius of gyration of the polymer, and the structures are referred to as "mushrooms". At very low grafting densities, where there are also strong attractive forces between the polymer chains and the substrate, the surface-grafted polymer may collapse completely, forming a flattened "pancake" morphology.

At sufficiently high grafting densities, polymer chains eventually touch and experience steric repulsion from their neighbours. This repulsion causes the chains to swell away from the substrate, forming brushes. The degree of swelling (or stretching) of the polymer chains increases with grafting density, and the thickness of the brush film increases accordingly.

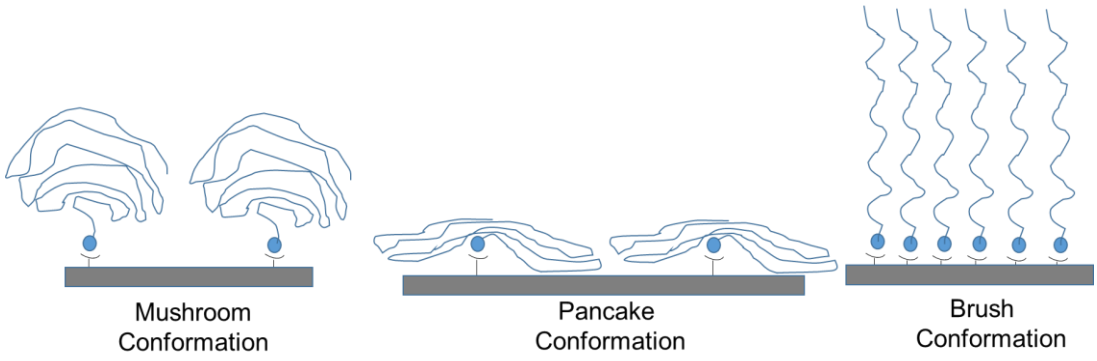

Figure 2-11: Diagram of the Three Different Polymer Conformation

These surface grafted polymers have been widely used to modify the properties of surfaces thereby conferring on them new properties that can lead to diverse applications in science, engineering and biomedical technology.[75,108] Preparation of graft polymers could be achieved via the grafting-to,[76,109-113] and the grafting-from[77] methods.

2.7.1 Grafting-To

The grafting-to protocol requires prefabricated reactive polymers to be coupled onto a polymer backbone. This enables the size and chemical structures of the brushes produced to be properly configured. However, this often results in limited grafting density owing to overcrowding by the grafted side chains, thus making it increasingly impossible for the incoming reactive polymer to be coupled to the prefabricated backbone. Just as in the immobilization on gold surfaces of pre-formed poly (sodium 4-styrenesulfonate) and poly (N,N-dimethylacrylamide).[114-117] To override this steric drawback, copper-catalyzed azide-alkyne cycloaddition (CuAAC) reaction has been incorporated because of its effective reactivity, decreased solvent sensitivity and increased functional group tolerance.[78-80,118-121]

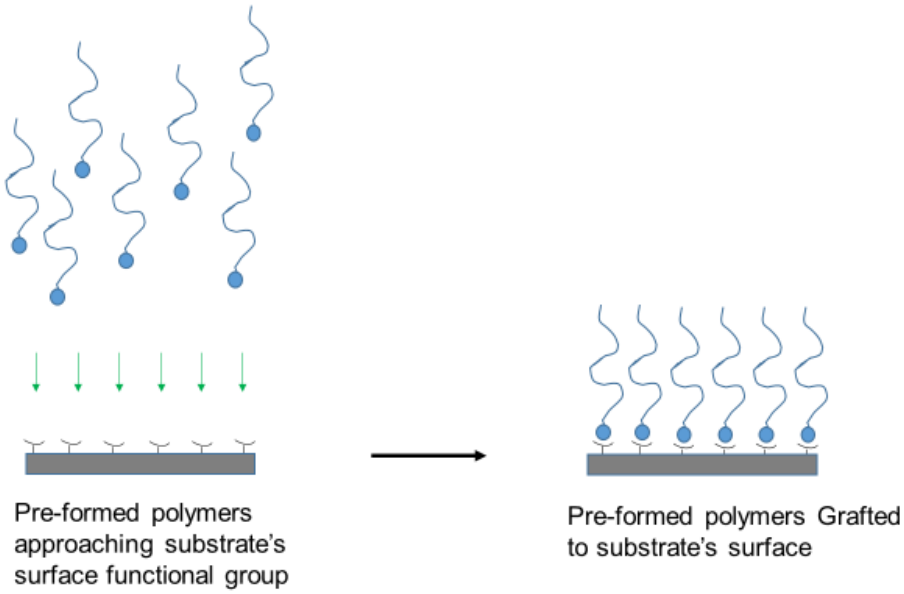

Figure 2-12: Schematic illustration of the Grafting-To process of polymer brush ATRP

2.7.2 Grafting-From

In grafting-from, polymer molecules are grown from a surface-bound initiator. Side chains may be prepared by grafting from the backbone. This technique facilitates the growing of dense polymer brush layers, although, side chain monomer conversion is limited, to inhibit radical-radical coupling occurring within and outside the polymer brushes. Recently these coupling effects have been avoided by deploying actuators which were sourced by electron transfer atom transfer radical polymerization.[81,122-126]

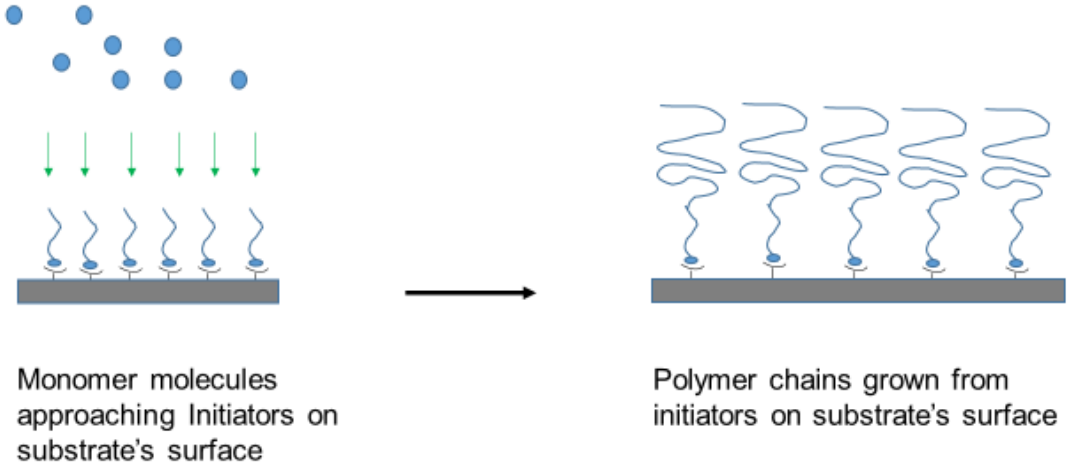

Figure 2-13: Schematic illustration of the Grafting-From process of polymer brush ATRP

2.8 Atom Transfer Radical Polymerization

The first report of atom transfer radical polymerization technique was by Matyjaszewski in 1995.[82,127,128] It involved growth of a polymer by a living radical mechanism from a surface bound initiator (a halogen). This technique was found to be capable of yielding controlled polymer growth. In a successful ATRP reaction no more than 5% of propagated polymers experience impromptu growth termination at the onset. However, most of the polymer chains are uniformly propagated chiefly due to the deployment of catalysts which

favour fast initiation step coupled with a swift reversible deactivation.[129,130] Although oxygen atoms present in the reaction media oxidize the metal of the catalyst which constitute a major hinderance to ATRP reaction, this factor is mitigated by the much higher catalyst concentration which overrides the concentration of the polymerizing radicals leading to prompt scavenging of the hindering oxygen atoms from the reaction.[83,131-135]

2.9 Activators Regenerated by Electron Transfer (ARGET) ATRP

Although ATRP is an indispensable technique for polymerization, it however, has some limitations. These drawbacks include: the dependence on organic solvent as a medium for reaction, the need for high monomer concentrations, high catalyst concentration, elevated temperature for reaction and its dependency on oxygen exclusion from reaction. These requirements do not favour large scale polymerization.[136-138] Consequently, activators regenerated by electron transfer (ARGET) ATRP, was introduced as a modified version to overcome these ATRP drawbacks. The ARGET-ATRP method lowers the amount of catalyst used by regeneration. This happens when copper (II) chloride and 2,2-bipyridyl are combined to form a Cu (II) complex that regenerates Cu (I) ions constantly with the help of a reducing agent (such as ascorbic acid).[84,139,140]

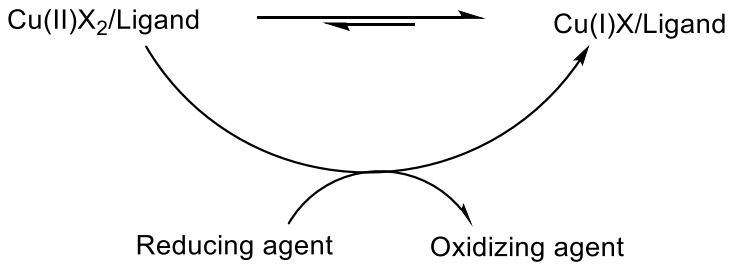

Figure 2-14: Reaction of the activated Cu (I) specie

The inclusion of this modification into ATRP ensures that the concentration of Cu (I) ion is low at the initial stage of polymerization thus lowering the concentration of free radical and optimizing their yield in the reaction. In addition, the improved ATRP protocol allows the addition of water into the reaction resulting in a significant enhancement in polymerization rates. The inclusion of water allows water soluble monomers to be polymerized completely in water as solvent thus facilitating the ease of polymerization because, lower monomer concentration is enabled (1% v/v in solution). The ease of polymerization brought about by these modifications on ATRP has made large scale polymerization viable.[84,141]

There has been an explosion of interest in ATRP owing to this simple polymerization reaction and the diversity of polymerization reactions with which it is capable. As well as the potential for well-controlled growth of polymer films and the compatibility with benign conditions (eg. use of water as solvent).[85,86] Atom transfer radical polymerization has become an important tool among the numerous techniques which have been employed in polymer synthesis of poly(methacrylates), polystyrene and poly(acrylates).[83,87] Many polymers with controlled surfaces and compositions are readily synthesized via atom transfer radical polymerization.[85,142]

Atom transfer radical polymerization mechanism entails the breakage of an alkyl halide bond (RX) with the aid of a transition metal complex to produce a higher oxidation state metal halide complex and a corresponding alkyl radical (R^*) which is capable of adding to a monomer.[87] Radicals are successfully added to monomers due to the existence of equilibrium which lies to left between the active and the dormant chains, thereby ensuring

a decreased concentration for propagating radicals and inhibiting termination step possibility.[88,143]

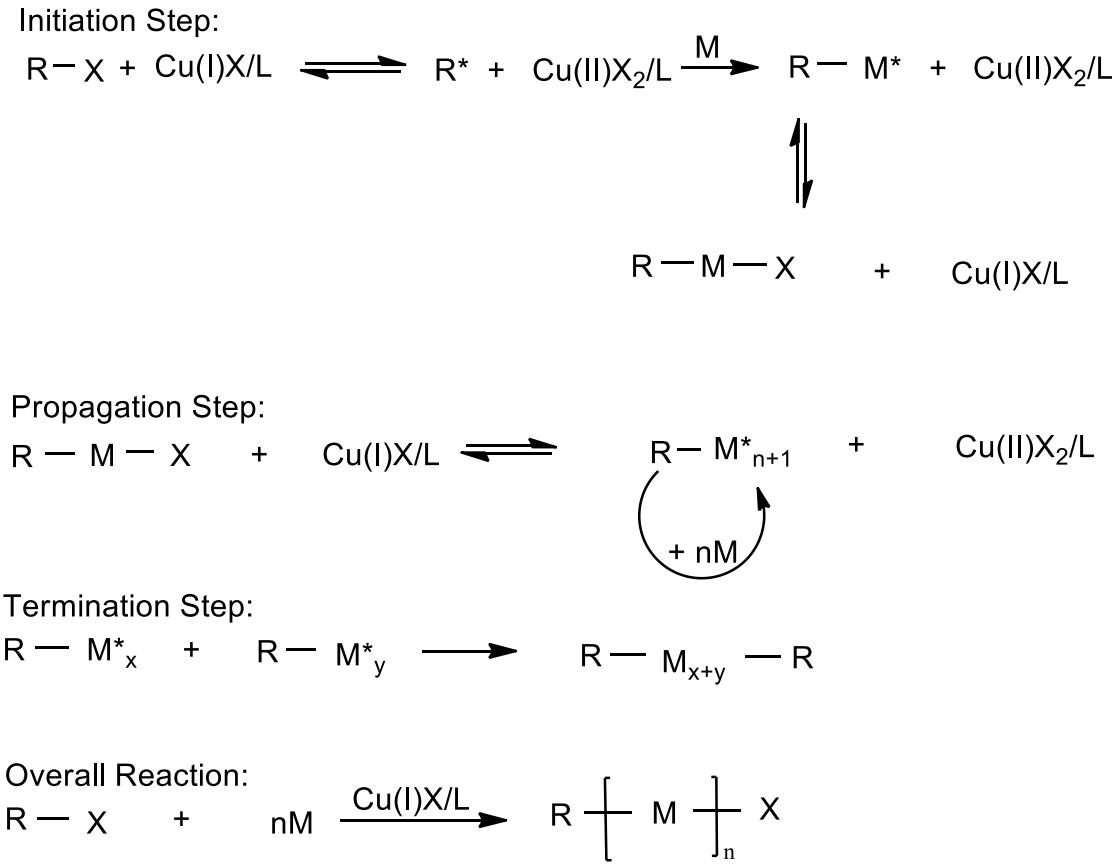

Figure 2-15: The ATRP mechanism according to Matyjaszewski et, al [83,84]

2.10 Surface Initiated Atom Transfer Radical Polymerization (SI-ATRP)

This technique of polymerization on a vast array of surfaces including planar and colloidal (inorganic) ones deploys the use of free initiators and Cu (II) which serves as an additional deactivator in polymerization process thus inducing molecularity weight control of the newly growing polymer chains. The free initiator addition also helps to lower the initial initiator to monomer ratio making the overall concentration of the initiator to be higher. Thus, facilitating the coupling effect of the radicals. 3-(2-bromopropionyloxy) propyl

dimethyl ethoxy silane (BIDS) which is an ATRP initiator that has been utilized for surface-initiated polymerization (SIP) alongside core shell CdS/SiO_2 nanoparticles.[89]

2.11 Surface Initiated Free Radical Polymerization

One of the most utilized techniques for polymerization is the free radical polymerization reaction. This technique involves the use of 2,2- azobis(isobutyronitrile) as initiator which is tethered on silica surface. There exist several similarities with a few differences in mechanisms mainly in the termination reaction compared to other forms of polymerization. A distinguishing feature of this initiator molecule is the ability to produce two radicals, where one radical gets tethered to the silica surface while the other radical gets diffused into the solution. This surface grafting attachment can be broken through hydrolysis, enabling the grafted polymers to be analyzed after polymerization. Termination reaction rates tends to decrease as the grafting density increases, owing to free radical chains dissolving into solution against concentration gradient, resulting in a situation where the number of already attached chains determine the molecular weight of the newly growing chains[90,91]

2.12 Living Anionic Surface Initiated Polymerization

This polymerization technique presents the best means of structure control. Anionic polymerization technique primarily facilitates formation of monodispersed homopolymers, star miktoarms and complex block polymer architectures. The term “living” refers to the chain end of a polymer molecule that is active and can be propagated continuously and not terminated. It is a living cation when its charge is positive and a living anion when it is negative. Polymer brushes have been grown from numerous small particles using this method such as those grown from silica gels carbon black and graphite. Although there

exist some constraints in the anionic polymerization process owing to the effects of moisture along with other impurities specifically with regards to clay surface polymerization.[92,93]

2.13 Surface Initiated Living Cationic Polymerization

This method utilizes end-functionalized 3D self-assembled monolayers adsorbed on gold nanoparticle surfaces via the technique of ‘’grafting-from’’. Thus, high density polymers brushes are obtained in a ‘’one-pot’’ multistep reaction. Utilizing suitable initiation protocol and monomers of 2-oxaziline, ring opening polymerization is propagated in a living manner. The amphiphilic gold/polymer nanocomposite that emanated from the use of 2-ethyl-2-oxaziline monomers in N,N-dioctadecylamine terminating agent was found to be very stable.[94-96]

2.14 Surface Initiated Ring Opening Metathesis Polymerization

This polymerization method entails the utilization of a transition metal-based catalyst ruthenium carbene ($Cl_2Ru(PCy_3)_2$-CHPh) and nanoparticles of gold and silica which were alkanethiol functionalized. The ease of adsorption of alkanethiols on Au-surfaces favour the immobilization of norbornenyl initiation sites which allows preferential block polymer growth on the nanoparticle surfaces, resulting in good control of polymer length, particle size and chemical composition.[97-99]

2.15 Surface Initiated Hyperbranched Polymerization

In this technique ultralow hyperbranched graft polymer functionalized surfaces were obtained on silicon, glass and zinc oxide substrates by self-condensing vinyl polymerization. The surfaces of ZnO nanoparticles were covalently linked to ATRP initiators accompanied by self-condensing vinyl polymerization of the inimer (initiator-

monomer) molecules which possess both a group that can be polymerized and an initiator group within the same molecule. Well-structured chains of polymers were conveniently propagated from these surfaces producing hybrid nanoparticles made up of ZnO cores and hyperbranched polymers which possessed functional end groups of chlorobenzyl. The grafting percentage obtained in a span of 6 hours was sufficiently high.[100]

2.16 Aims

The goal of this PhD project is to develop microsystems that enable the *in-situ* measurements of membrane transport processes. The basic concept is the formation of compartmentalized regions (‘’corrals’’) which define supported lipid bilayers that contain integral transmembrane proteins. The systems are to be designed in such a way that they incorporate reporters for the *in-situ* measurements of membrane transport.

Figure 2.16 shows a schematic diagram of the type of system that we envisage. Regions functionalized with PCysMA cushions for lipid membranes are enclosed within POEGMA walls that contain integral pH-sensitive dye reporters that yield spectral changes as the pH changes. This enables in situ monitoring of changes in the local pH in response to transmembrane proton transport. A limitation of this system is that it is open: the POEGMA walls are not encapsulated by a lipid bilayer, meaning that protons may diffuse through them. Thus, the system is effectively under kinetic control. Nevertheless, it is a suitable starting point, enabling proof of concept investigation of the feasibility of brush-based microsystems for modelling membrane transport processes. The first challenge, however, is to design a synthetic strategy to enable production of the required surface-grafted polymers. This is the main goal of this PhD thesis.

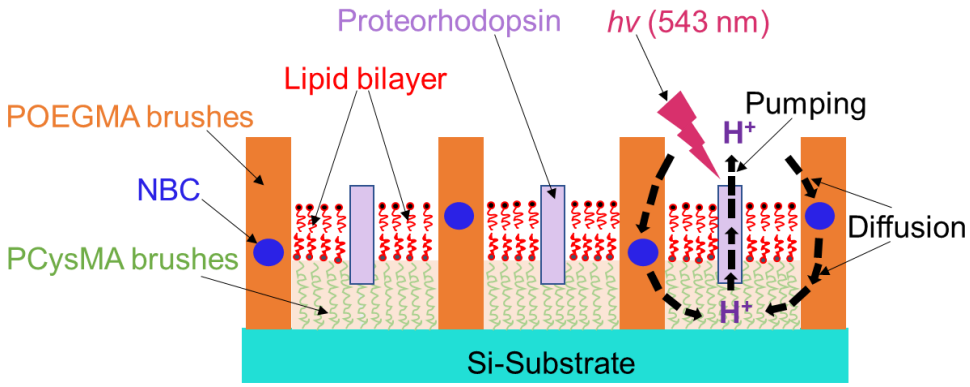

Figure 2-16: A Model of the Polymer Brush Microsystem

The steps needed to achieve these goals include:

- Deposition of an initiator monolayer for growth of polymer brushes by ATRP.
- Patterning the initiator monolayers by UV exposure to define and enable cell compartmentalization.
- Use polymer brushes to build the cell walls and the corrals.
- Transfer lipid bilayers to the cells as suitable attachments sites for the membrane proteins.

This thesis is composed of an introduction to microsystem development along with a review of related literatures in chapters 1 and 2, as well as a description of relevant surface analysis experimental techniques employed for the development of a viable microsystem in chapters 3, while the experimental results and discussions are represented and described in chapters 4, 5 and 6. Chapter 4 focusses on the ATRP of sufficiently controlled thicknesses of PCysMA and POEGMA brushes on brominated and chlorinated films on silicon surfaces. Chapter 5 dwells on the incorporation and end-capping of pH-responsive Nile blue dye into the brush structures. Finally, chapter 6 deals

with photo-modifications of surfaces by UV-exposures and polymer brush growth on photopatterned films to establish a binary structured platform. The final chapter in this thesis captures the conclusion and recommendation for future work.

CHAPTER 3: EXPERIMENTAL METHODS

3.1 Materials

All chemicals used were analytical reagent grade. 2-bromoisobutyrylbromide (BIBB) 98% purity, Triethylamine (TEA) 99% purity, 3-aminopropyltriethoxysilane (APTES) 98% purity, 2,2-bipyridyl 99% purity, L-cysteine, Bis[2-(-bromoisobutyryloxy) undecyl] disulfide, 3-(acryloyloxy)-2-hydroxypropylmethacrylate, Oligoetheleneglycolmethacrylate, (OegMA), Dimethyphenylphosphine (DMPP), Dicyclohexylcarbodiimide (DCC), Nile blue carbamate (NBC) dye, Glycerol, Sulphuric acid and Ascorbic acid were purchased from Sigma Aldrich (Gillingham, UK). 4-Chloromethylphenyltrichlorosilane (CMPTS) and Diethyl-12-mercaptododecylphosphonate were purchased from Alfa-Aesar (Lancashire, UK). Gold wire 99,999% purity was purchased from Goodfellow UK. Chromium chips 99.99% purity was sourced from Agar Scientific Limited (Stansted Essex, UK). Other HPLC graded items were gotten from the University of Sheffield stores these include Ethanol, Isopropyl alcohol, Dichloromethane, Hydrogen peroxide, Acetone, Toluene, Methanol, Ammonium hydroxide, and Ethyl acetate. De-ionized water was obtained from an Elgar purification unit (Elgar, pure nanopore 16 MΩ) stationed in the Laboratory.

3.2 Glassware and Substrate Slides Cleaning Methods

All glassware was cleaned by immersion in piranha solution, a mixture of concentrated sulfuric acid (70%) and hydrogen peroxide (30%) for 90 min. (Note: Piranha solution can easily detonate spontaneously when in contact with materials that are organic, due to its extremely strong oxidizing capability). Extreme care must be employed when making use of piranha solution because of it being potentially very dangerous and its usage must always be inside a fume cupboard with the aid of a blast shield, goggles and very thick

rubber gloves as personal protective equipment (PPE). The cleaning solution was poured slowly into a dilution tank filled with water. The glassware and substrates were subsequently rinsed with deionized water sonication for 10 min.

3.3 Sample Handling

To avoid surface contamination of the sample substrates, only cleaned (using acetone and ethanol for cleaning before being dried with N_2 gas) tweezers were used for handling the slides, to ensure they are free of contaminants. Furthermore, this cleaning protocol was done on diamond cutter and metal ruler including the glass platform which were used to cut the sample slides into appropriate sizes for use.

3.4 Preparation of BIBB-APTES Initiator

Piranha-cleaned silicon substrates were immersed in a solution of 2% 3-aminopropyltriethoxysilane in ethanol for 30 min at 20^{o}C. The silicon substrate was rinsed with ethanol and dried under a stream of nitrogen gas, followed by subsequent annealing at 120^{o}C for 30 min in a vacuum oven. The annealed APTES coated substrates were immersed in clean glass tubes containing a solution of 2-bromoisobutyrylbromide (0.37 mL, 3 mmol) and triethylamine (0.41 mL, 3 mmol) dissolved in 60 mL of dichloromethane for 30 min at 20^{o}C. The BIBB-APTES functionalized substrates were rinsed with dichloromethane and ethanol before drying in a stream of nitrogen gas prior to characterization.

3.5 Preparation of 4-(Chloromethylphenyl) trichlorosilane (CMPTS) Initiator Films

Clean silicon substrates were immersed in a solution of 100 µL of CMPTS in 30 mL of dry toluene contained within a carousel in a nitrogen atmosphere for 30 min at 20^{o}C. The

CMPTS functionalised substrate was retrieved and washed with a mixture of toluene and ethanol before drying under a stream of nitrogen gas. Samples were annealing for 30 min at 120^{o}C in a vacuum oven prior to characterization.

3.6 Thiol Monolayer

Metal substrates used in SAMs can be made through physical vapour deposition or electrodeposition techniques. Thiol SAMs produced by adsorption from solution are usually made by substrate's immersion into diluted solutions of alkane thiols in ethanol. Metal film deposition was performed using an Edwards Auto 306 Thermal Evaporator System (BOC Edwards, Crawley, UK). Substrates were primed with a layer of Cr (thickness ca 2-5 nm) before deposition of ca 20 nm layer of gold at evaporating rates of ca 0.1 nm sec^{-1} and 0.4 nm sec^{-1} for Cr and Au respectively.

3.7 Cysteine Methacrylate (CysMA) Synthesis

L-cysteine (15.13 g, 124.88 m mol) was measured and dissolved in 100 mL deionized water and 3-(acryloyloxy)-2-hydroxypropyl methacrylate (29.43 g, 137.36 m mol) was added. Catalyst dimethyl phenyl phosphine (20 μL, 1.47 x 10^{-1} m mol) was transferred into the aqueous solution which was constantly stirred at room temperature for 2 h with the help of a magnetic stirrer. The monomer formed was washed twice by dispersion in 50 mL of ethyl acetate. The organic phase was separated from the aqueous phase and discarded. Finally, a further phase separation step was carried out using dichloromethane (2 x 50 mL). CysMA was isolated from purified aqueous solution as a pure white solid by utilizing the Freeze-drying technique.

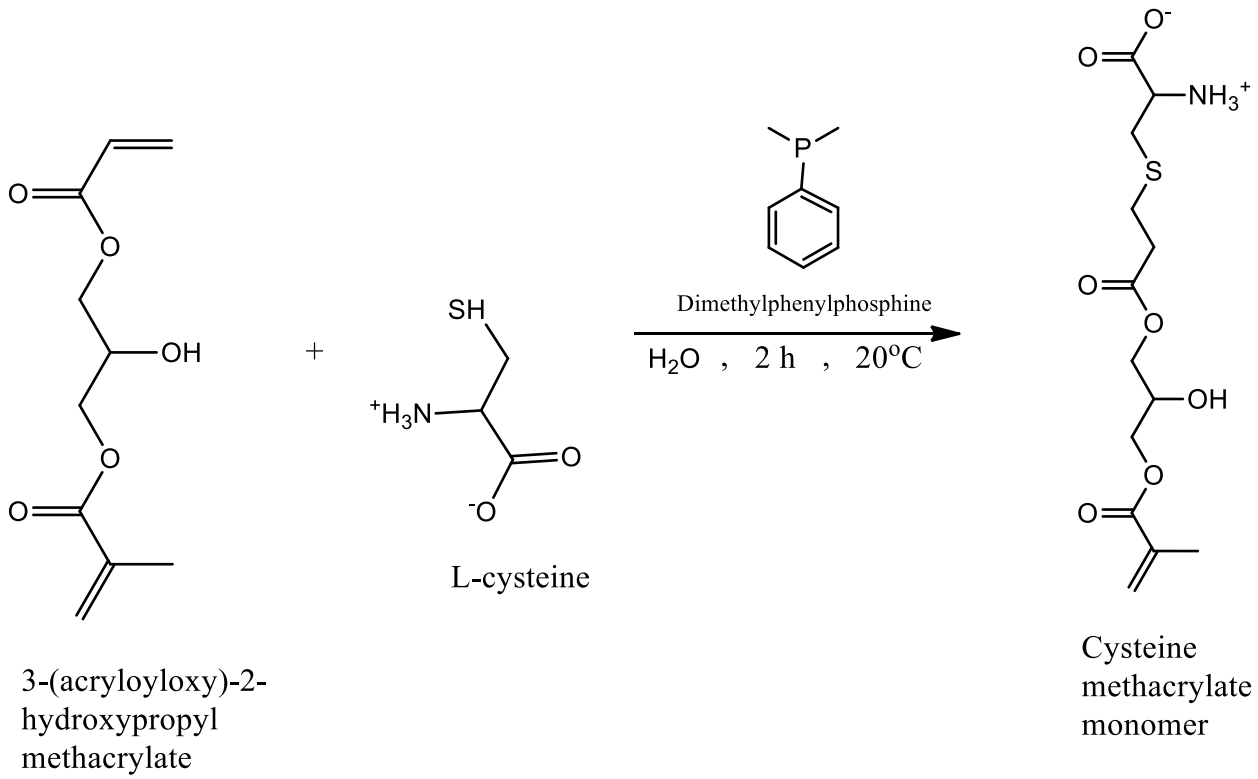

Figure 3-1: Schematic Representation of Synthesis of Cysteine Methacrylate Monomer

3.8 Preparation of Poly (Cysteinemethacrylate) (PCysMA) Solution for ATRP

0.75 g of cysteine methacrylate (CysMA) monomer was placed in a clean 50 mL capped glass tube. 4 mL of deionized water was added to the monomer and shaken to ensure proper dissolution of the CysMA monomer. To this solution, 0.18 mL of a solution 100.1 mg (0.1001 g) of ascorbic acid was dissolved in 10 mL deionized water. 38.8 mg (0,0388 g) of 2,2-bipyridyl was dissolved into 5 mL of ethanol contained in a 10 mL clean capped glass tube. To this was added a solution of 14.6 mg (0.0146 g) of $CuCl_2$ dissolved in 5 mL deionized water. 0.35 mL of this resulting solution was then added to the monomer

solution. The resulting mixture was shaken once only and allowed to settle without further agitation. This final solution was used for ATRP.

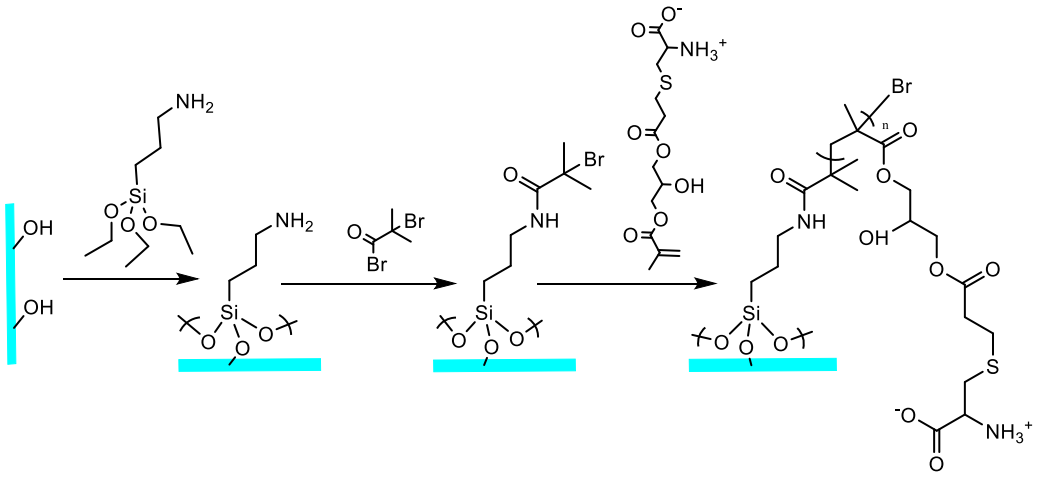

Figure 3-2: Schematic representation of reactions producing PCysMA on substrates

3.9 Preparation of Poly (Oligoethylene glycol methyl ether methacrylate) (POEGMA) Solution for ATRP

4.6 mL of Oligoethylene glycol methyl ether methacrylate (OEGMA) monomer was transferred into a clean suba-sealed 50 mL round bottom flask containing 11.2 mL of deionized water in a nitrogen atmosphere. 0.07g of 2,2-bipyridyl was added into the monomer solution along with 0.011g of copper (II) bromide and 0.023g of copper (I) bromide catalyst with adequate stirring of the reaction solution. This was added to an initiator-functionalized substrate placed inside a carousel tube in a nitrogen atmosphere. ATRP was carried out for the required polymerization time

3.10 Photo-Patterning of Initiator Functionalized Substrate Surfaces

Micro-scale patterned, and un-patterned samples were achieved via argon ion laser beam source (Coherent Innova 300C FreD, UK). The argon ion laser source has a wavelength

emission capacity of 244 nm. To make the laser source instrument function optimally, it was turned on for 40 min prior to usage for proper stabilization of the laser beam intensity.

Sample slides to be used for micro-patterned and non-patterned laser exposure were cut to a dimension of 5 mm x 7 mm rectangular shapes. Ethanol was used for cleaning the sample surface after cutting and dried under a stream of nitrogen gas before UV light exposure. The apparatus deployed for micro-patterning comprised of a converging lens along with a mirror placed at 45^{o} to the incident beam. The laser beam was focused on to the sample covering an area of about 2 mm^2.

An electron microscope Cu grid mask which consisted of patterns of square meshes (Agar, Cambridge, UK), was used for masking. This Cu grid square patterned mesh was placed on the sample surface and held in position with the aid of a cleaned quartz disc during exposure. At the end of the exposure period, the sample was removed and cleaned with ethanol before being dried under a nitrogen gas stream. The argon ion laser exposure time on sample surface was derived from the equation:

$$t = \frac{D \cdot \pi \cdot r^2}{LP}, \quad \text{..... (3.1)}$$

Where *t* is the Exposure time [sec], *D* is the Dose of exposure [J/m^2], *r* is the sensor radius ($0.25 \cdot 10^{-2}$ m), *LP* is the Laser power on sample [W], and π = 3.14.

3.11 Surface Characterization

3.11.1 Contact Angle

Contact angle is the term used to refer to the angle between the solid-liquid and liquid-vapour interfaces within a solid-liquid-vapour system. It provides information about the

thermodynamics of the solid liquid interface. Contact angle (θ_o) can be accomplished in two ways: Advancing Contact Angle (θ_A) and Receding Contact Angle (θ_R).

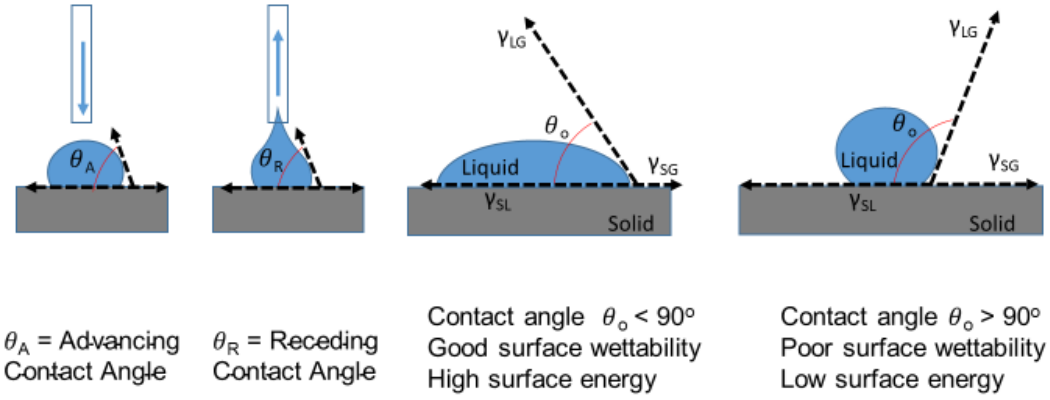

Figure 3-3: Contact Angle (C.A) diagram showing Advancing C.A, Receding C.A, a Hydrophilic surface, and a hydrophobic surface

The measurement of an advancing contact angle is achieved at the instance when dropping the water droplet onto the substrate's surface, while that of receding angle is measured at the instance when the water droplet is withdrawn from the surface. The liquid droplet which rests on the substrate's surface, has a shape that depends largely on the thermodynamic equilibrium around its perimeter. Measurement of contact angle can be achieved with the aid of microscope fitted with a goniometer scale (Ram Hart sessile-drop goniometer). The relationship between the interfacial tension and the contact angle of the surface is given by Young's equation:

$$\gamma_{SV} = \gamma_{SL} + \gamma_{LV} \cos\theta_o \quad \ldots\ldots\ldots\ldots\ldots\ldots (3.2)$$

Where: γ_{SL} is the solid-liquid interfacial tension, γ_{LV} is the liquid-vapour interfacial tension, γ_{SV} is the solid-vapour interfacial tension, θ_o is the contact angle.

3.11.2 Spectroscopic Ellipsometry

Ellipsometry is a non-invasive and non-destructive optical technique in surface chemistry. It is used to investigate the dielectric properties of films of molecules immobilized on surfaces of substrates. This is achieved by assessing changes in the polarization states of light when it is transmitted or reflected from surfaces. The ellipsometer can reveal information about the composition, thickness, roughness, crystalline properties and other material properties on functionalized surfaces.

Figure 3-4: Image of Spectroscopic Ellipsometry Instrument.[102]

In this study a J.A. Woolan M-2000 V spectroscopic ellipsometer was used. It consists of an optical part, which is made up of a light source, polarizing elements referred to as a photodetector and an analyzer and polarizer units. It deploys a quartz tungsten halogen lamp with a beam diameter of 2-5 mm and a 370-1000 nm range of spectrum. Including an incident angle of 75^{o} which enables both *in-situ* and ex-situ characterizations.

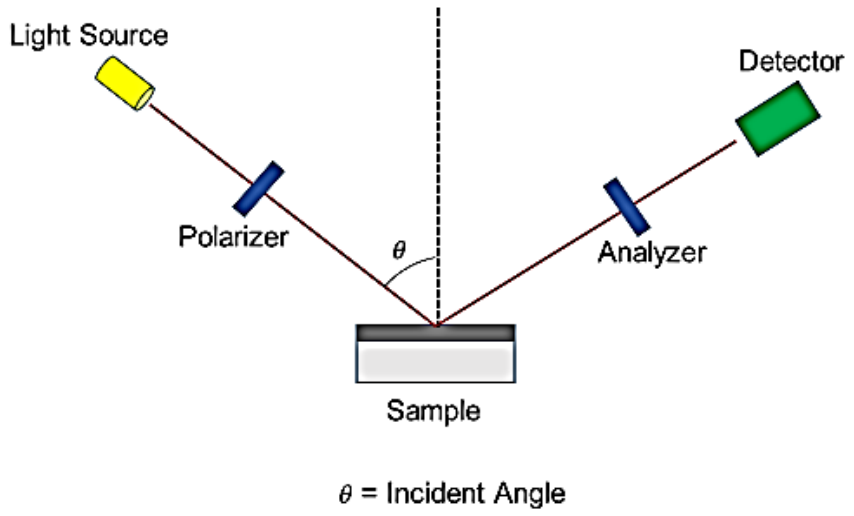

Figure 3-5: Schematic illustration of an Ellipsometry Equipment

Spectroscopic ellipsometry executes measurement of two cross polarized positions that are recalculated as ellipsometry angles of ψ and Δ, which represent functions of wavelength and incidence angle. Optical constant and film thickness can be extracted using a model-based analysis.

Firstly, ψ and Δ experimental data are gathered within the range of spectrum at desired incidence angle. An optical structure model of the sample was constructed, followed by the prediction of expected ψ and Δ values for each wavelength. Lastly, the measured ψ and Δ values are compared with the predicted values of the model. This procedure of analysis is called Data-fitting.

The mean squared error (MSE) is used to quantify the variations between the predicted values and the experimental values. It is normalized by the standard deviations on the experimental data, such that the noisy data are weighted insignificantly. The smaller values of MSE suggest a better fit to data.

$$MSE = \frac{1}{2N-M} \sum_{i=1}^{N} \left(\frac{\psi_i^{mod} - \psi_i^{Exp}}{\sigma\psi_i^{Exp}} \right)^2 + \left(\frac{\Delta_i^{mod} - \Delta_i^{Exp}}{\sigma\Delta_i^{Exp}} \right)^2 \quad \ldots\ldots\ldots\ldots\ldots\ldots (3.3)$$

The incident light beam passes a polarizer where it is linearly polarized and reflected by the sample on to an analyzer before detection. Ellipsometry evaluates the complex reflectance ratio (ρ) whose parameters are defined by ψ and Δ The polarization of the incident beam of light is built up of two components s and p which oscillates perpendicularly and parallel to the plane of incidence respectively. The amplitudes after reflection of s and p components are denoted by r_s and r_p respectively. The ratio of these amplitudes describes the complex reflectance ratio (ρ).[102]

$$\rho = \frac{r_P}{r_S} = tan\,(\psi) e^{i\Delta} \quad \ldots\ldots\ldots\ldots\ldots\ldots\ldots\ldots (3.4)$$

3.11.3 Atomic Force Microscopy

AFM was performed using a Multimode NanoScope instrument (Bruker, Coventry, UK) operating in contact mode. V-shaped silicon nitride probes (k = 0.06 Nm^{-1}) were used. The nominal radius of curvature of the tip was 20 nm, while the spring constant was derived from the cantilever parameters. The AFM like all other scanning probes uses a sharp tipped probe which moves over the surface of a sample substrate in a raster (horizontal) scan pattern. The probe is situated at the end of the cantilever tip which bends in response to the force between the tip and the sample surface. Unlike other microscope, scanned-probe systems do not use lenses, therefore the resolution limit is determined by the size of the probe as well as its nature of interaction.[103]

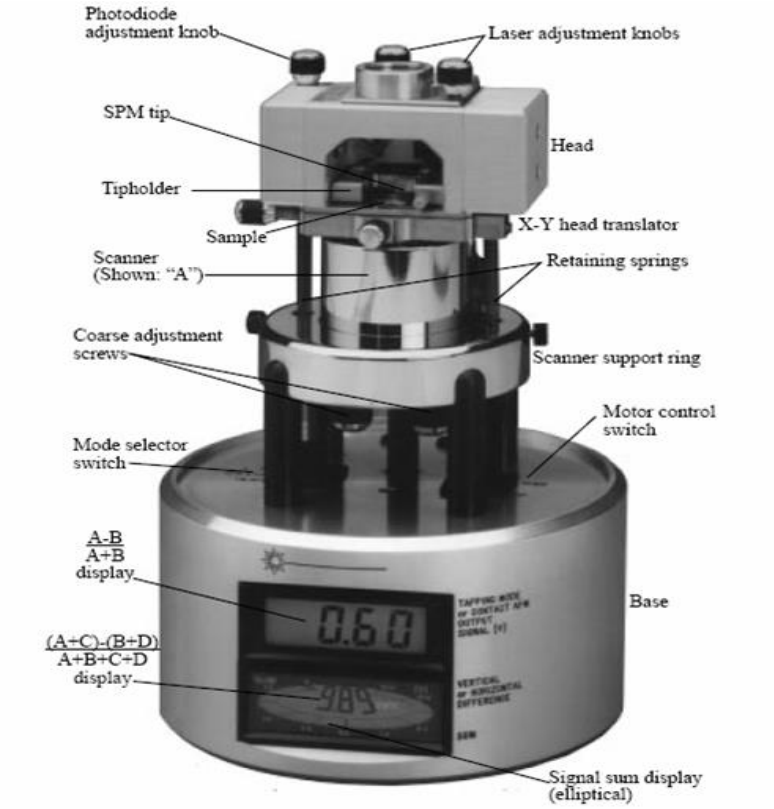

Figure 3-6: Image of an Atomic Force Microscope.[103]

Operations of the AFM is based on the interactive forces between the tip of the probe and the surface of the sample substrate. As the probe tip is brought into proximity with a sample surface, the force acting between the tip and the sample generates a deflection of the cantilever in accordance with Hooke's law.

$$F = - kx \qquad \ldots\ldots\ldots\ldots\ldots\ldots\ldots\ldots \quad (3.5)$$

Where: F = the force, k = the spring constant (Nm^{-1}) and x = the cantilever deflection.

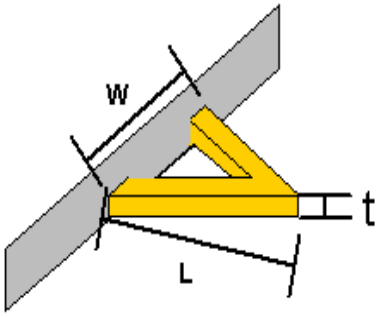

Figure 3-7: Image of a Cantilever.[104]

The spring constant *k* (Nm^{-1}) strongly depends on the physical dimensions of the cantilever which are the width (*w*), the length *(L*) and the thickness (*t*) and the value of modulus of elasticity (*E)*. The spring constant for the triangular cantilever is approximately expressed by

$$k = \frac{Et^3w}{4L^3} \qquad \text{..... (3.6)}$$

Interatomic forces or Van der Waals forces are the most common forces associated with AFM. The cantilever is held at the contact region less than a couple of Angstroms (10^{-10} m) from the surface of the sample substrate and the Van der Waal's forces acting between the sample surface and the cantilever is repulsive. While the cantilever is held at the non-contact region in the order of tens of hundreds of angstroms from the surface of the sample with an attractive Van der Waals force between the cantilever and the sample surface. AFM scanning modes operating within the different regions of the curve are represented below. The non-contact mode functions within the attractive region of the inter atomic forces, the contact mode operates within the repulsive region of the inter atomic forces while the tapping mode fluctuates between the two regions.

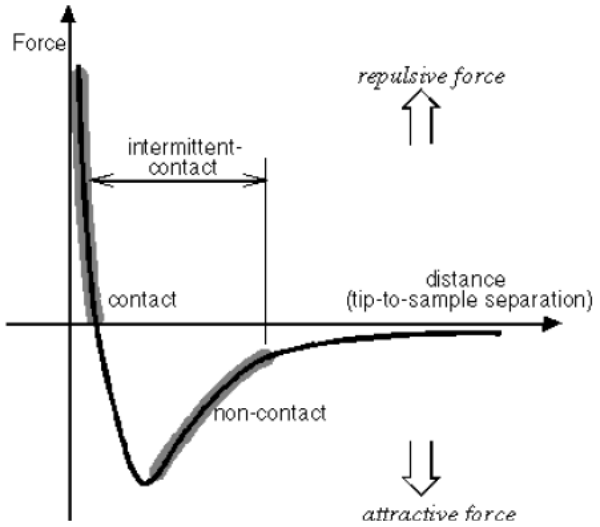

Figure 3-8: Diagram showing Relationship between Van der Waals Forces and Distance.[105]

3.11.3.1 Beam Deflection Detection System

Fluctuations were monitored between the Tip-Sample interactions via an optical cantilever detection system, where a beam of laser is reflected from the cantilever and collected by a detector that is position sensitive which consist of two photodiodes that are closely spaced and connected to a different amplifier. The cantilever's angular displacement results in one photodiode collecting more of the light than the other photodiodes, yielding an output signal that is proportional to the cantilever deflection. Specific operating parameters and AFM settings were maintained while scanning at constant level generating images through feedback loops situated between the piezoelectric scanners and the optical detection system. Scanning was achieved above a stationary probe tip on the sample surface.

3.11.3.2 AFM Contact Mode

The contact mode AFM functions by scanning a probe tip which is attached to the end of a cantilever across the surface of the sample at the same time monitoring fluctuations in the cantilever deflections using a split photodiode detector. The close-range contact between the repulsive regions of the inter-molecule force curve. A constant deflection between the cantilever and the sample surface is maintained through a feedback loop by moving the scanner vertically at each (x,y) points for a set point deflection to be maintained.

The force between the sample surface and tip remains constant by maintaining a constant deflection of the cantilever. The AFM can operate in an environment which is either in liquid or gaseous phase. Data of the scanner's vertical positions at each (x,y) point was generated and stored as topographic images of sample surfaces in the computer.

3.12 AFM Tapping Mode

This is an AFM operational imaging procedure that is widely used next to contact mode imaging technique. It involves high resonance frequency oscillation of the cantilever at about 300kHz, where the tip strikes the sample surface. Adjustment of the feedback loop enables the tip-surface interaction to be controlled. Thus, maintaining a set-point owing to the modified oscillation amplitude at a constant value leading to the generation of a topographical image. These cantilevers are made from large spring constant silicon compared to those of contact mode technique. The advent of tapping mode operational technique has diminished the contact and lateral forces existing between the sample surface and the cantilever tip. Thus, favouring it as a highly sought out technique for soft material imaging.[103]

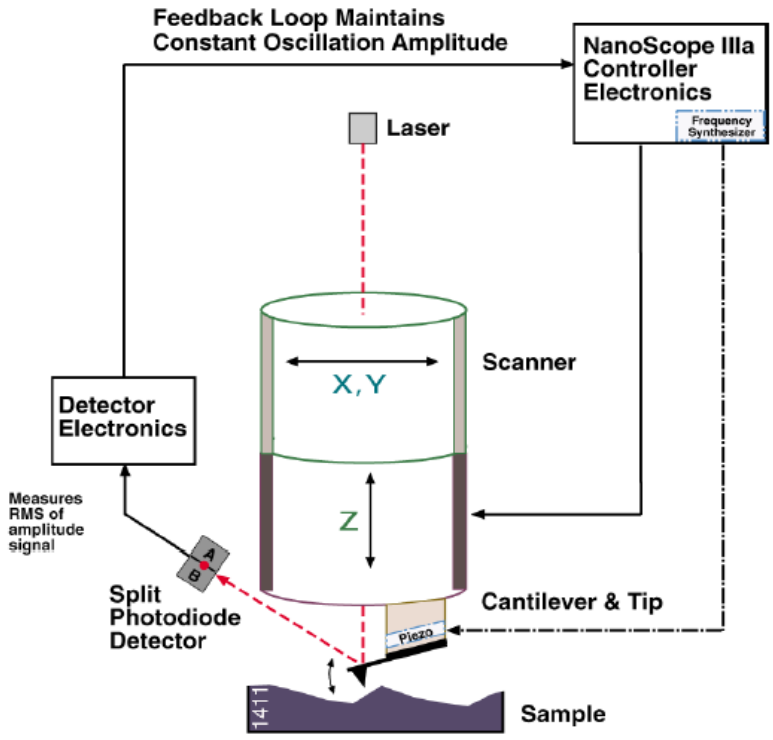

Figure 3-9: Schematic diagram of contact mode scanning probe.[103]

The AFM contact mode has the advantage of a high-speed scanning and the ability to scan samples that are rough and possess immense changes in vertical topography. However, the major disadvantage of the contact mode AFM is that the probe tip can easily damage when it accidentally touches sample surface.[103]

3.12.1.1 AFM Probes

The probes used in this research are made up of silicon cantilever which has a sharp silicon nitride tip integrated to its end. Contact mode AFM requires a cantilever which is soft enough to be deflected by minute forces and possess a high resonant frequency to avoid susceptibility to vibrations. This intrinsic cantilever property is achieved by making it short to provide a resonant frequency that is high and making the cantilever thin, which confers on it a small force constant. The silicon nitride probe has four cantilevers possessing different geometries attached to it, yielding four differing spring constants.

The AFM (NanoScope IIIa Multimode) instrument used in this research is kept on an antivibration platform to reduce vibrational noise interference.

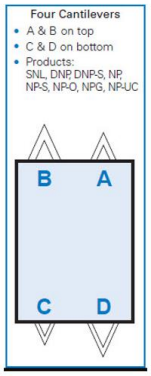

Figure 3-10: Diagram of DNP-10 probe cantilever layouts.[103]

3.12.2 X-ray Photoelectron Spectroscopy

Analysis by X-ray photoelectron spectroscopy was performed at the Sheffield Surface Analysis Centre (SSAC), using a Kratos Supra/Ultra X-ray photoelectron spectrometer equipped with a monochromatic Al X-ray source and a delay-line detector.

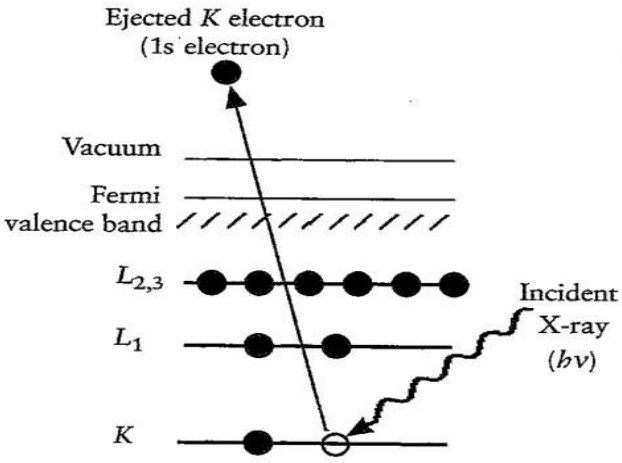

Figure 3-11: XPS Image Showing Ejected Electron from Surface of Core Shell

The operation of this instrument is enabled by the photoelectric effect on surfaces. The sample is irradiated with X-rays (Usually Al X-rays). This causes electrons to be ejected from the core shell orbitals. Excess energy from the X-ray photon gives the photoelectron kinetic energy. Since the energy and the number of incoming photoelectrons is known from the measurements on the detector, then the binding energy of the electron can be calculated:[107]

$$E_{Binding} = E_{Photon} - (E_{Kinetic} + \phi) \qquad \text{..... (3.7)}$$

The work function ϕ is typically about a few eV. It is the energy barrier that photoelectrons must overcome to be emitted and reach the detector. The binding energy is characteristic of the orbital electron and is indicative of the nature of bond leading to the analysis of the surface of the sample material.

The X-ray source operates at 15 KV (voltage) with a filament current of 15 mA. Surface charge is neutralized using a filament that ejected low energy electrons. With the utilization of ion pumps, an ultra-high vacuum is achieved. Survey spectra and core level pass energies were set at 160 eV and 20 eV respectively.

Survey scans collected at 1 eV resolution between 1200 – 0 eV with one 300 sec sweep. High resolution scans were collected at 0.1 eV energy resolution over an appropriate energy range. Typically, one 300 sec sweep was collected for C1s, O1s, Si2p and Br3d spectrum and two 300 sec sweeps for N1s and S2p. The Br3d spectrum was always collected first because of the risk of debromination.

The analysis of the data acquired was achieved by CASA XPS software, which was calibrated to C1s (285.0 eV). Baseline fitting was achieved through a Shirley background and Gaussian-Lorentzian peaks were used to fit the line shapes.

CHAPTER 4: POLYMERIZATION KINETICS OF POEGMA AND PCYSMA BRUSHES

4.1 Introduction

The emergence of ATRP in recent years as a highly fruitful synthetic tool for the preparation of polymers with controlled molecular weights, has facilitated the assemblage of an array of synthetic polymeric structures. The ability to propagate and execute controlled reactions of these polymers with desirable outcome is crucial for the design of microsystems via ATRP. ATRP is essentially a unique reaction path that deploys a transition metal complex capable of existing in two varying oxidation states.[143,144] This initiates the interaction of an alkyl halide from an ATRP initiator with the complex possessing the lower oxidation state to produce an alkyl radical with the emergence of a halide coordinated complex metal carrying a higher oxidation state in a reversible reaction that could also regenerate the alkyl halide and the lower oxidation state metal complex.[123,127]

Polymerization occurs when the alkyl radical reacts with a monomer yielding a polymeric chain or a halogen terminated dormant state polymer which potentially could be reactivated again by a complex metal catalyst. This technique has engineered the evolution of polymers grown on surfaces forming a thick layer of brush-like structures referred to as polymer brushes.[145,146] The polymer brush structures thus formed, have since been found to be useful in the fabrication of nanostructured devises with probing capabilities.

A major distinguishing quality of polymer brushes revolves around their non biofouling nature. This has triggered a great deal of research aimed at surface modification with a

view towards polymer brush usage and control.[97,99,106] Biofouling essentially implies the spontaneous undesirable biomolecule adsorption on surfaces. To keep this issue in check, it is imperative to understand the factors that encourage biofouling. These could be the hydrophilic nature of the surface or its hydrophobicity.[59,118]

There are a few ways of achieving biofouling control. One of these is the coating of the surface with suitable polymer brushes. The Leggett group has achieved significant experience in the engineering of silicon surfaces by coating with polymer brushes via atom transfer radical polymerization (ATRP) as a means of conferring antibiofouling or other desirable properties on surfaces.[60,84,147]

The achievement and control of surfaces with polymer brushes have been extensively accomplished via monolayer deposition of polar organic molecules.[59,60,148] Self-assembled monolayers are essentially an aggregation of chains of smaller molecules which are formed by the spontaneous adsorption of active surfactants from an organic solvent onto suitable substrate's surfaces.[61,63,149] These one-molecule layer thick array of ordered organic materials can be absorbed onto a surface either in their solution or gaseous phases in readiness for polymer brush ATRP.[61,62,64,150]

This work seeks to illustrates the ability to grow polymer brushes as tools deployed for the functionalization and control of silicon surface. It aims to establish reliable and optimum procedures for growing desirable polymer brush thickness from different functionalized surfaces with greater ease of repeatability.

In this work, our goal is to develop microsystems that enable the *in-situ* measurement of membrane transport process. The basic concept is the formation of compartmentalized

regions (''corrals'') made up of polymer brushes serving as confined structures housing integral sensors, as well as accommodating supported lipid bilayers that contain integral transmembrane proteins. The microsystems are to be designed in such a way that they incorporate reporters for the *in-situ* measurements of membrane transport. Silane films of 3-(2-bromoisobutyramido) propyltriethoxysilane (BIBB-APTES) and 4-(chloromethylphenyl) trichlorosilane (CMPTS) initiator monolayers were deployed to achieve significant functionalization and control of various silicon surface chemistry. The formation of these self-assembled monolayers on surfaces is to usher in a uniform optimal condition for surface modification via polymer brush growth.

The reaction process leading to the formation of these organosilane films on silicon surfaces is thought to have evolved through the hydrolysis of their head group forming cross-linked structures with each other before being adsorbed onto the hydrated silicon surface in a condensation reaction.

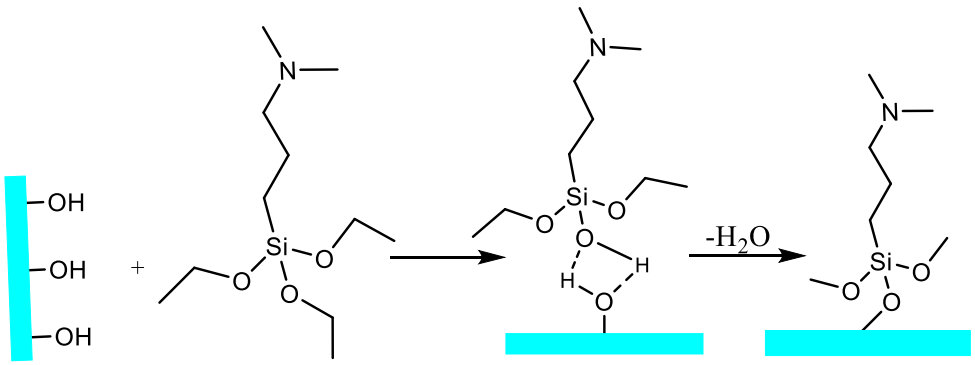

Figure 4-1: Reaction Showing Formation of Monolayer on Hydrated Silicon Surface

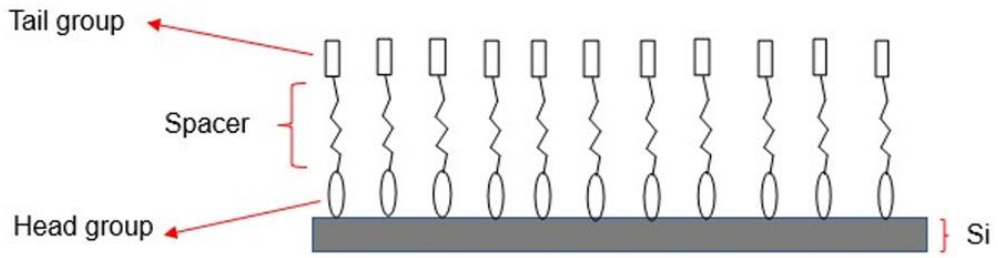

Figure 4-2: Diagram of Self Assembled Monolayer Molecules on the Surface of Silicon

4.2 Experimental Method

4.2.1 Materials

Analytical reagent grade 2-bromoisobutyrylbromide (BIBB) 98% purity, triethylamine (TEA) 99% purity, 3-aminopropyltriethoxysilane (APTES) 98% purity, 2,2-bipyridyl 99% purity were supplied by Sigma Aldrich (Gillingham, UK). 4-(chloromethylphenyl)trichlorosilane was supplied by Alfa-Aesar (Lancashire, UK). Other HPLC grade chemicals were obtained from Fisher Scientific (Loughborough, UK). These included: ethanol, isopropyl alcohol, dichloromethane, hydrogen peroxide, acetone, toluene, methanol, and ethyl acetate. De-ionized water was obtained from an Elgar purification unit (Elgar, pure nanopore 16 MΩ).

4.2.2 Preparation of BIBB-APTES Layer

Piranha-cleaned silicon substrates were immersed in a solution of 2% 3-aminopropyltriethoxysilane in ethanol for 30 min at 20^{o}C. The silicon substrate was rinsed with ethanol and dried under a stream of nitrogen gas, followed by subsequent annealing at 120^{o}C for 30 min in a vacuum oven.

The annealed APTES coated substrates were immersed in clean glass tubes containing a solution of 2-bromoisobutyrylbromide (0.37 mL, 3 mmol) and triethylamine (0.41 mL, 3

mmol) dissolved in 60 mL of dichloromethane for 30 min at 20°C. The BIBB-APTES functionalized substrates were rinsed with dichloromethane and ethanol before drying in a stream of nitrogen gas prior to characterization.

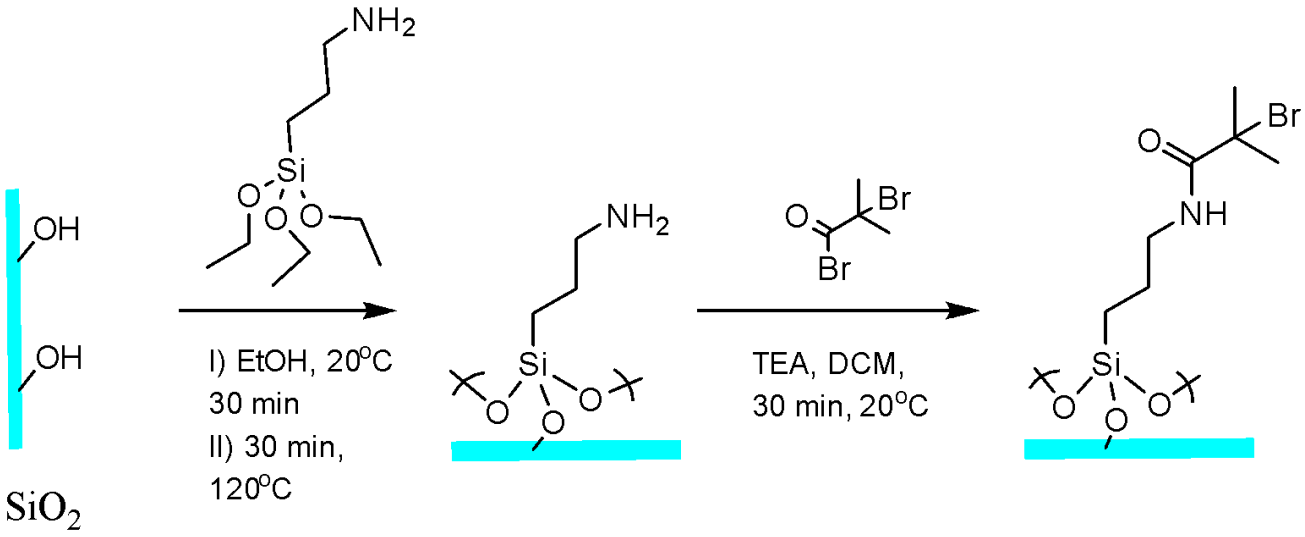

Figure 4-3: A representation of Formation of BIBB-APTES Layer

4.2.3 Preparation of 4-(Chloromethylphenyl)trichlorosilane (CMPTS) Layer

Clean silicon substrates were immersed in a solution of 100 µL of CMPTS in 30 mL of dry toluene contained within a carousel in a nitrogen atmosphere for 30 min at 20°C. The CMPTS functionalised substrate was retrieved and washed with a mixture of toluene and ethanol before drying under a stream of nitrogen gas. Samples were annealing for 30 min at 120°C in a vacuum oven prior to characterization.

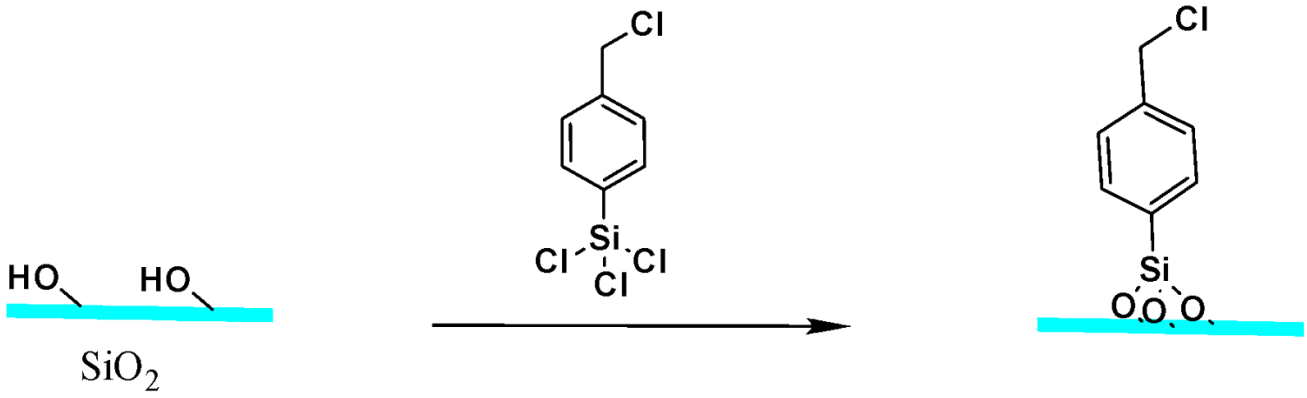

Figure 4-4: Schematic Representation of Formation of CMPTS Layer

4.2.4 Synthesis of Cysteine methacrylate monomer (CysMA)

L-cysteine (15.13 g, 124.88 mmol) was dissolved in 100 mL deionized water and 3-(acryloyloxy)-2-hydroxypropyl methacrylate (29.43 g, 137.36 mmol) was added. Catalyst dimethyl phenyl phosphine (20 µL, 1.47 x 10^{-1} mmol) was transferred into the aqueous solution which was constantly stirred at room temperature for 2 h with the help of a magnetic stirrer. The monomer formed was washed twice by dispersion in 50 mL of ethyl acetate. The organic phase was separated from the aqueous phase and discarded. Finally, a further phase separation step was carried out using dichloromethane (2 x 50 mL). CysMA was isolated and purified from the aqueous solution as a pure white solid by utilizing the freeze-drying technique.

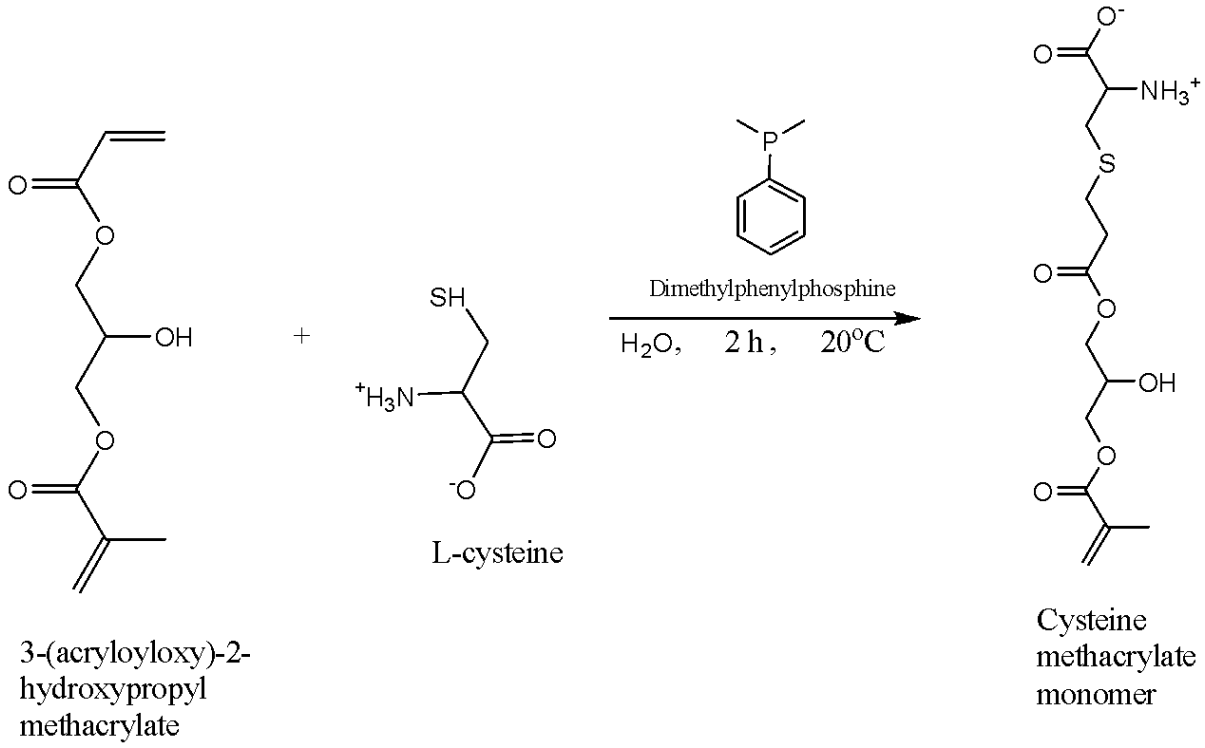

Figure 4-5: Schematic Representation of Synthesis of Cysteine Methacrylate Monomer

4.2.5 Preparation of Poly Cysteine methacrylate (PCysMA) Solution

0.75 g of cysteine methacrylate (CysMA) monomer was placed in a clean 50 mL capped glass tube. 4 mL of deionized water was added to the monomer and shaken to ensure proper dissolution of the CysMA monomer. To this solution, 0.18 mL of a solution 100.1 mg (0.1001 g) of ascorbic acid was dissolved in 10 mL deionized water. 38.8 mg (0,0388 g) of 2,2-bipyridyl was dissolved into 5 mL of ethanol contained in a 10 mL clean capped glass tube. To this was added a solution of 14.6 mg (0.0146 g) of $CuCl_2$ dissolved in 5 mL deionized water. 0.35 mL of this resulting solution was then added to the monomer solution.

The resulting mixture was shaken once only and allowed to settle without further agitation.

This final solution was used for ATRP.

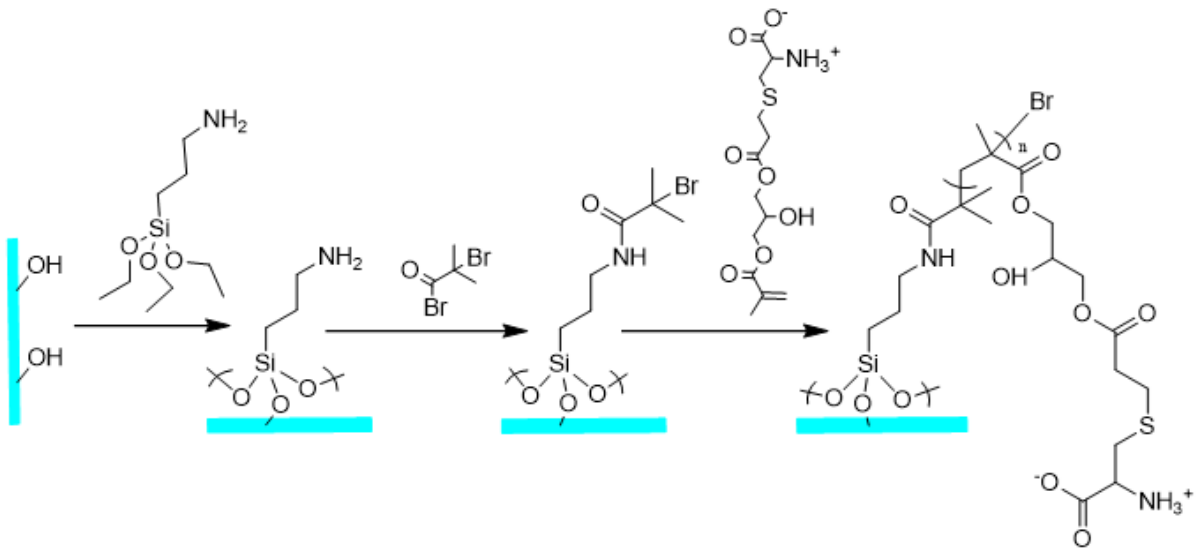

Figure 4-6: Schematic representation of reactions producing PCysMA on BIBB-APTES substrate

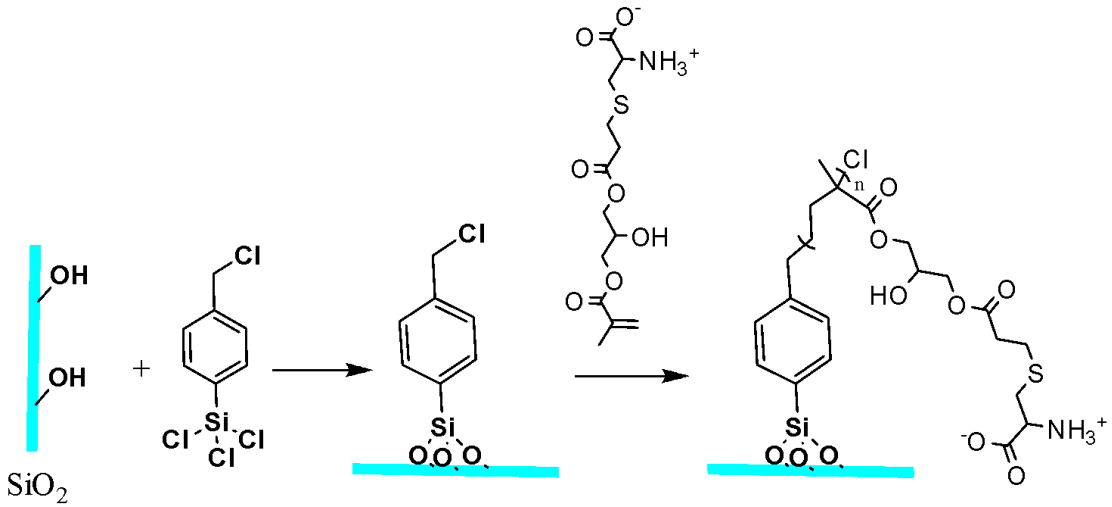

Figure 4-7: Schematic representation of reactions producing PCysMA brushes on CMPTS substrate

4.2.6 Preparation of Oligoethylene glycol methyl ether methacrylate (POEGMA) Solution

4.6 mL of Oligoethylene glycol methyl ether methacrylate (OEGMA) monomer was transferred into a clean suba-sealed 50 mL round bottom flask containing 11.2 mL of deionized water in a nitrogen atmosphere. 0.07g of 2,2-bipyridyl was added into the monomer solution along with 0.011g of copper (II) bromide and 0.023g of copper (I) bromide catalyst with adequate stirring of the reaction solution. This was added to an initiator-functionalized substrate placed inside a carousel tube in a nitrogen atmosphere. ATRP was carried out for the required polymerization time.

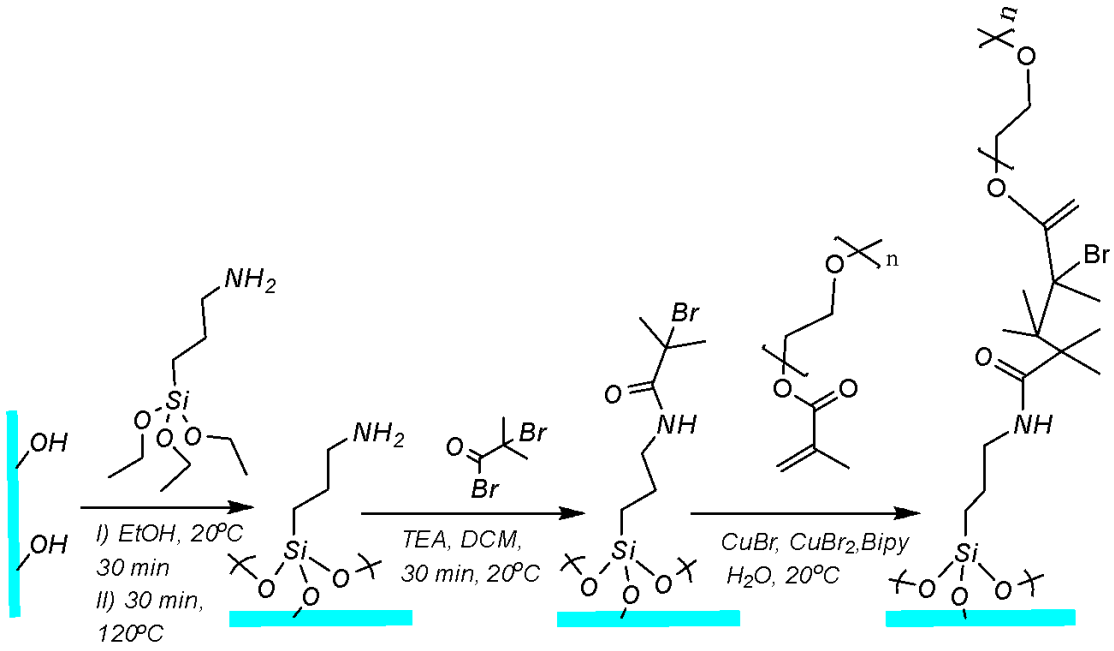

Figure 4-8: Schematic representation of reactions producing POEGMA brushes on BIBB-APTES Substrate

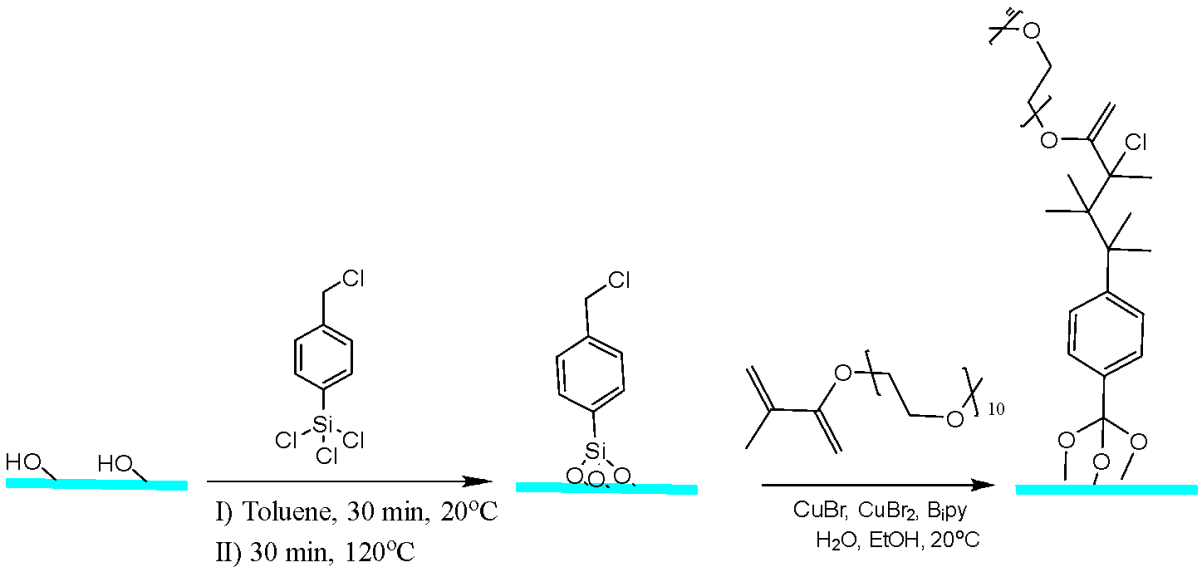

Figure 4-9: Schematic representation of reactions producing POEGMA brushes on CMPTS substrate

4.3 Surface Characterization

Advancing water contact angles of the functionalized surfaces were measured using a Rame-Hart model 100-00 goniometer via the sessile drop method. The quoted values are the means of at least three different measurements.

The thickness of the organosilane film was measured by spectroscopic ellipsometry using an M-2000V Ellipsometer (J.A Woollam Co. inc). The Complete Ease software was used to analyse the data. The mean thickness for each sample was determined from at least three different measurements.

Topographic roughness of the surface was measured in triplicate from Tapping Mode AFM images acquired using a Bruker Nanoscope (v) Multimode Atomic Force Microscope (Bruker. Coventry, UK).

X-ray photoelectron spectroscopy was performed using an Axis Ultra/Supra DLD X-ray Photoelectron spectroscopy (Manchester, UK). Data were analysed using Casa XPS software.

4.4 Results and Discussion

4.4.1 Water contact Angle Characterization of Self-Assembled Monolayers

Silicon substrates functionalized with APTES were immersed in a solution of BIBB triethylamine as a base to produce BIBB-APTES functionalized substrates (as described in figures 2-10 and 4-3). Contact angles were measured for glass and silicon slides coated with APTES monolayer and BIBB-APTES initiator layers. The measurements are shown in Table 4-1 below. Contact angles of 56 ± 4^{o} and 47 ± 3^{o} were measured for glass and silicon substrates, respectively, after adsorption of APTES. These contact angles increased to 61 ± 2^{o} and 58 ± 1^{o} for glass and silicon, respectively, after reaction with BIBB. These data are consistent with a previous report which showed a contact angle record of up to 60^{o} for BIBB-APTES layer and about 50^{o} for APTES layer. A contact angle value of less than 12^{o} was measured for hydroxyl terminated piranha clean substrates.

Table 4-1: Water Contact Angle of APTES, BIBB-APTES, and Piranha Cleaned Silicon Surfaces

Surface	C.A (θ) Glass	C.A (θ) Silicon	Cos (θ) Glass	Cos (θ) Silicon
Piranha Cleaned	9.0 ± 0.7^{o}	12.0 ± 1.1^{o}	1.0	1.0
APTES	56.0 ± 3.6^{o}	47.0 ± 2.8^{o}	0.6	0.7
BIBB-APTES	61.0 ± 2.3^{o}	58.0 ± 0.9^{o}	0.5	0.5

Table 4-2: Ellipsometry Thickness of BIBB-APTES on Glass and Silicon

Sample ID	Average Ellipsometric Thickness
BIBB-APTES on Glass	1.29 ± 0.07 nm
BIBB-APTES on Silicon	1.10 ± 0.21 nm

4.4.2 Spectroscopic Ellipsometry

Ellipsometric data were obtained from modelling two components of native oxide and Cauchy layers revealed an average ellipsometric thickness for BIBB/APTES on Glass as 1.29±0.07 nm while the average ellipsometric thickness of BIBB/APTES on Silicon showed a measured value of 1.10±0.21 nm. This is indicative of an initiator layer deposition on clean substrate as outlined in previous reports.

4.4.3 AFM Surface Roughness for BIBB-APTES

The topographies of BIBB-APTES films were characterized by Tapping Mode AFM. Figure 4-10 shows a representative height image. The surface morphology is smooth. The roughness was characterised by determining the root mean square roughness which is equivalent to 0.15 ± 0.03 nm layer of BIBB-APTES initiator film on substrate.

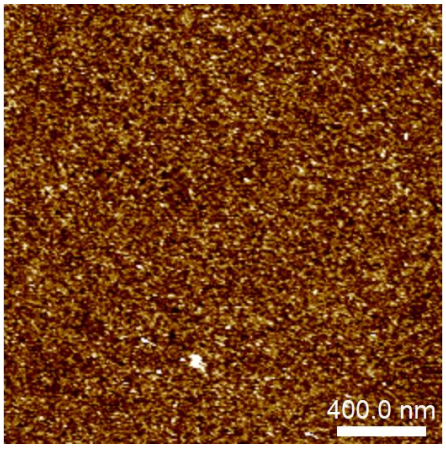

Figure 4-10: Surface Roughness for BIBB-APTES on Si-Substrate ‘’z scale 0 to 1.02 nm’’

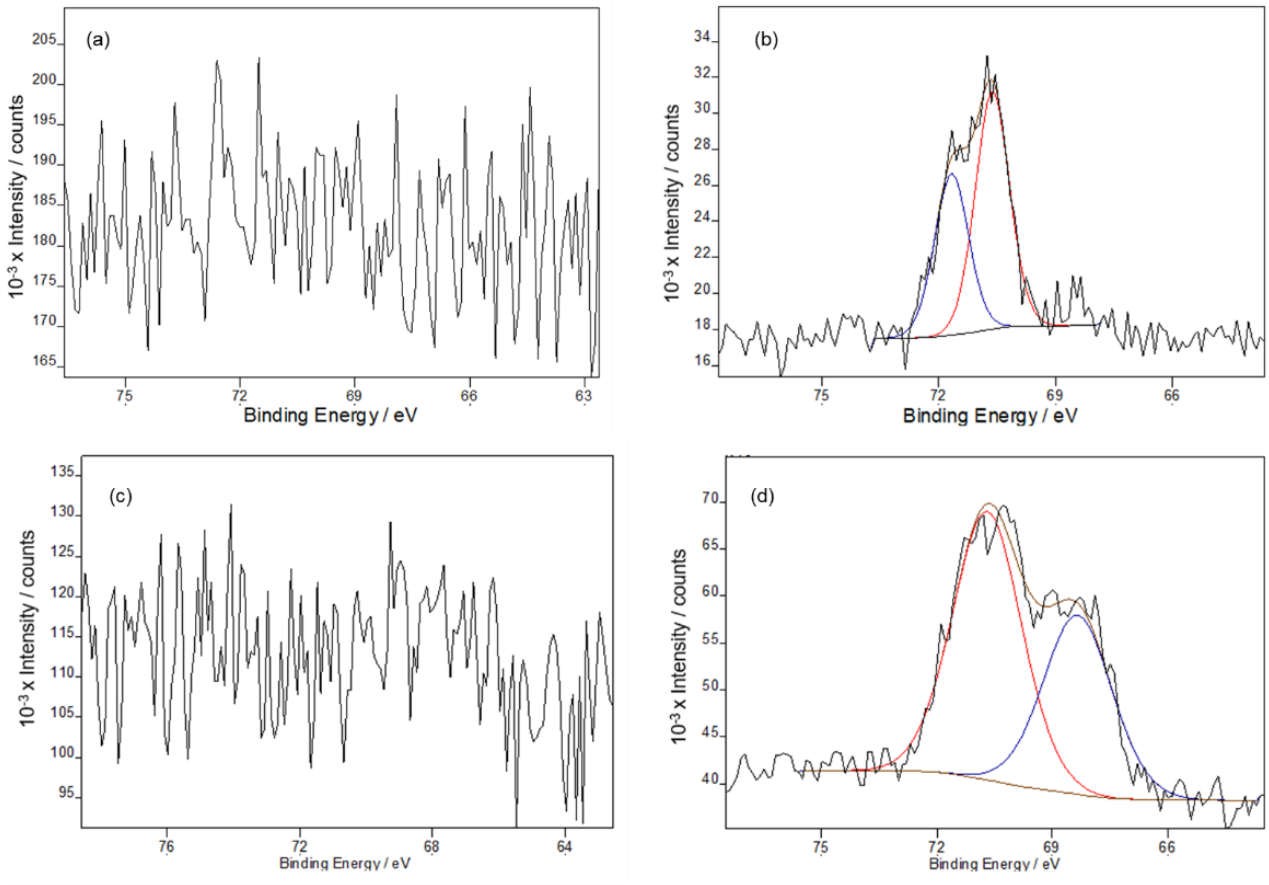

Figure 4-11: XPS Spectra of (a) Cleaned Glass, (b) BIBB-APTES Br3d Peak on Glass (c) Cleaned Silicon and (d) BIBB-APTES Br3d Peak on Silicon

Table 4-3: XPS High Resolution Spectra Showing % Atomic Compositions of BIBB-APTES layer on Substrates

Sample ID	Br3d	O1s	N1s	C1s	S2p	Si2p
Cleaned Glass	0.0	65.8	0.0	6.1	0.0	28.1
Cleaned Silicon	0.0	27.1	0.0	4.5	0.0	68.4
BIBB-APTES Glass	1.7	47.1	2.5	21.3	0.0	27.5
BIBB-APTES Silicon	0.3	32.5	3.2	25.5	0.0	38.4

The chemical composition of the BIBB-APTES layers was analysed using XPS. High resolution spectra. Three components were used for fitting the C1s spectrum at binding energies of 285 eV, 286 eV and 289 eV, attributed to C-C, C-N/C-Br and O=C, respectively. The experimental ratios of 4.5 : 2.1 : 1, were in agreement with the theoretical ratios of 4 : 2 : 1. The high resolution spectrum of Br3d was fitted using two components having relative intensities in the ratio of 1 : 1.5, corresponding to the Br3d3/2 and Br3d5/2 components, attributed to spin orbit coupling with binding energies of 71 eV and 70 eV, respectively. The atomic ratio of Br/N was 2 : 1 suggesting that about 80% of surface amine groups of APTES had effectively coupled with 2-bromoisobutyryl bromide, producing a dense BIBB-APTES layer.

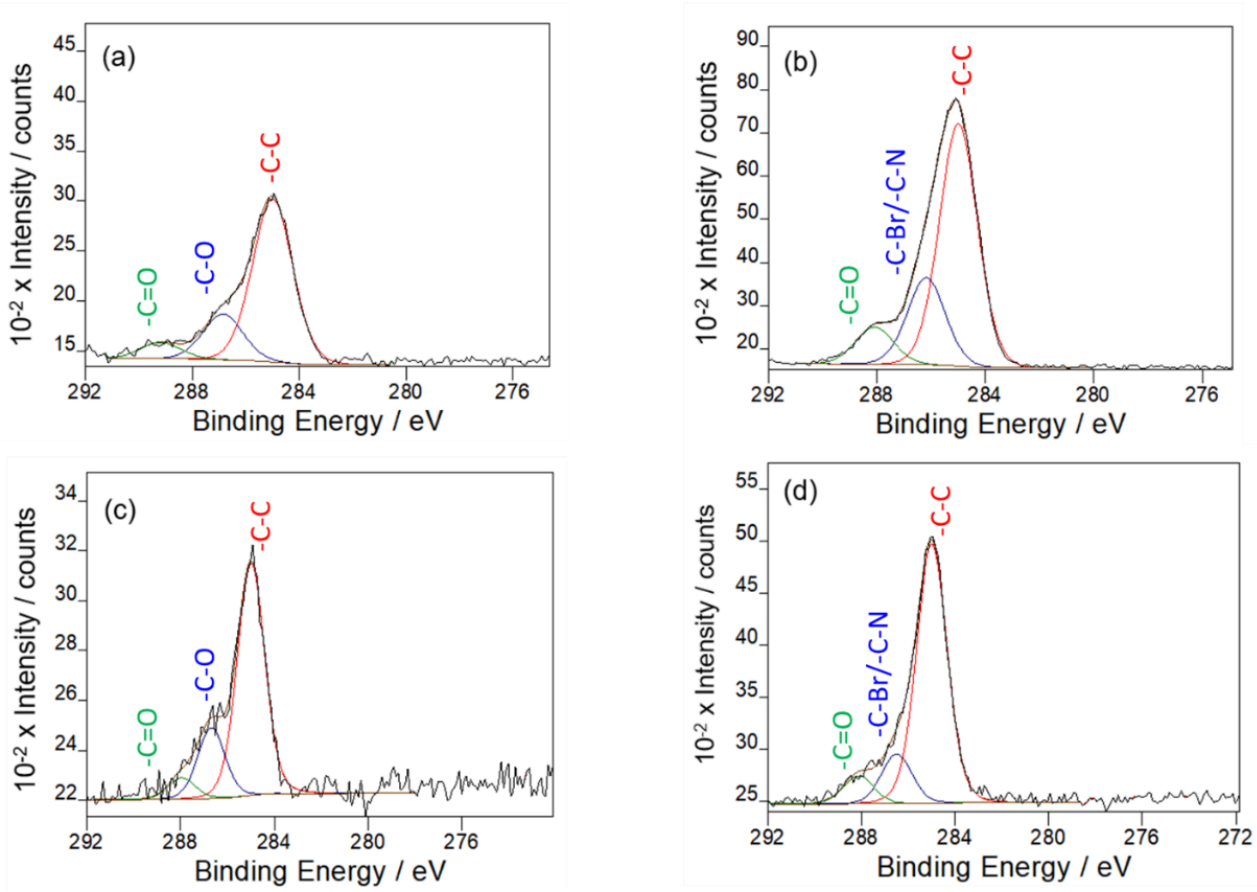

Figure 4-12: Figure 4 11: XPS C1s Spectra of (a) Cleaned Glass, (b) BIBB-APTES on Glass (c) Cleaned Silicon and (d) BIBB-APTES on Silicon

Table 4-4: Water Contact Angle of CMPTS and Piranha Cleaned Silicon Surfaces

Surface	C.A (degree) Glass	C.A (degree) Silicon	Cos (θ) Glass	Cos (θ) Glass
Piranha Cleaned	9.0 ± 0.7^{o}	12.0 ± 1.1^{o}	1.0	1.0
CMPTS	71.0 ± 2.1^{o}	73.0 ± 1.8^{o}	0.3	0.3

Table 4-5: Ellipsometric Thickness of CMPTS on Glass and Silicon

Sample ID	Average Ellipsometric Thickness
CMPTS on Glass	0.87 ± 0.18 nm
CMPTS on Silicon	0.87 ± 0.14 nm

Ellipsometric data acquired and modelled as Cauchy layers containing the native oxide modelling indicated that the mean thickness of CMPTS on Glass was 0.87 ± 0.18 nm, while the average thickness of CMPTS on Silicon was 0.87 ± 0.14 nm. This is consistent with initiator layer deposition on clean substrate as outlined in previous reports.

4.4.4 AFM Surface Roughness for CMPTS

The topographies of the chlorine initiator-terminated films were characterized by AFM. Figure 4-13 shows AFM images of CMPTS. The surface roughness was analysed by determining the root mean square roughness which is equivalent to 0.15 ± 0.02 nm layer of CMPTS initiator film on substrate.

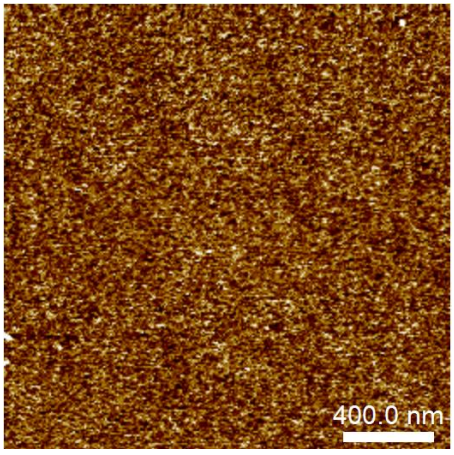

Figure 4-13: AFM CMPTS Surface Roughness ‘’z scale 0 to 1.05 nm‘’

The chemical composition of the CMPTS layers on substrates was analysed using XPS high resolution spectra. Two components were used for fitting the C1s peak, at binding energies of 285.0 eV and 286.0 eV, which represented C-C, and C-Cl respectively. The peak area ratio of 7 : 1 was in good agreement with theoretical ratio. Cl2p peak displayed a doublet due to Spin-orbit coupling, with an area ratio of 7 : 1 corresponding to Cl2p1/2 and Cl2p3/2 at binding energies of 200 eV and 199 eV respectively.

Table 4-6: XPS High RESOLUTION Spectra Showing % Atomic Compositions of CMPTS layer on Substrates

Sample ID	Cl2p	O1s	N1s	C1s	S2p	Si2p
Cleaned Glass	0.0	65.8	0.0	6.1	0.0	28.1
Cleaned Silicon	0.0	27.1	0.0	4.5	0.0	68.4
CMPTS Glass	1.3	59.2	0.0	13.7	0.0	25.8
CMPTS Silicon	0.9	55.3	0.0	12.0	0.0	31.7

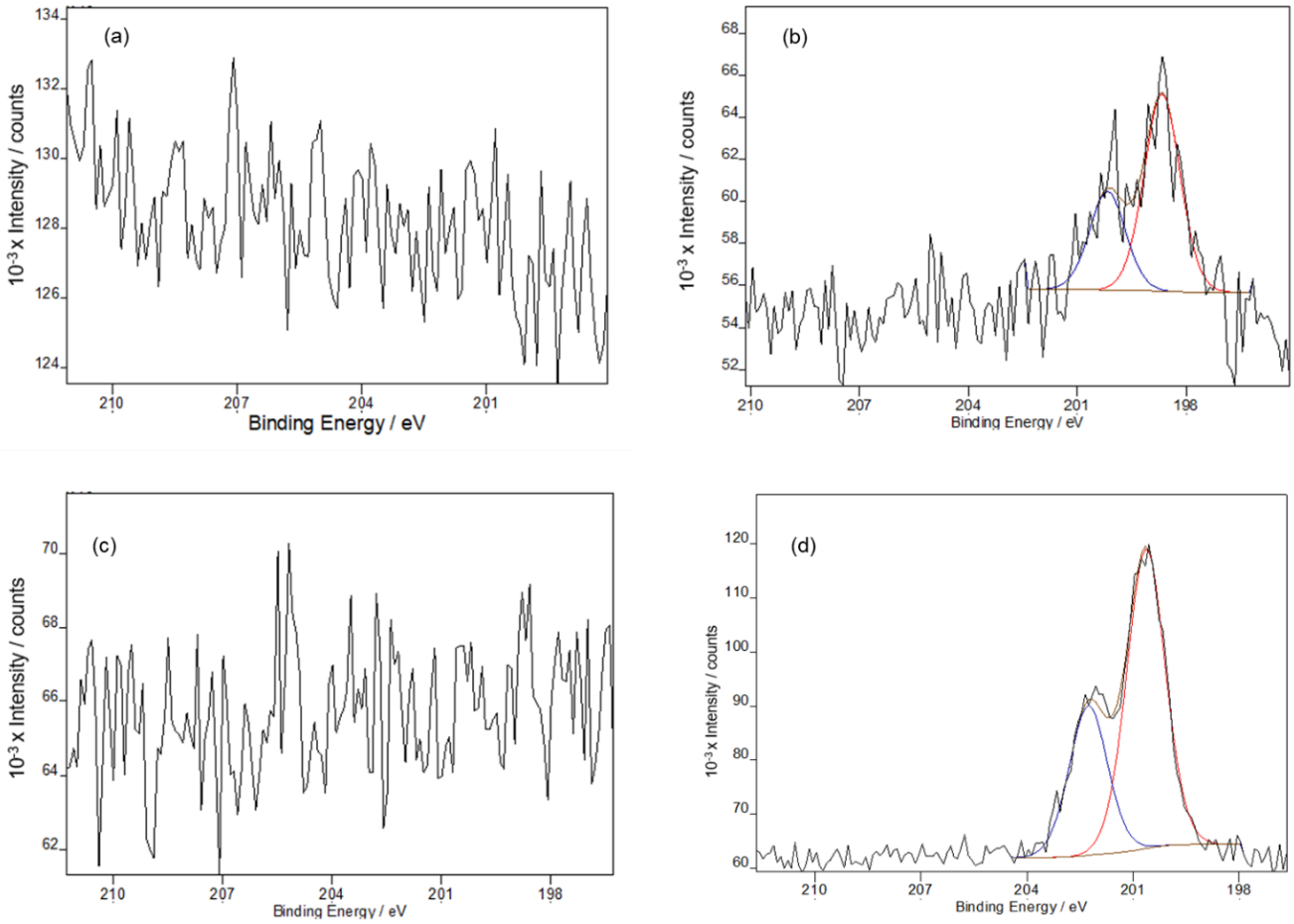

Figure 4-14: XPS Spectra of (a) Cleaned Glass, (b) CMPTS Cl2p Peak on Glass (c) Cleaned Silicon and (d) CMPTS Cl2p Peak on Silicon

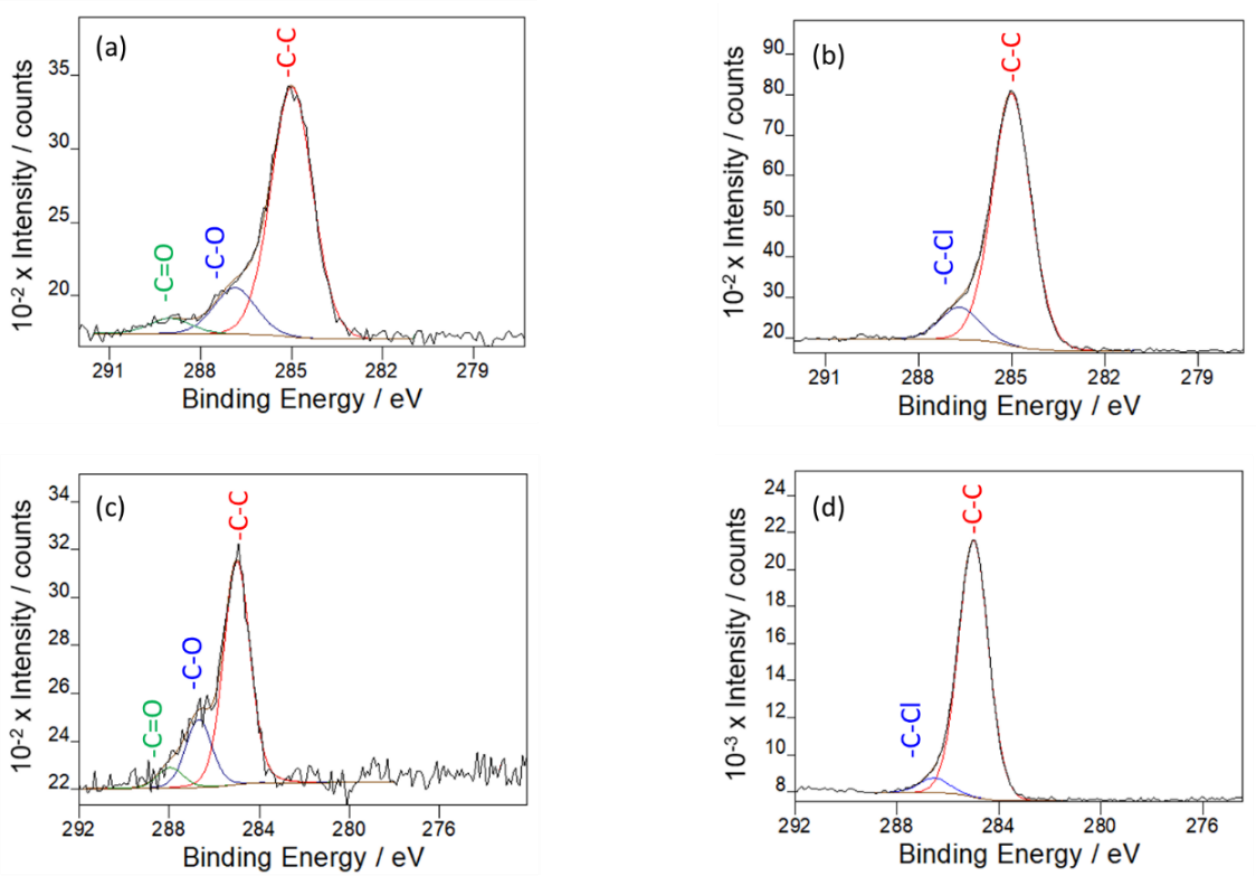

Figure 4-15: XPS C1s Spectra of (a) Cleaned Glass, (b) CMPTS on Glass (c) Cleaned Silicon and (d) CMPTS on Silicon

4.4.5 CysMA Monomer Synthesis

The monomer was prepared as described in the experimental section and a yield of 94%, was achieved. The product analysis has as follows:

^{1}H-NMR (400.13 MHz, D_2O, 298 K) δ (ppm): 1.89 (s, 3H, -CH_3); 2.68 – 3.17 (m, 6H, -S-CH_2-CH_2-COO-, -S-CH_2-CH(COO^-)NH_3^+); 3.79 (m, 1H, CHOH); 3.90 (m, 1H, -CH(COO^-)NH_3^+); 4.20 – 4.30 (m, 4H, -CH_2-CHOH-CH_2-); 5.70 (s, 1H, Vinyl); 6.13 (s, 1H, Vinyl). The result from the ^{1}H-NMR spectra of CysMA monomer analyzed, showed that the spectral

peak data obtained agree with the spectral peaks expected as shown in the work of Alswieleh et al[108].

^{13}C-NMR (400.13 MHz, D_2O, 298 K) δ (ppm): 17.31 (-CH_3); 26.29 (-S-CH_2-CH_2-); 32.08 (-S-CH_2-); 33.86 (-S-CH_2-CH_2-); 53.49 (-CH_2-CHOH-CH_2-); 65.17, 65.27 (2C, -CHOH-CH_2-); 66.83 (-CH(COO^-) NH_3^+); 127.13, 135.50 (2C, Vinyl); 172.76, 174.10 (3C, Carbonyl). The result from the ^{13}C-NMR spectra of CysMA monomer analyzed, showed that the spectral peak data obtained agree with the spectral peaks expected as shown in the work of Alswieleh et al[108].

Mass Spectrometry

($M+H^+$): Relative molecular mass of the product was calculated to be 336.39 amu, while it was found from Mass Spectrometric data to be 336.1 amu. The correlation shown by the two atomic masses indicate that the monomer obtained is CysMA monomer. The result from the Mass spectrum of CysMA monomer analyzed shows that the spectral peak data obtained agree with the spectral peaks expected as shown in the work of Alswieleh et al[108].

4.4.6 ATRP of PCysMA Brushes on BIBB-APTES Films

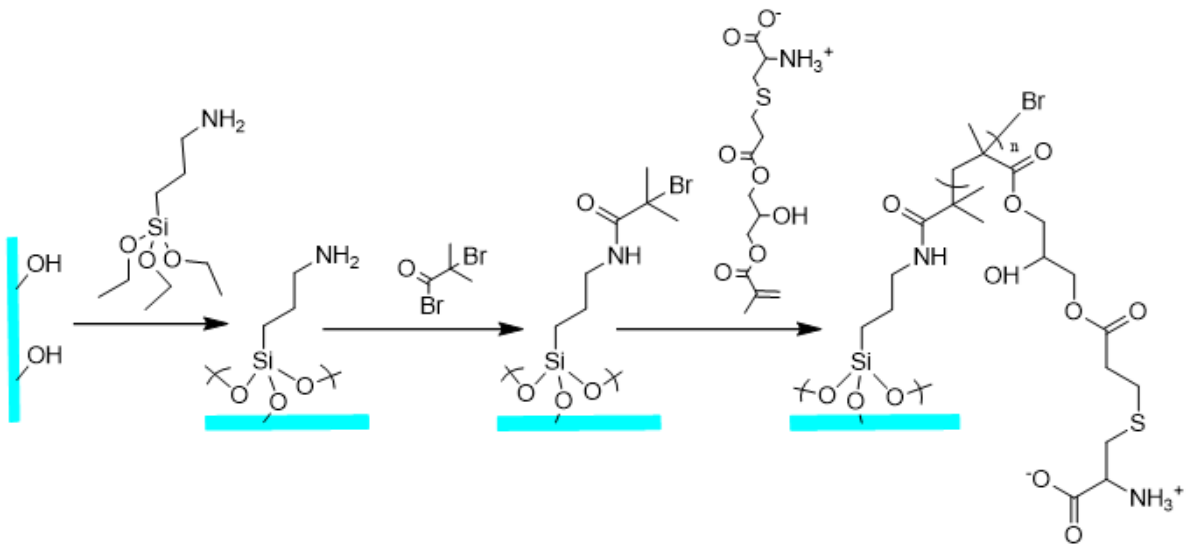

Figure 4-16: Schematic representation of reactions producing PCysMA on BIBB-APTES substrate

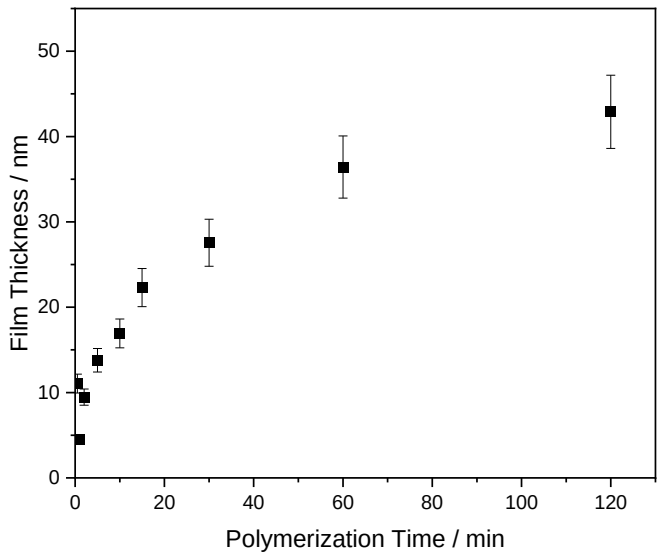

Figure 4-17: Growth of Film Thickness with Polymerization Time for PCysMA Brushes Grown by ATRP from BIBB-APTES Initiator Functionalized Surfaces

Atom Transfer Radical Polymerization (ATRP) of CysMA monomer was done on BIBB-APTES functionalized surface. The film thickness was measured as a function of the polymerization time using spectroscopic ellipsometry. The brush average thickness increased rapidly at first reaching 40 nm after 70 min. Subsequently, the rate of increase in film thickness slowed, with a thickness of 42 nm being reached after 120 min of polymerization time. Contact angles were measured for BIBB-APTES PCysMA brush films after a range of polymerization times. The values changed very little, from 49.0 ± 0.3^{o} at 10 min, to 51.0 ± 0.2^{o} at 160 min of polymerization time.

Table 4-7: Contact Angle Data of PCysMA Brush Surfaces on BIBB-APTES at Different Polymerization Time

BIBB-APTES PCysMA Polymerization Time (min)	Contact Angle (θ)	Cos (θ)
0	61.0 ± 2.3^{o}	0.50
10	49.0 ± 0.3^{o}	0.66
20	51.0 ± 0.8^{o}	0.63
40	46.0 ± 0.5^{o}	0.69
80	44.0 ± 0.4^{o}	0.71
160	51.0 ± 0.2^{o}	0.63

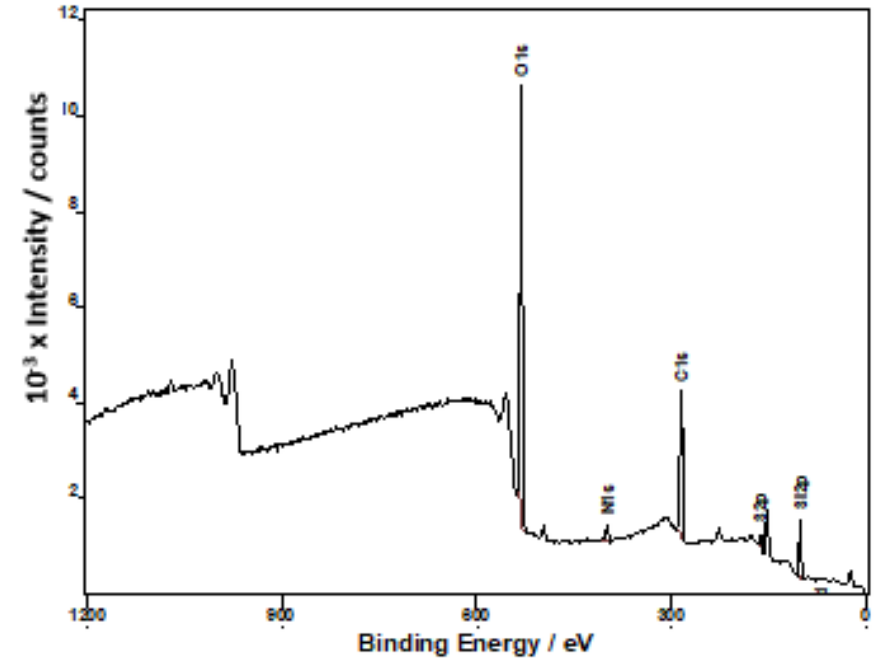

Figure 4-18: XPS Survey Scan of BIBB-APTES Initiator on Si Substrate

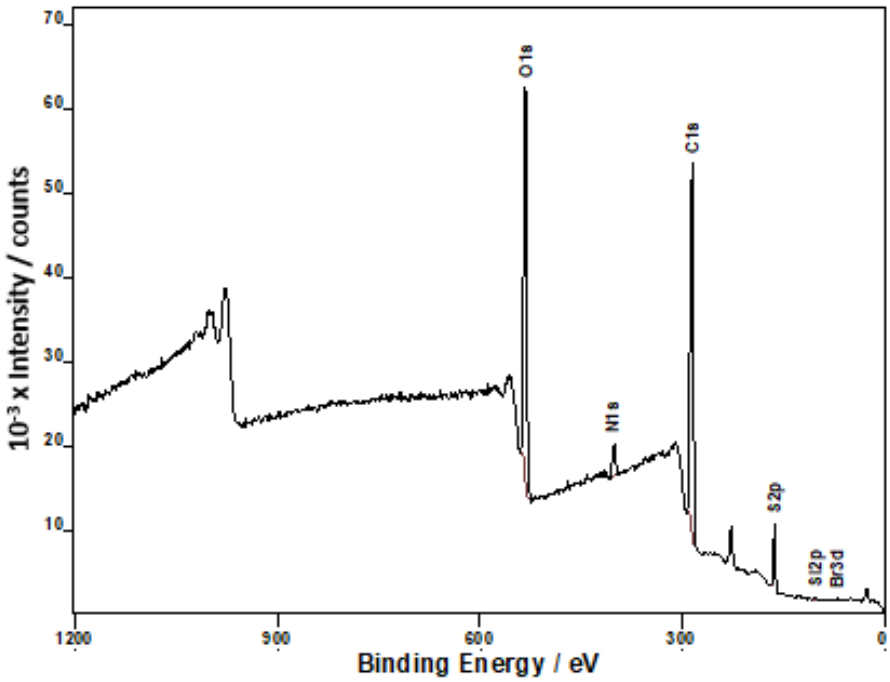

Figure 4-19: XPS Survey Scan of BIBB-APTES PCysMA Brushes on Si Substrate at 120 min Polymerization Time

Table 4-8: XPS Atomic Compositional Percent Data of PCysMA Polymerization on BIBB-APTES Substrate

Sample ID	Br2d	O1s	N1s	C1s	S2p	Si2p
Clean Silicon	0.00	27.13	0.00	4.52	0.00	68.35
APTES	0.00	22.24	0.75	14.93	0.00	62.10
BIBB-APTES	0.57	22.52	0.91	13.99	0.00	62.00
BIBB PCysMA 1 min	0.16	22.21	1.78	32.73	0.00	43.11
BIBB PCysMA 2 min	0.07	22.13	2.21	53.22	0.00	22.38
BIBB PCysMA 5 min	0.00	25.55	2.73	59.29	3.43	9.00
BIBB PCysMA 10 min	0.00	27.09	2.86	62.31	3.91	3.83
BIBB PCysMA 15 min	0.00	26.92	3.11	64.58	4.7	0.70
BIBB PCysMA 30 min	0.00	27.82	3.15	63.84	4.91	0.27
BIBB PCysMA 60 min	0.00	27.51	3.29	63.91	4.8	0.49
BIBB PCysMA 120 min	0.00	26.65	3.10	65.25	4.75	0.25

PCysMA brush grown from BIBB-APTES films were analysed by XPS (Figure 4-18 and Table 4-8). In the wide scan of BIBB-APTES a strong peak was observed at 530 eV corresponding to O1s. However, C1s peak at 285 eV (Figure 4-18) was weaker with an area about a third of the O1s peak because the thin BIBB-APTES layer occupied a small fraction of the XPS sampling depth. A strong Si2p peak was detected originating from the silicon substrate. Similarly, Br3d and N1s peaks at 69 eV and 400 eV respectively appeared as traces of less than $1x10^{-3}$ intensity/counts due to their low prevalence ratio in the thin layer of BIBB-APTES initiator.

After growth of a PCysMA brush from BIBB-APTES, the Si2p is reduced as observed in figure 4-18. Even after just 5 min polymerisation, the Si2p concentration is reduced from 62 atomic % to 9 atomic %, and in15 min is less than 1 atomic %. The decline in the Si peak intensity results from the increasing thickness of the polymer overlayer, which attenuates the photoelectron intensity. Br3d remains largely undetected for polymer brush samples. A very small Br3d peak is observed for 1 min and 2 min polymerisation, but it is undetectable at longer times. As polymerisation progresses, there are terminations of the chain ends, so the Br concentration in the brush layer is expected to decline with time.

4.4.7 ATRP of PCysMA brushes on CMPTS Films

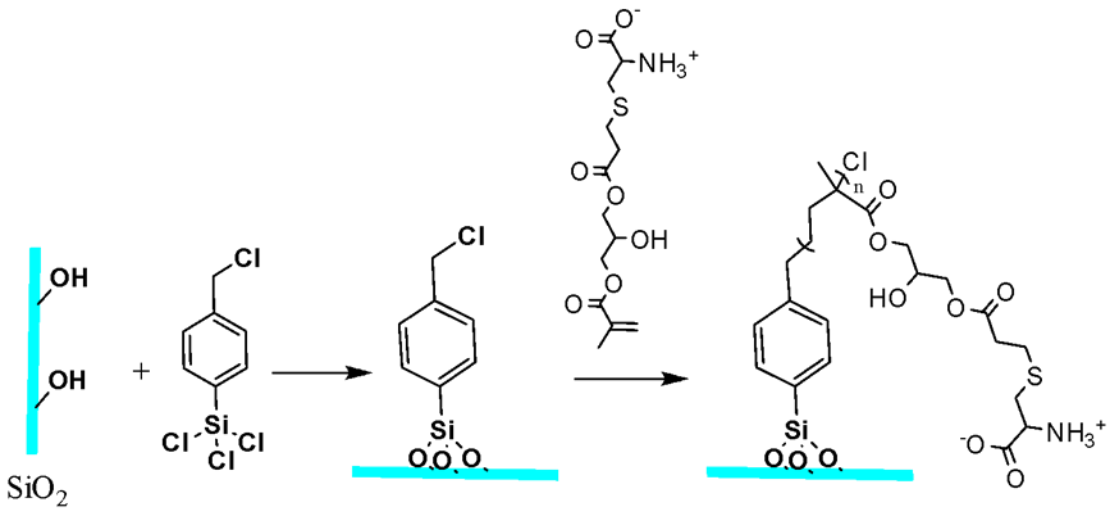

Figure 4-20: Schematic representation of reactions producing PCysMA brushes on CMPTS substrate

Figure 4-21 shows the increase in PCysMA films thickness as a function of polymerization time for brushes grown by ATRP from CMPTS films. Table 4-9 below displayed a set data for contact angle measurements at different polymerization times for PCysMA brushes on CMPTS surfaces. The values ranged from 50 ± 0.61º at 10min to 51 ± 0.74º at 40min

all through to 160 min of polymerization, which showed a contact angle of 48 ± 0.87°. These values do not show significant changes as the polymerization time progressed.

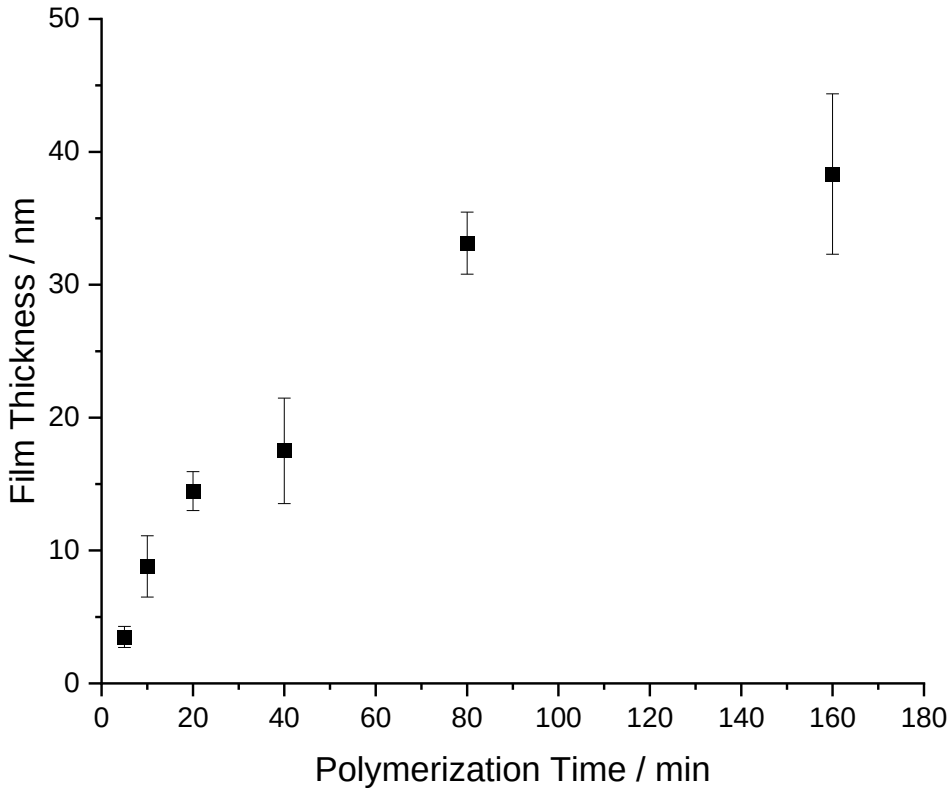

Figure 4-21: Spectroscopic Ellipsometry Measurements of CMPTS PCysMA Brush Thickness (Recipe details: CysMA : Bpy : Asco : Cu(II)Cl 51 : 2.7 : 7 : 1)

Table 4-9: Contact Angle Data of PCysMA Brush Surfaces on CMPTS at different Polymerization time

CMPTS PCysMA Polymerization (min)	Contact Angle (θ)	Cos (θ)
0	73.0 ± 1.8°	0.30
10	50.0 ± 0.6°	0.76
20	43.0 ± 0.5°	0.73

40	51.0 ± 0.7°	0.63
80	44.0 ± 0.6°	0.72
160	48.0 ± 0.9°	0.67

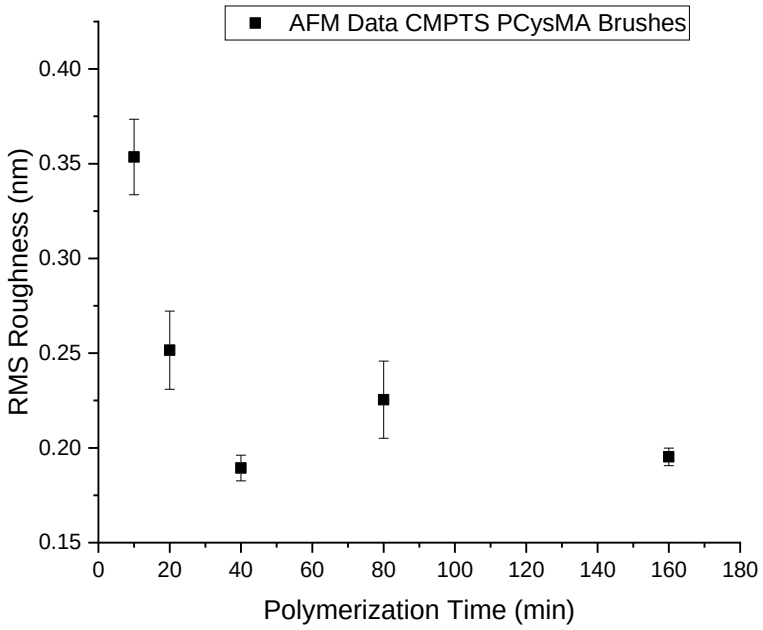

Figure 4-22: Dependence of the RMS roughness of PCysMA brushes grown from CMPTS films on the polymerization time

Figure 4-22 shows the variation in the RMS roughness of PCysMA brushes grown from CMPTS films on the polymerization time. After 10 min of growth, the RMS roughness is 0.35 nm, but this steadily declines to 0.20 nm at 160 min.

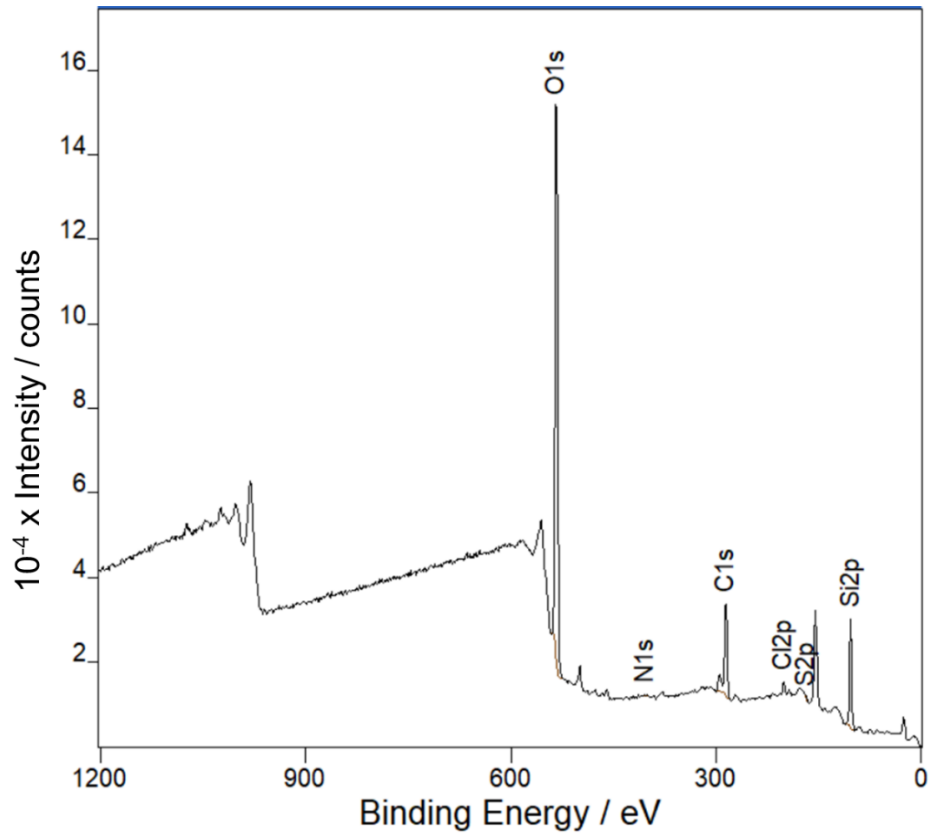

Figure 4-23: XPS Survey Scan of CMPTS Initiator on Si Substrate

XPS analysis were carried out to ascertain the chemical composition of the CMPTS and PCysMA brush surfaces. The results can be seen in the wide scan spectral peaks displayed in Figures 4-23 and 4-24. The CMPTS spectrum in Figure 4-23 showed a high intensity for O1s at about 530 eV, but no peak was seen for N1s at 400 eV. C1s showed a low intensity at 285 eV which a quarter compared to O1s. Unlike N1s spectral peak, which was absent, Cl2p can significantly be noted at 200 eV.

After ATRP a significant peak was observed for N1s at 400 eV, while the Cl2p peak disappeared as observed in figure 4-24. The intensity of the C1s peak was found to have

increased from about a quarter of the O1s peak to about three quarters of its intensity. As expected, the Si2p peak was found to be significantly reduced in intensity after ATRP. These changes in atomic compositions (percentage) are an indication that the CMPTS surfaces had been covered by PCysMA brushes.

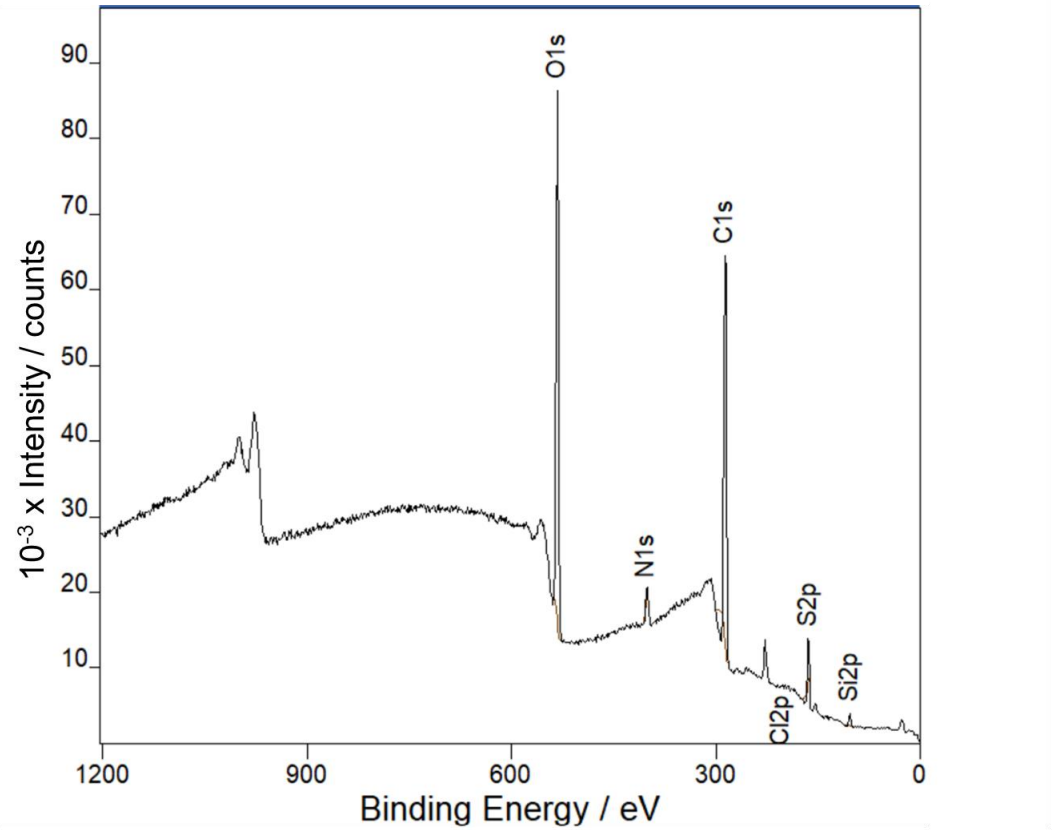

Figure 4-24: XPS Survey Scan of CMPTS PCysMA Brushes on Si substrate at 120 min Polymerization Time

Table 4-10: XPS Compositional Atomic Concentration (Percent) Data of PCysMA Polymerization on CMPTS Substrate

Sample ID	Cl2p	O1s	N1s	C1s	S2p	Si2p
Cleaned Glass	0.00	64.18	0.00	5.25	0.00	30.59
CMPTS	2.62	51.97	0.00	18.83	0.00	26.58
CMPTS PCysMA 2 min	0.89	34.38	2.20	50.45	2.58	9.51
CMPTS PCysMA 5 min	0.67	33.32	2.62	52.54	2.77	8.07
CMPTS PCysMA 10 min	0.63	33.34	2.54	53.31	3.03	7.24
CMPTS PCysMA 15 min	0.45	32.42	3.26	55.13	3.39	5.38
CMPTS PCysMA 30 min	0.33	31.34	3.14	57.67	3.48	4.03
CMPTS PCysMA 60 min	0.00	30.67	3.08	60.41	4.04	1.80
CMPTS PCysMA 90 min	0.00	32.01	3.12	58.53	3.90	2.45
CMPTS PCysMA 120 min	0.00	31.16	2.78	59.95	4.02	2.06
CMPTS PCysMA 180 min	0.00	30.41	3.02	60.88	4.25	1.43

Detailed quantitative characterization was carried out by analysing high resolution spectra (Table 4-10). It showed a gradual decline in the percentage atomic composition from 3%, 52% and 27% corresponding to Cl2p, O1s and Si2p respectively at the start of polymerization at 0 min to about 40 min where it reached a depletion point corresponding to 0%, 31% and 4% for Cl2p, O1s and Si2p respectively.These remained relatively unchanged from 40 min all through to 180 min of polymerization.

On the other hand, the trend in percentage atomic composition for N1s, C1s and S2p revealed an increasing trend from the start of polymerization at 0min for N1s, C1s and S2p from 0%, 19% and 0% respectively. This increasing trend continued steadily until a saturation point of 70 min was arrived at before it levelled up all through to 180 min of polymerization where an average percentage atomic composition of 3%, 60% and 4% for N1s, C1s and S2p respectively was maintained.

4.4.8 The kinetics of growth of POEGMA brushes from CMPTS films

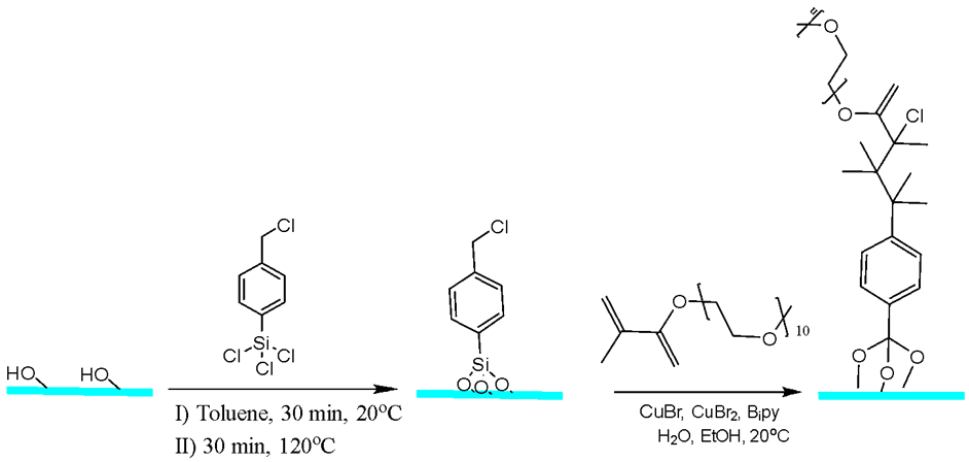

Figure 4-25: Schematic representation of reactions producing POEGMA brushes on CMPTS substrate

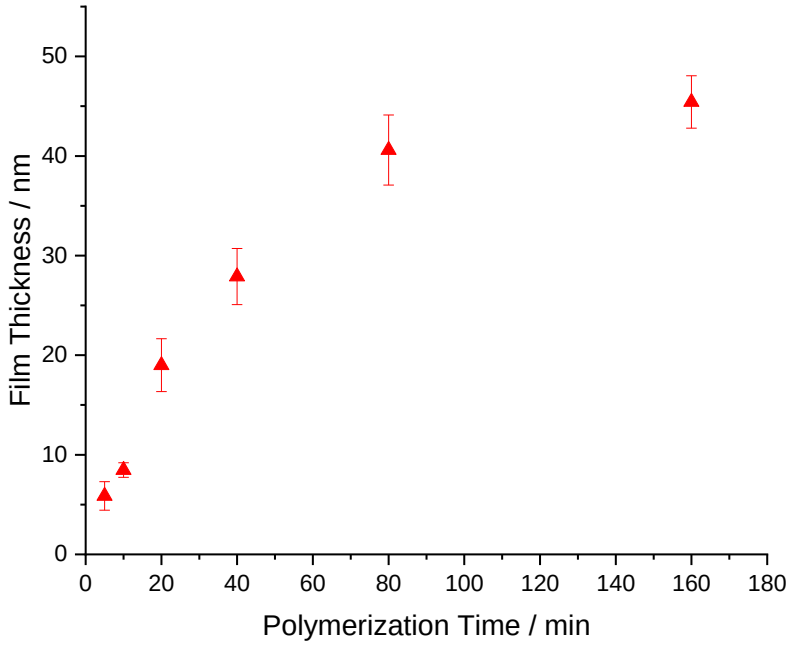

Figure 4-26: Spectroscopic Ellipsometry Measurements of CMPTS POEGMA Brush Thickness [Recipe details: OegMA : Bpy : Cu(I)Br : Cu(II)Br / 455 : 2. : 6 : 1]

The kinetics of growth of POEGMA brushes from CMPTS films were analysed using spectroscopic ellipsometry. The thickness of the brush layer was found to increase rapidly at first, but after 40 min the rate of growth began to slow and by 160 nm the rate of reaction was very low. However, up to 40 min, there was an approximately linear dependence of the brush thickness on the polymerisation time, indicating that the kinetics were very well controlled.

Table 4-11 below shows contact angle measurements at different polymerization times for POEGMA brush grown from CMPTS surfaces. The values ranged from 38 ± 0.41^{o} at 20min to 32 ± 0.72^{o} at 80min all through to 160min of polymerization, which showed a contact angle of 31 ± 0.46^{o}. These values do not show significant changes as the

polymerization time progressed but are a little lower than the average contact angle recorded for PCysMA brushes on CMPTS surface.

Table 4-11: Contact Angle Data of POEGMA Brush Surfaces on CMPTS at Different Polymerization Time

CMPTS POEGMA	Contact Angle (θ)	Cos (θ)
0 min	73.0 ± 1.8^o	0.30
10 min	46.0 ± 0.4^o	0.69
20 min	38.0 ± 0.4^o	0.78
40 min	47.0 ± 2.8^o	0.68
80 min	47.0 ± 2.8^o	0.84
160 min	47.0 ± 2.8^o	0.85

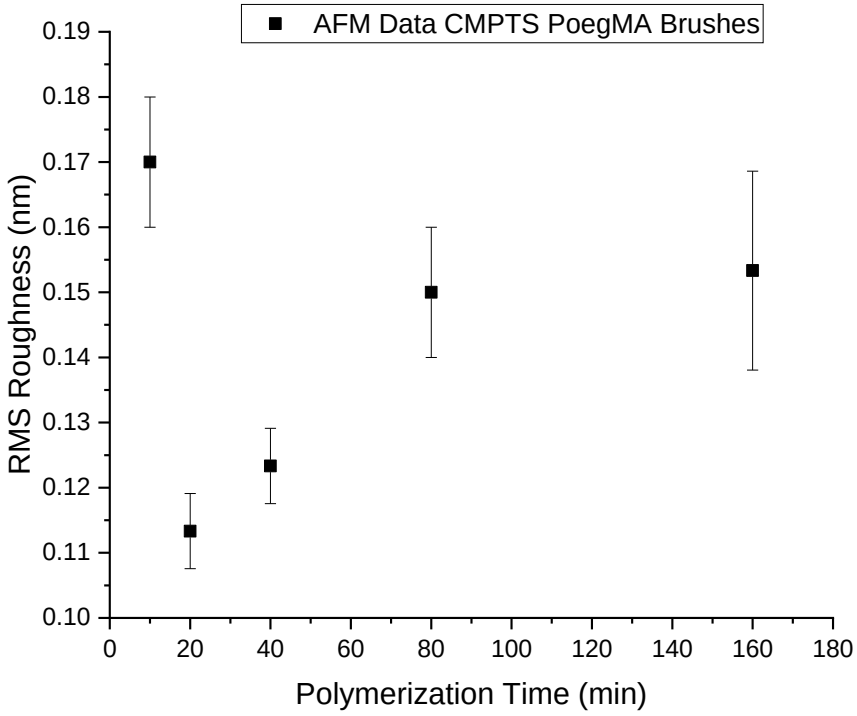

Figure 4-27: AFM Roughness for CMPTS POEGMA Brushes

POEGMA brushes grown from CMPTS films were characterised by Tapping Mode AFM. The RMS roughness was determined using the nanoscope software and is shown as a

function of the polymerisation time in Figure 4-27. Except for the t = 10 min point, which appeared to be anomalous, the RMS roughness was found to increase with the polymerisation time, reaching a plateau of 0.15 nm at 80 min, before levelling up at 160 min polymerization, where the brush roughness approached a limiting value.

XPS analysis were carried out to ascertain the chemical composition of the CMPTS and POEGMA brush surfaces. The results can be seen in the wide scan spectral peaks displayed in figure 4-28. The CMPTS spectrum in figure 4-23 above, showed a high intensity for O1s reaching $15x10^{-3}$ intensity/counts at about 530 eV, but no peak was seen for N1s at 400 eV. C1s showed a low intensity of about $3x10^{-3}$ intensity/counts at 285 eV compared to O1s. Unlike N1s spectral peak that was absent, Cl2p spectral peak with an intensity/count of $1.8x10^{-3}$ can significantly be noted at 200 eV.

On the other hand, in figure 4-28 which is the wide scan spectrum of CMPTS POEGMA brushes, there is a significant peak seen for O1s at 530 eV while the Cl2p spectral peak which was initially noted in CMPTS at 200 eV had disappeared after POEGMA polymerization. Similarly, C1s spectral peak which used to be about a fifth of the O1s peak intensity, can be seen to have risen to about three quarters. In addition, the Si2p spectral peak that was significantly shown with an intensity/count of $3x10^{-3}$, had diminished completely into less than a tenth of its initial intensity. These changes in percentage atomic compositions are an indication that the CMPTS surfaces had been covered by POEGMA brushes.

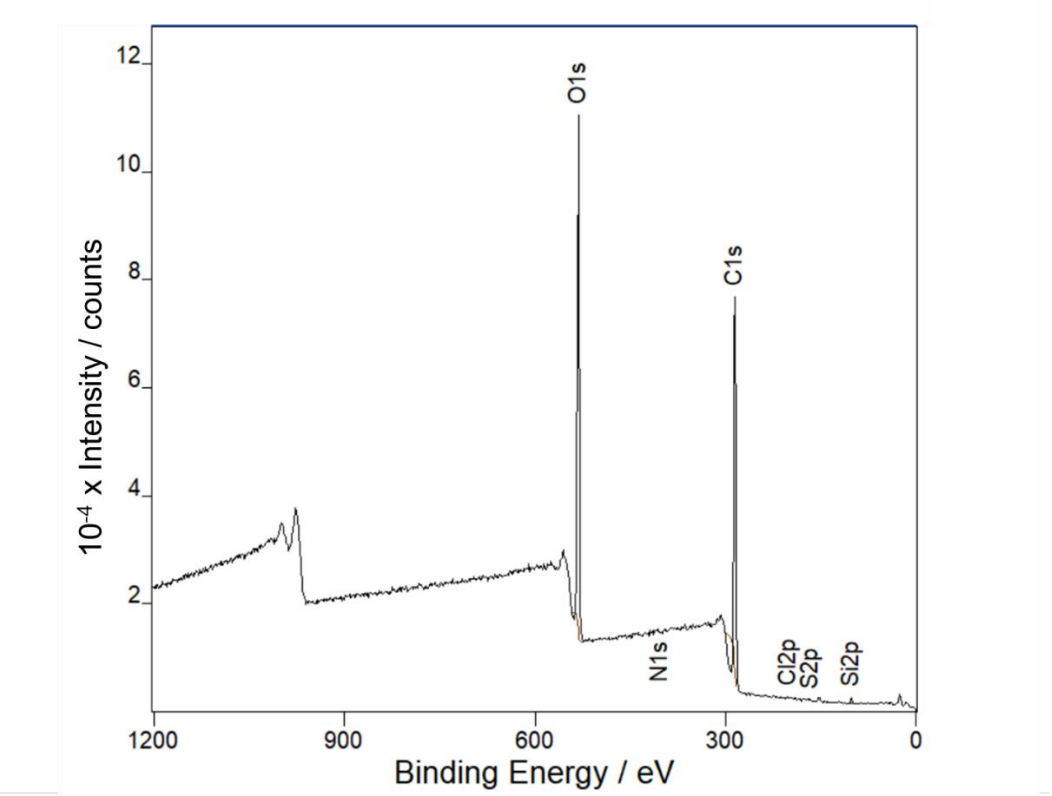

Figure 4-28: XPS Survey Scan of CMPTS POEGMA Brushes on Si Substrate after 180 min of Polymerization Time

Table 4-12: XPS Compositional Percent Data of POEGMA Polymerization on CMPTS Substrate

Sample ID / Polymerization Time	Cl2p	O1s	C1s	Si2p
Cleaned Glass	0.00	66.58	3.94	29.48
CMPTS	3.08	51.55	18.44	26.94
CMPTS POEGMA 2 min	2.03	48.91	26.79	22.27
CMPTS POEGMA 5 min	1.36	40.72	40.42	17.5
CMPTS POEGMA 10 min	0.43	35.67	53.93	9.97
CMPTS POEGMA 15 min	0.34	33.69	58.27	7.71
CMPTS POEGMA 30 min	0.00	31.78	65.57	2.66
CMPTS POEGMA 60 min	0.00	31.87	66.95	1.18
CMPTS POEGMA 120 min	0.00	31.51	68.23	0.27
CMPTS POEGMA 180 min	0.00	31.75	67.47	0.79

Furthermore, XPS high resolution scan data as shown in Table 4-12, reveal the percentage chemical compositions of POEGMA brush samples as a function of increasing polymerization time. Cl2p, O1s and Si2p are seen with initial atomic composition of 3%, 52% and 27% steadily declined to 0%, 32% and 3% respectively after 30 min then remained relatively constant all the way to 180 min of polymerization. Whereas, C1s atomic composition as seen in Table 4-12, rose initialy at 18% to 66% after 30 min before levelling up to 67% after 180 min of polymerization.

4.4.9 ATRP of POEGMA Brushes on BIBB-APTES Films

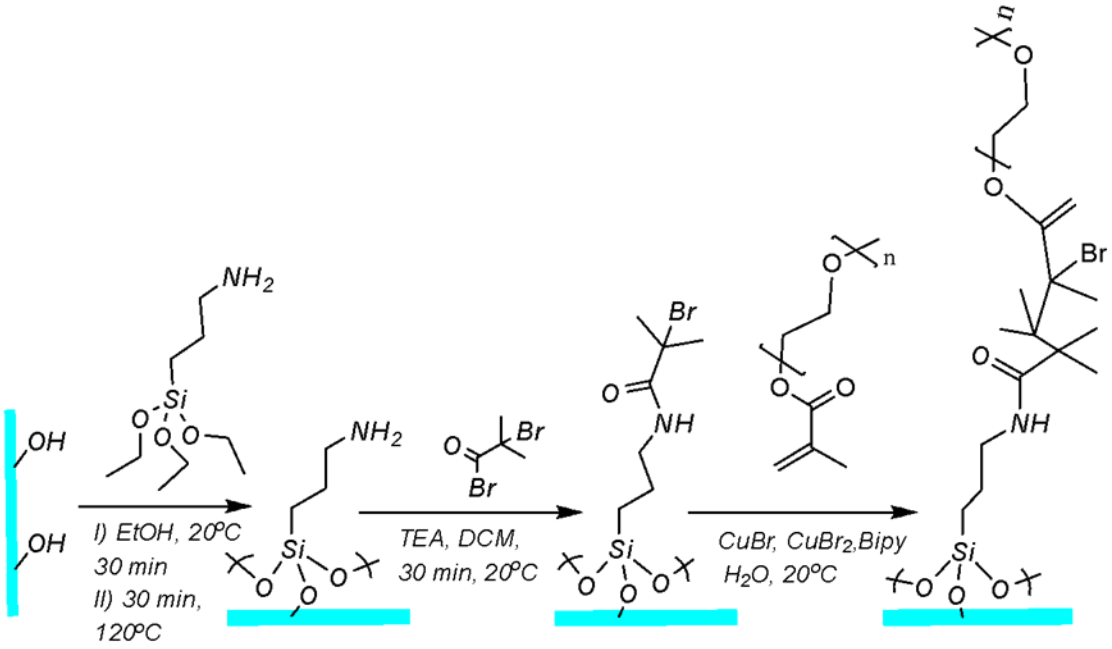

Figure 4-29: Schematic representation of reactions producing POEGMA brushes on BIBB-APTES Substrate

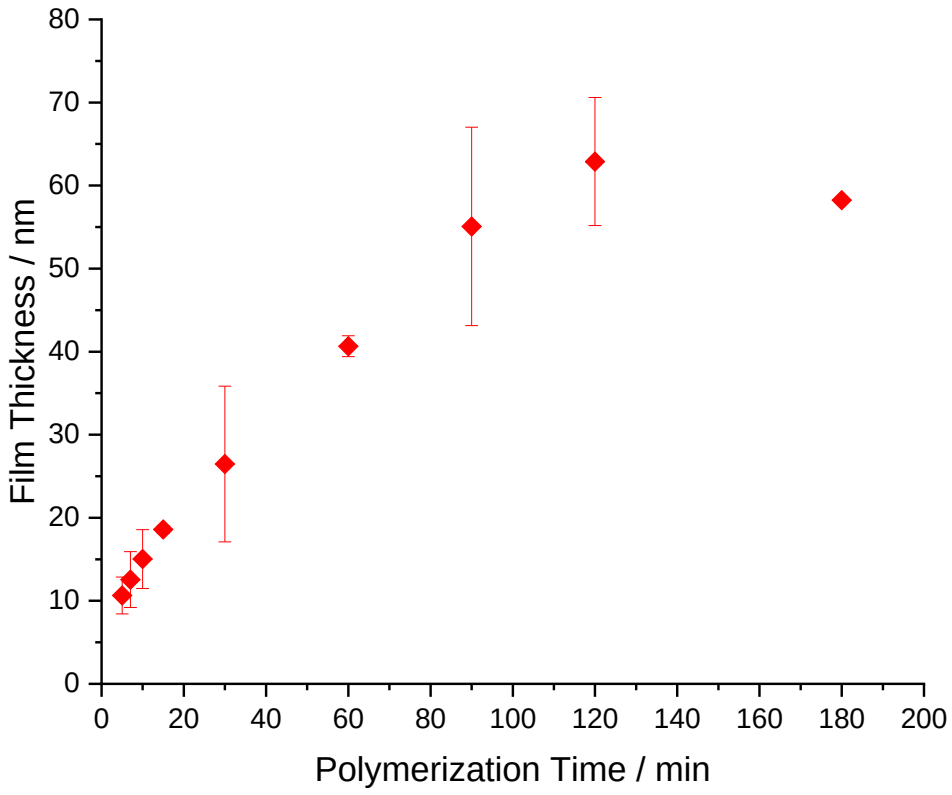

Figure 4-30: Spectroscopic Ellipsometry Measurements of BIBB/APTES POEGMA Brush Thickness [Recipe details: OEGMA : Bpy : Cu(I)Br : Cu(II)Br / 455 : 2 : 6 : 1]

Figure 4-30 shows the variation in the brush thickness as a function of the polymerization time. The film thickness increases rapidly with polymerization time at first, with the rate of film thickness increasing slowly as polymerization proceeds. The brush average thickness grew from 10 nm at 5 min reaching an average maximum height of about 64 nm corresponding to 120 min, then decreased slightly to 58 nm at 180 min of polymerization time.

Contact angles were measured as a function of the polymerization time for POEGMA brushes grown from BIBB-APTES films. The values ranged from an average of 42.0 ±

0.8^{o} at 20 min, to 39.0 ± 0.6^{o} at 80 min before decreasing to 36.0 ± 1.0^{o} at 160 min of polymerization. This is an indication that the wettability and surface energy of POEGMA brushes for both. Tables 4-11 and 4-13 are similar.

Table 4-13: Contact Angle Data of POEGMA Brush Surfaces on BIBB-APTES at different Polymerization time

BIBB-APTES POEGMA Polymerization Time (min)	Contact Angle (θ)	Cos (θ)
0	61.0 ± 2.3^{o}	0.50
10	48.0 ± 0.8^{o}	0.67
20	42.0 ± 0.8^{o}	0.74
40	41.0 ± 0.6^{o}	0.75
80	39.0 ± 0.6^{o}	0.78
160	36.0 ± 1.0^{o}	0.81

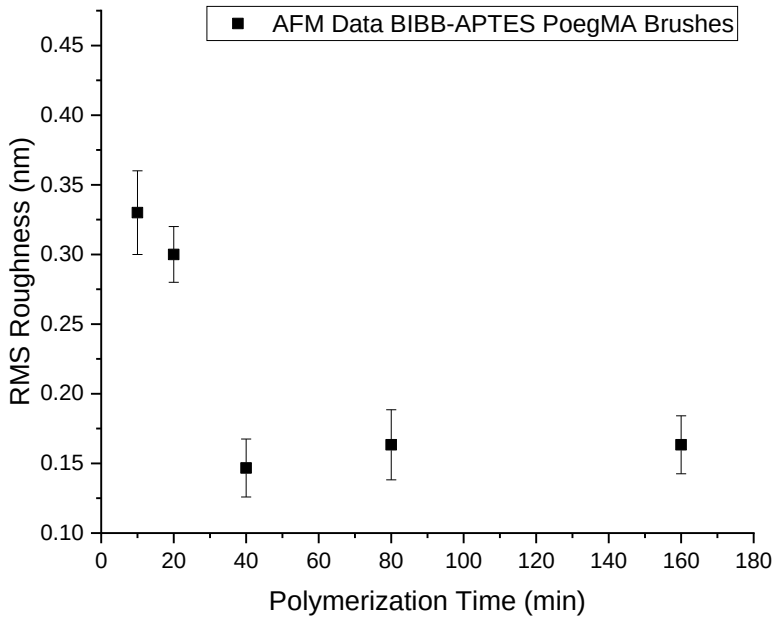

Figure 4-31: AFM Roughness for BIBB-APTES POEGMA Brushes

RMS roughness data of POEGMA brushes on BIBB-APTES as determined from AFM images, are shown in Figure 4-31. There is a steady drop in RMS values from 0.33 nm to 0.15 nm as the polymerization proceeds from 10 min to 40 min respectively, before levelling to about 0.16 nm at 160 min.

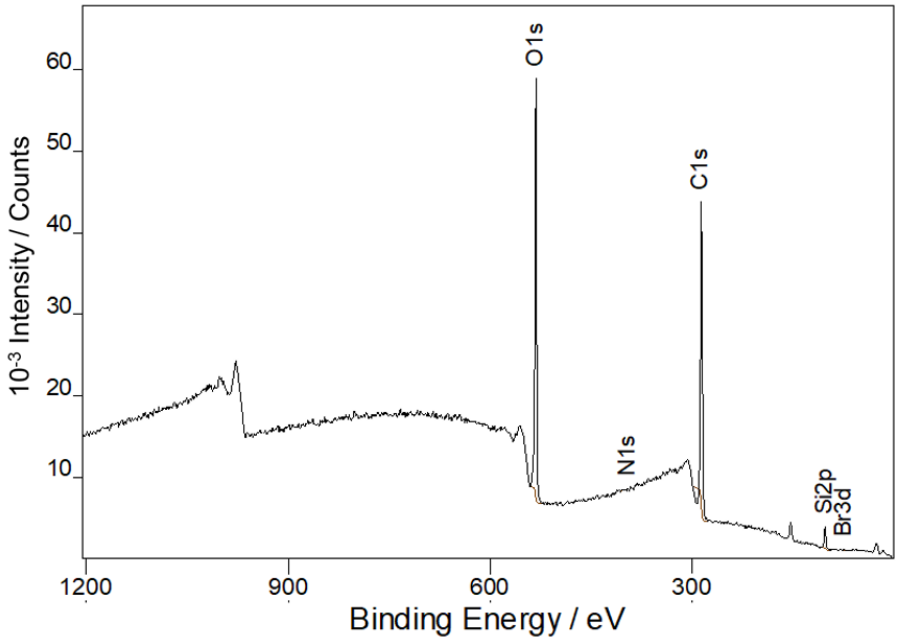

Figure 4-32: XPS Survey Scan Showing BIBB-APTES POEGMA Brushes on Si Substrate after 160 min of Polymerization Time

Table 4-14: XPS Compositional Percent Data of POEGMA Polymerization on BIBB-APTES Substrate

Sample ID / Polymerization Time	Br3d	O1s	N1s	C1s	Si2p
Cleaned Glass	0.00	60.76	0.00	5.11	34.19
APTES	0.00	49.81	1.32	16.59	32.39
BIBB-APTES	0.20	47.43	1.11	20.16	31.49
BIBB-APTES POEGMA 5 min	0.17	44.73	1.13	25.33	28.87
BIBB-APTES POEGMA 10 min	0.17	44.50	0.91	26.35	28.85
BIBB-APTES POEGMA 15 min	0.15	41.11	0.82	32.45	25.47
BIBB-APTES POEGMA 30 min	0.10	35.55	0.60	45.12	18.63
BIBB-APTES POEGMA 60 min	0.06	31.04	0.39	53.29	15.23
BIBB-APTES POEGMA 90 min	0.01	27.69	0.10	63.88	8.31
BIBB-APTES POEGMA 120 min	0.00	27.28	0.00	67.13	8.31
BIBB-APTES POEGMA 180 min	0.00	26.39	0.00	68.97	4.67

X-ray photoelectron spectroscopy (XPS) analysis conducted on BIBB-APTES and POEGMA brushes show a surface chemical composition as seen in Table 4-14. The XPS wide scan analysis for BIBB-APTES initiator layer in Figure 4-18 showed in the spectrum, a record of strong peak at $11x10^{-3}$ intensity/count for O1s at 530 eV, owing to the high

oxide level in the substrate. C1s showed an initial peak with intensity/count of $1.8x10^{-3}$ at 285 eV. Si2p appeared at 102 eV with a peak of $2.0x10^{-3}$ intensity/counts. Whereas N1s and Cl2p peaks at 400 eV and 200 eV respectively remained as trace levels, largely due to a very thin BIBB-APTES layer on the substrate. Thus, allowing the Si2p peak of the substrate at 102 eV to be noticed more than the intensity of C1s peak.

Compared to the XPS spectral representation of BIBB-APTES (Figure 4-18), the POEGMA on BIBB-APTES spectral peaks on Figure 4-32, showed Br3d and N1s peaks absent completely. In addition, figure 4-32 revealed much more stronger peaks for O1s and C1s corresponding to $58x10^{-3}$ and $45x10^{-3}$ intensity/counts respectively with Si2p which appeared as a fourth of its initial intensity. These marked increases in spectral peak intensities are due to the thick POEGMA brush layer on the substrates surface. The disappearance of the Br3d and Si2p peaks from Figure 4-32 served as confirmation that Br3d got used up for polymerization to generate a thick brush layer that masked the appearance of Si2p from the surface as well.

Furthermore, XPS high resolution scan data as shown in Table 4-14, revealed the percentage chemical compositions of the different atoms in POEGMA brushes on BIBB-APTES surface as a function of increasing polymerization time. Br3d, O1s, N1s and Si2p showed a sharp decline in their atomic compositions from 0.2%, 48%, 1% and 32% to a reduced atomic composition of 0%, 26%, 0% and 8% respectively after 80 min before levelling up to 180 min of polymerization. While the C1s atomic composition rose from 20% to 60% after 80 min before levelling all the way to 68% at 180 min of polymerization.

4.5 Conclusion

PCysMA and POEGMA brushes of varying dry thicknesses have been prepared at room temperature using ATRP. XPS data analysis confirmed that these polymer brush layers have been successfully deposited on the substrate surfaces. For PCysMA, the limiting thickness of the polymer brushes was 37 nm when grown from CMPTS films and 42 nm when grown from BIBB-APTES films. The rate of film growth was slower when Cl was the initiator and faster when Br was the initiator. For POEGMA, the limiting thickness of the polymer brushes was 45 nm when grown from CMPTS films and 64 nm when grown from BIBB-APTES films. The rate of film growth was slower when Cl was the initiator and rapid when Br was the initiator. From this observation, it can be said that BIBB-APTES initiator yields the thickest films and fastest growth, and OEGMA monomer yields the thickest films and fastest growth.[62,117,139,151]

The growth profile exhibited by the polymer brush structures grown from different surfaces of varying compositions suggest that a form of control has been established in the growth of these polymers and can be repeatedly achieved. From the results of the polymerization kinetics seen of chlorinated and brominated initiator films in Figures 4-17, 4-21, 4-26 and 4-30, it showed that brominated initiator films grow thicker brushes compared to the chlorinated films. This was recently observed in the work of Parkatzidis et. al, 2021. They stated that initiator films with chlorinated end group, cause lower activation rates compared to their brominated counterparts under identical conditions. The growth profile exhibited by the polymer brush structures grown from different surfaces of varying compositions suggest that a form of control has been established in the growth kinetics

of these polymers and can be repeatedly achieved. Thus, constituting a platform for the incorporation of Nile blue dye which will serve as a *ratiomeric* pH sensors.

CHAPTER 5: FORMATION OF DYE-FUNCTIONALIZED POLYMER BRUSHES

5.1 Introduction

Polymer brushes provide a simple and effective means to control surface properties and interactions. PolyCysMA and polyOEGMA are attractive polymers for applications in biology because they exhibit low rates of biofouling.[152] The main aim of the research conducted during this project was to develop microsystems for the *in-situ* monitoring of membrane processes. Optically active molecules (dyes) can be effective as reporters for such processes, because they yield signals that can be detected simply and inexpensively using a variety of means, including UV-vis spectroscopy and fluorimetry. Thus, there has been extensive interest in the derivatisation of polymer brushes with dye molecules. Fluorescent dye incorporation into antibodies serving as binders are readily available reporters used in fluorescence microscopy, microplate assays as well as flow cytometry.[152-154]

Thousands of fluorescent dyes can be coupled to polymer scaffolds with single antibody attachment yielding fluorescent signals that are comparable to the intensities derived from recent immunofluorescence technology. However, to maintain an effective fluorescent property, it is necessary that the degree of dye labelling should be less than 10 dyes per IgG (antibody), which is equivalent to a low modification fraction with individual dyes. An example is the case of a labelled antibody with up to 6 fluorophores per protein exhibiting a decrease in specificity and binding affinity.[152] On the other hand, specific site labelling with exactly one molecule of dye such as linker labelling of block co-polymers or chain-

end-labelling as well as attachment of fluorescent dyes by post polymerization modifications invariably are still the preferred methods.[155]

In previously published literature, the emphasis has been placed on the introduction of small concentrations of dye molecules in a polymer brush matrix. Where qualitative readout is required, that may be satisfactory; moreover, the use of low concentrations of dye molecules also makes the polymer chemistry straightforward, because many brushes are solvated by polar solvents, while many common dyes are large hydrophobic molecules with uncertain compatibility with the interior of the brush layer.

However, for some potential applications it would be desirable to be able to bind dyes with higher concentrations in the brush layer. For example, Madsen et al have described the use of Nile Blue as a *ratiomeric* pH sensor. In *ratiomeric* sensors, the pH change is detected by a *shift* in the emission spectrum rather than by a change in the fluorescence intensity.[156] Compared to probes based solely on emission *intensity,* such probes are less susceptible to problems arising from non-specific quenching, photobleaching, variations in the intensity of the light source and background scattering. However, it is necessary to be able to achieve adequate signal-to-noise; thus, optimisation of the concentration of the reporter molecules (dye) in the polymer brush matrix is important.[157]

Madsen and co-workers described an approach to the labelling of polymer brushes with Nile Blue by adding dye-labelled monomer at a concentration of ~1% to the reaction mixture used for ATRP. Like many other dyes, Nile Blue acts as a radical trap, and is thus able to terminate the living radical polymerisation mechanism that is the basis for ATRP. To minimise the termination rate, the dye concentration must be maintained at a very low

concentration. Madsen et al demonstrated that UV-vis spectra could be measured from Nile Blue labelled PCysMA and POEGMA brushes, but the signal to noise was poor.

The aim of this chapter is to explore an alternative route to the synthesis of Nile Blue functionalised polymer brushes, based on the covalent coupling of the dye to the surface-grafted polymer. Three approaches are examined to determine how to optimise the binding of Nile Blue to POEGMA and PCysMA. First, a dye-labelled acrylic monomer, Nile Blue 2-Methacryloyloxy ethyl carbamate, will be added to the reaction solution along with the catalyst and monomer solution to achieve incorporation of Nile Blue into the backbone of the surface grafted polymer as shown in Figure 5-2 below. This follows directly the method of Madsen et. al, 2018. They added dye at low concentration to minimise the extent to which the dye would cause termination. Thus, the degree of incorporation of dye molecules must be small while nevertheless being large enough to yield significant optical activity.

The second approach relies upon the fact that Nile Blue is a radical trap and reacts with the living chain ends of polymers during ATRP. In this approach, Nile Blue will be added to the reaction mixture to act as a terminator (Fig. 5-3), binding to the chain ends of the surface-grafted polymers. This will yield a maximum of one dye molecule per polymer chain.

The third method involves the covalent attachment of the dye to the polymer, with the aim being to achieve a high degree of derivatisation. Two alternative reactions are compared. First, PCysMA is incubated with glutaraldehyde, a dialdehyde which reacts with pendant amine groups via the formation of an imine bond. Thus, a significant fraction of pendant amine groups is expected to be converted to aldehydic functional groups. These

derivatised films are then incubated with a solution of Nile Blue that has been modified to introduce an amine linker, which again reacts with a free aldehyde group or an active ester group to couple the dye to the polymer via the formation of either a further imine bond or an amide bond. Glutaraldehyde has been used extensively for surface conjugation in an analogous fashion.[158] Secondly, PCysMA is incubated with dissuccinimidyl suberate, a bifunctional linker containing two succinimidyl ester groups that are highly reactive towards primary amines. One end of the linker couples to an amine on the polymer scaffold, and the other is available to bind Nile Blue that has been modified to introduce an amine linker. N-hyroxysiccinimidyl ester reagents are widely used for the conjugation of biological molecules to solid phases.[157]

5.2 Experimental Method

5.2.1 Synthesis of Nile Blue 2-Methacryloyloxy ethyl carbamate

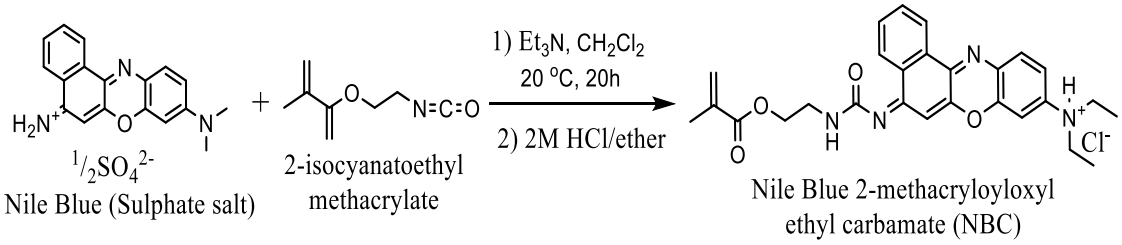

Figure 5-1: Synthesis of Nile Blue 2-methacryloyloxy ethyl carbamate (NBC)

Nile Blue (sulphate salt, 1.1141 g) was dissolved in 25 mL of dichloromethane and thoroughly mixed under nitrogen. To this solution, 3.6 g of triethylamine was added, and the mixture was kept for on ice for 15 min. 0.55g of 2-isocyanatoethyl methacrylate was dissolved in 10 mL of dichloromethane and added to the reaction solution. The mixture was stirred for 20 h. Finally, 2 mL of methanol was introduced to halt the reaction.

The solvent was evaporated over 6 h, and the residue was washed with 50 mL of water. The precipitate was added to 10 mL of dichloromethane dissolved in 500 mL of diethyl ether. A solution of 2 M HCl in 2.5 mL ether was added. The precipitate was filtered, washed with 250 mL of diethyl ether and vacuum-dried to yield 0.83g of product.

The product was purified further on silica column with a 9 : 1 dichloromethane : methanol mixed eluent.

5.2.2 ATRP of POEGMA and NBC

4.6 mL of oligoethylene glycol methyl ether methacrylate (OEGMA) monomer was transferred into a clean 50 mL round bottom flask sealed with a Suba-seal and containing 11.2 mL of deionized water in a nitrogen atmosphere. 70 mg of 2,2-bipyridyl was added into the monomer solution with 11 mg of copper (II) bromide and 23 mg of copper (I) bromide catalyst. The reaction solution was stirred continuously. NBC was added to the reaction solution to yield the desired concentration, and the solution was transferred under nitrogen to a carousel tube containing an initiator-functionalised substrate under a nitrogen atmosphere. ATRP was carried out for the required time. After termination of the polymerisation reaction, the substrate was washed with deionised water and ethanol and dried in a stream of nitrogen gas.

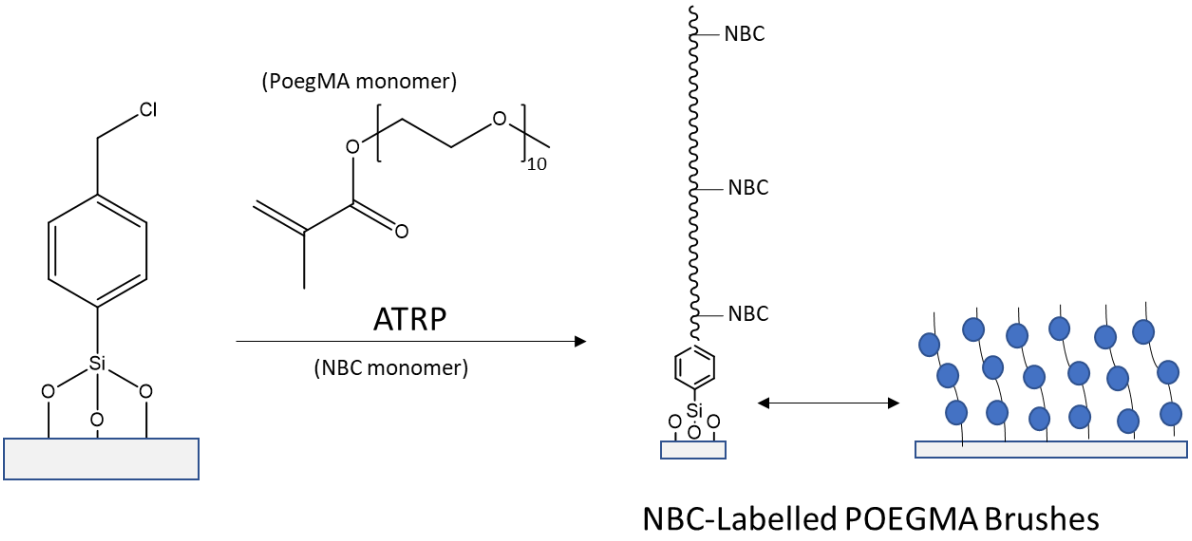

Figure 5-2: Figure 5 2: NBC-Labelled POEGMA Brush Formation

5.2.3 ATRP of POEGMA and NBC end-capping

4.6 mL of oligoethylene glycol methyl ether methacrylate (OEGMA) monomer was transferred into a clean 50 mL round bottom flask sealed with a Suba-seal and containing 11.2 mL of deionized water in a nitrogen atmosphere. 70 mg of 2,2-bipyridyl was added into the monomer solution with 11 mg of copper (II) bromide and 23 mg of copper (I) bromide catalyst. The reaction solution was stirred and then transferred to a carousel tube containing an initiator-functionalised substrate under a nitrogen atmosphere. ATRP was carried out for the required time. After termination of the polymerisation reaction, the substrate was washed with deionised water and ethanol and dried in a stream of nitrogen gas. The dried POEGMA functionalized substrate was placed into a degassed NBC solution purged with Nitrogen and left for 16 h at room temperature. The sample was washed and dried under nitrogen and characterised.

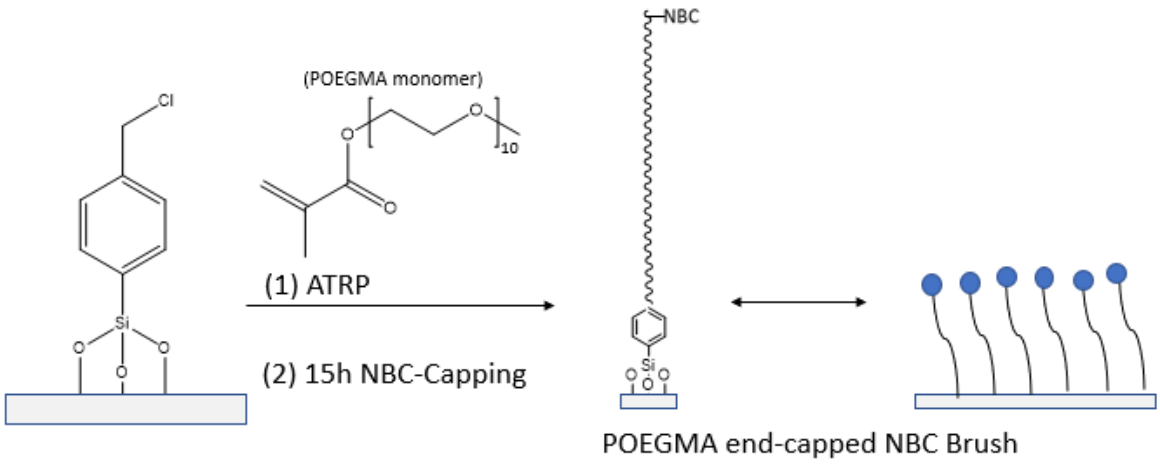

Figure 5-3: NBC-Capped POEGMA Brush Formation

5.2.4 Gluteraldehyde-Mediated Coupling of Nile Blue to PCysMA Brushes

CMPTS substrates functionalised by growth of PCsyMA by ATRP were immersed in a solution consisting of 0.2 mL of 25% gluteraldehyde in water dissolved in 10 mL of deionised water and heated at 50^{o}C for 24 h. After completion of the reaction, the samples were washed with water and ethanol before nitrogen gas stream drying. The dry aldehyde-functionalised brushes were immersed in a solution of amine-modified Nile Blue in ethanol and incubated for 24 h at 50^{o}C. Finally, the Nile Blue-functionalized substrate was washed with ethanol and dried in a stream of nitrogen gas.

5.2.5 Dissuccinimidyl Suberate (DSS)-Mediated Coupling of Nile Blue to PCysMA Brushes

PCysMA brush-coated substrates were immersed in a solution of 0.0117g dissuccinimidyl suberate (DSS) in 4.5 mL of 7.5 phosphate buffer solution in a small vail and heated for 24 h at 50^{o}C. The sample was washed with water and ethanol and dried in a stream of nitrogen gas. The resulting succinimidyl ester-functionalised brush was immersed in a

solution of the amine-modified Nile Blue and heated for 24 h at 50^{o}C. The resulting Nile Blue-functionalized substrate was washed with ethanol and dried in a stream of nitrogen gas prior to characterisation.

5.3 Characterization

Absorbance intensity was determined by using UV-visible spectrophotometer. Spectroscopic Ellipsometry was used to measure the brush thickness after NBC was added to the monomer catalyst reaction solution and the documented thicknesses are a mean of ot least three measurements. XPS wide scan and high resolution spectra was used to determine the chemical composition of the polymer layer on substrate.

5.4 Results and Discussions

5.4.1 Synthesis of NBC

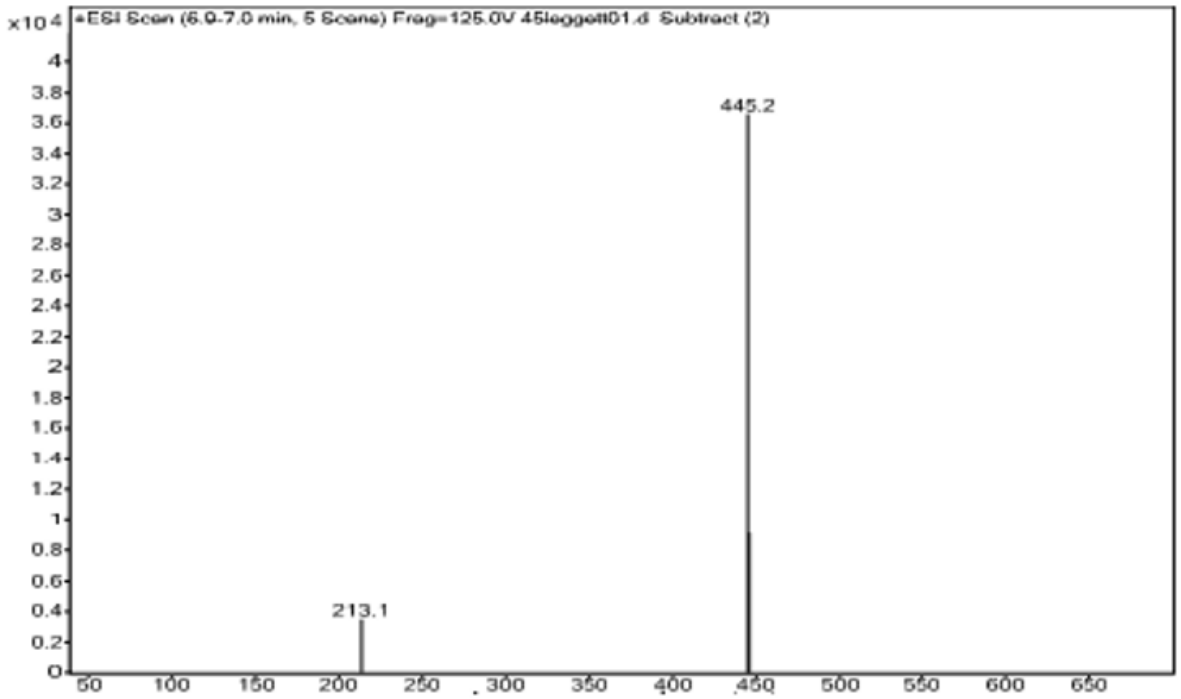

Figure 5-4: Electron impact (m/z) mass spectrum of NBC

^{13}C NMR $(400\ MHz,\ 3{:}1\ CDCl_3 : CD_3OD)$ δ 167.32, 161.54, 147.85, 140.79, 136.29, 130.96, 130.30, 128.59, 125.38, 123.45, 122.17, 121.95, 120.67, 115.54, 110.83, 106.33, 105.48, 100.56, 96.28, 92.21, 63.54, 46.42, 38.71, 17.10, 7.90 ppm

^{1}H NMR $(400\ MHz,\ CD_3OD)$ $\delta\ 9.05\ (br, 1H), 8.72\ (br, 1H), 8.35\ (d, 1H, J = 8.2\ Hz), 7.95\ (m, 3H), 7.70\ (br, 1H), 7.25\ (br, 1H), 6.21\ (s, 1H), 5.70\ (s, 1H), 4.46\ (t, 2H, J = 5.38\ Hz), 3.91\ Hz\ (br, q, 4H), 3.70\ (t, 2H, J = 5.14\ Hz), 1.90\ (s, 3H), 1.44\ (t, 6H, 7.09\ Hz)\ \ ppm$

The yield of NBC was 74.5% after purification and drying. The mass spectrum of the product (Figure 5-4) exhibited a dominant peak at m/z 445.2. the calculated molecular mass of NBC is 445 g mol^{-1}, thus this peak in the Mass Spectrum is attributed to the molecular ion.

5.4.2 Spectroscopic characterization of NBC dye in methanol

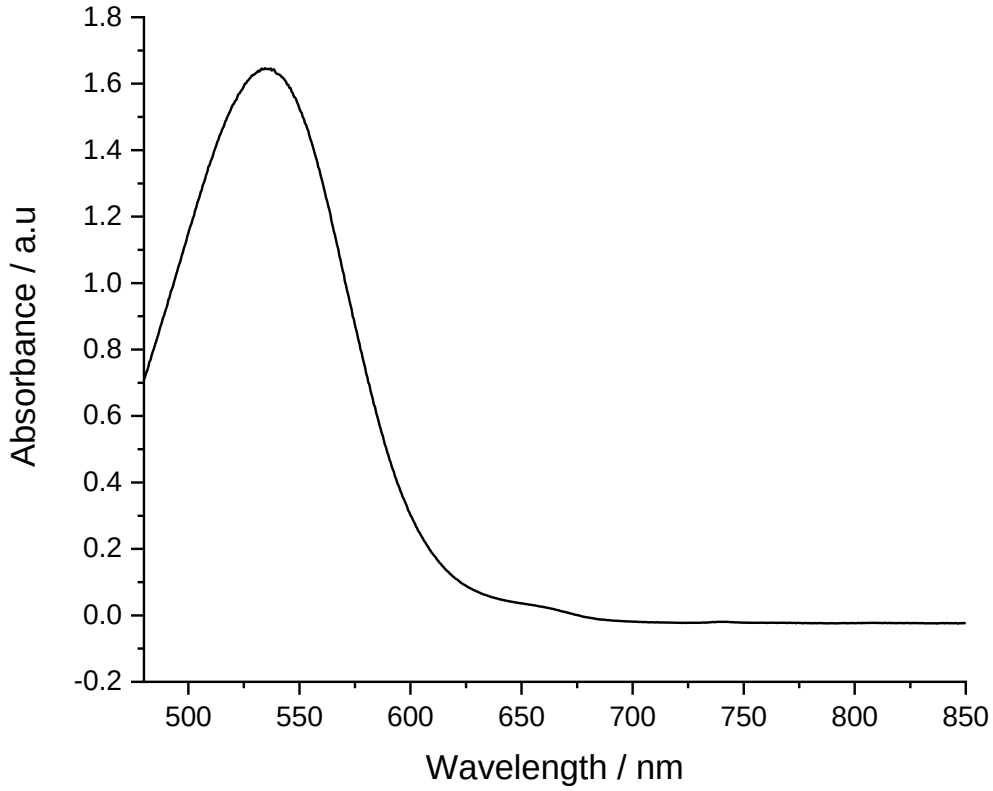

Figure 5-5: Absorbance spectrum for NBC dissolved in methanol

Figure 5-5 shows the uv-vis spectrum of NBC dissolved in ethanol to form a very diluted solution. The spectrum exhibits a strong absorption maximum at 540 nm (absorbance 1.6 a.u).

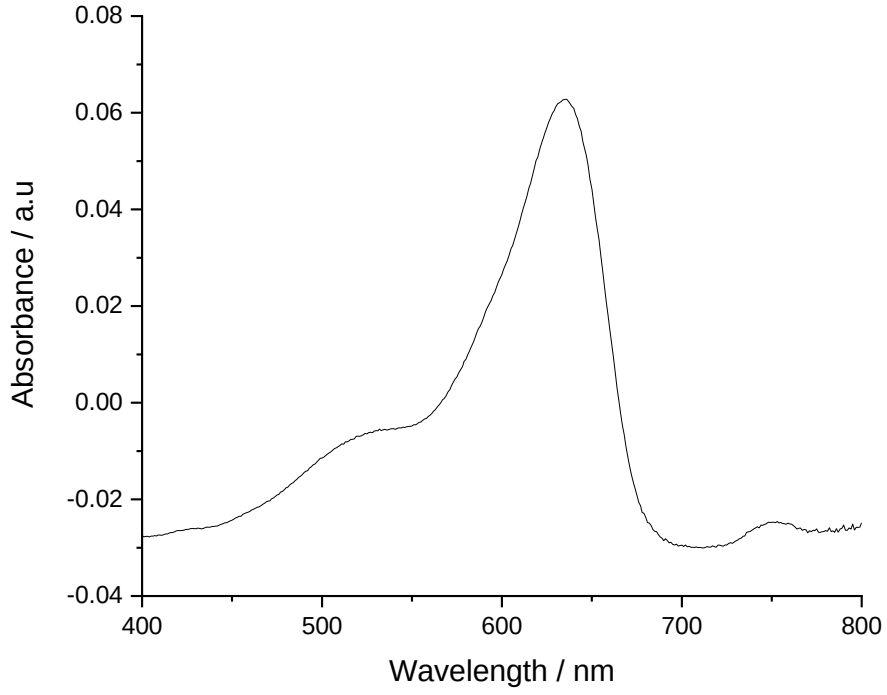

Figure 5-6: Wavelength of Absorbance for Amine-Modified Nile Blue in ethanol

Figure 5-6, shows the modified NB dye dissolved in ethanol to form a very diluted solution and transferred into a cleaned cuvvette for measurement. Analysis of the data obtained revealed a very clear absorption peak intensity of about 0.06 a.u was recorded at about 640nm.

5.4.3 Spectroscopic characterization of dry POEGMA brush

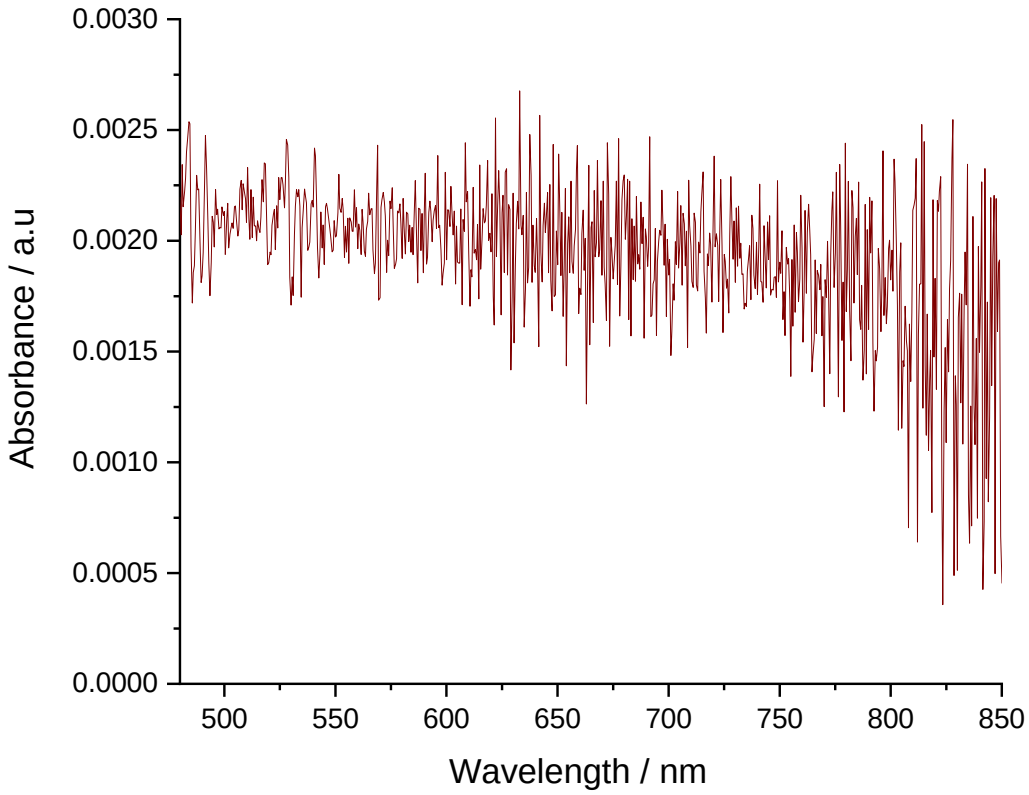

Figure 5-7: Absorption Spectrum of 20 nm thick POEGMA Brush on CMPTS Layer

POEGMA brushes were grown from glass CMPTS surfaces for 40 min, yielding films with a dry brush thickness of 20 nm determined by spectroscopic ellipsometry measurements. The absorbance was measured for these brushes in the absence of any dye, to establish the intrinsic absorbance of the polymer film. Figure 5-7 shows a representative spectrum. In the range of wavelength studied, no peak is seen for POEGMA brushes.

5.4.4 Spectroscopic characterisation of POEGMA brushes following co-polymerisation with NBC

UV-vis spectroscopy was carried out for POEGMA brushes grown from glass CMPTS substrates for times ranging from 2.5 to 160 min, expected to yield dry brush thicknesses of 3 to 46 nm in the absence of dye. NBC was included in the reaction mixture. Because of the tendency of NBC to act as a radical trap, causing chain terminations, the concentration was varied. It was expected that at low concentrations, dye concentrations in the resulting films would be too small to detect measurable fluorescence, whereas at high NBC concentrations, high rates of termination would be expected, leading to thinner films and reduced amounts of dye binding overall.

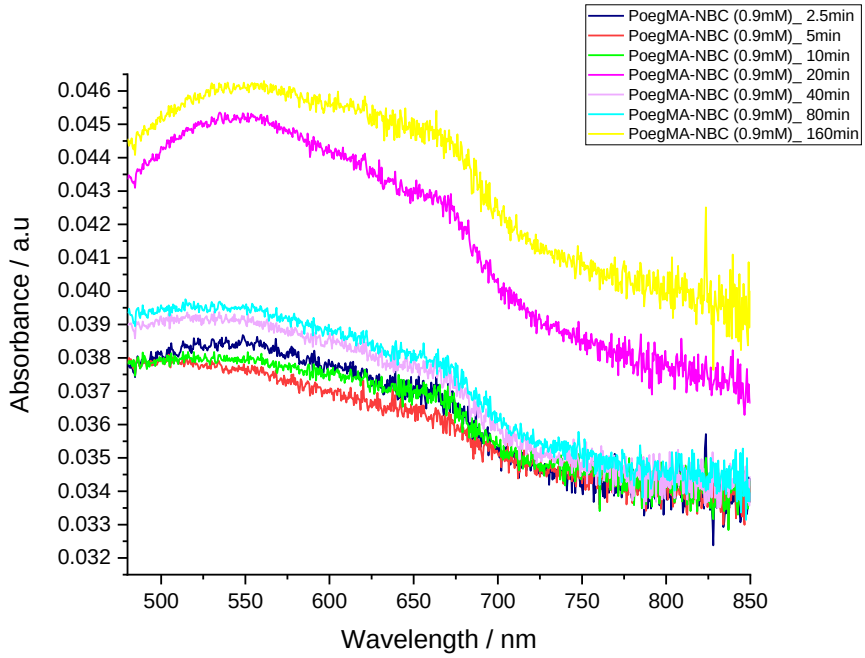

Figure 5-8: Spectral Peaks Showing Absorbance Intensities for POEGMA NBC (0.9mM) at Different Polymerization Times

Figure 5-8 shows absorption spectra acquired for POEGMA brushes grown using a polymerisation mixture containing 0.9 mM NBC. It can be seen that the highest peak intensity of 0.046 a.u at 535 nm observed for brush grown for 160 min with 0.9 mM NBC while the lowest peak intensity of 0.037 a.u at 535 nm was observed for the brush grown for 5 min polymerization.

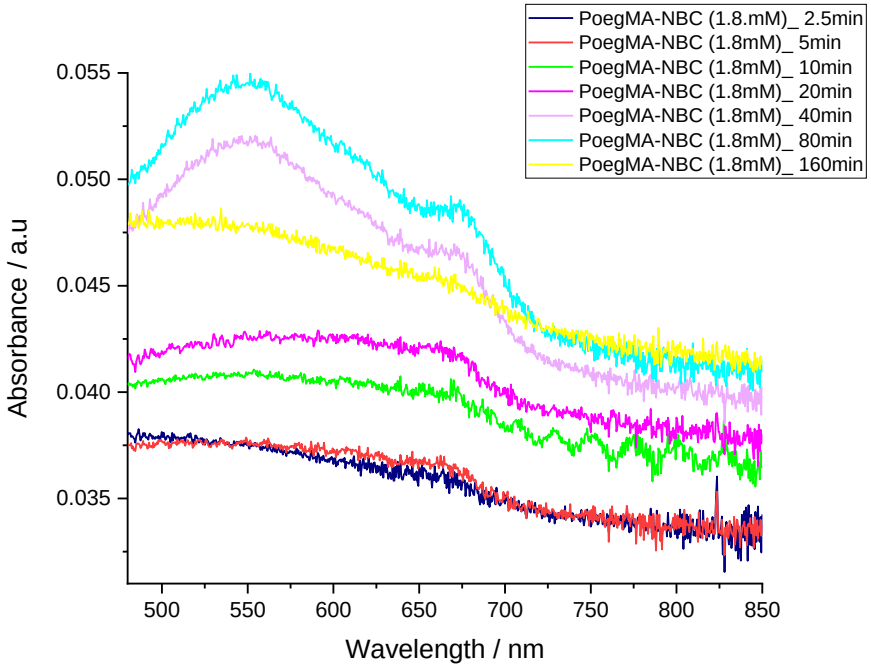

Figure 5-9: Spectral Peaks Showing Absorbance Intensities for POEGMA NBC (1.8mM) at Different Polymerization Times

Similarly in figure 5-9, the highest peak intensity of 0.055 a.u at 535 nm was observed for brush grown for 80 min with 1.8 mM NBC while the lowest peak intensity of 0.038 a.u at 535 nm was observed for the brush grown for 2.5 min polymerization.

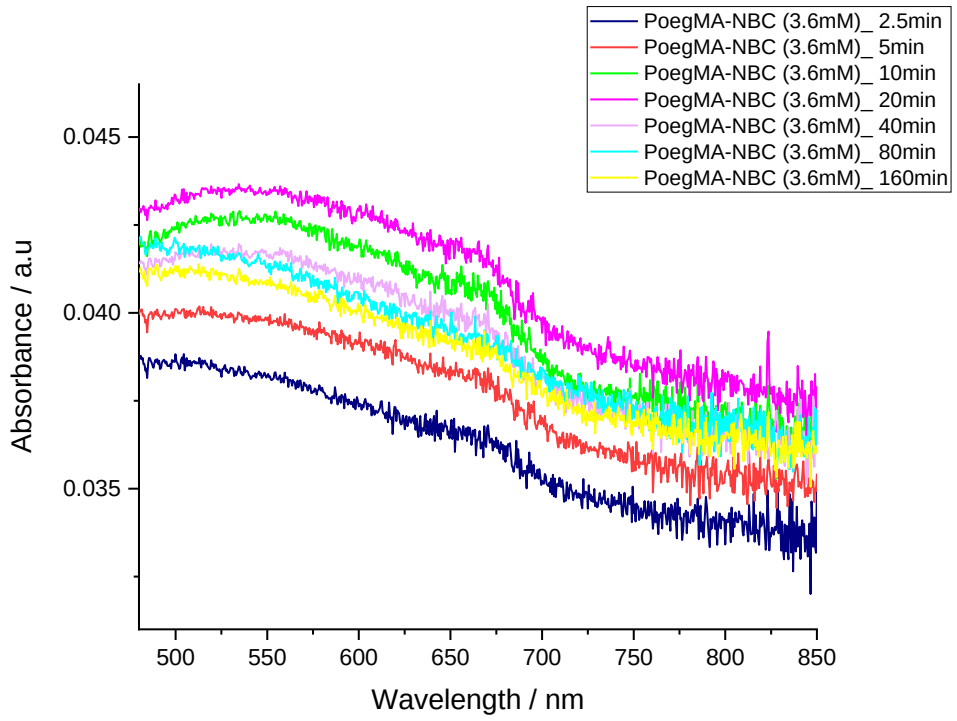

Figure 5-10: Spectral Peaks Showing Absorbance Intensities for POEGMA NBC at Different Polymerization Times

Furthermore, figure 5-10, has its highest peak intensity of 0.043 a.u at 535 nm observed for brush grown for 20 min wirh 3.6 mM NBC while the lowest peak intensity of 0.038 a.u at 535 nm was observed for the brush grown fo 2.5 min polymerization.

5.4.5 Spectroscopic characterisation of POEGMA brushes following end-capping with NBC

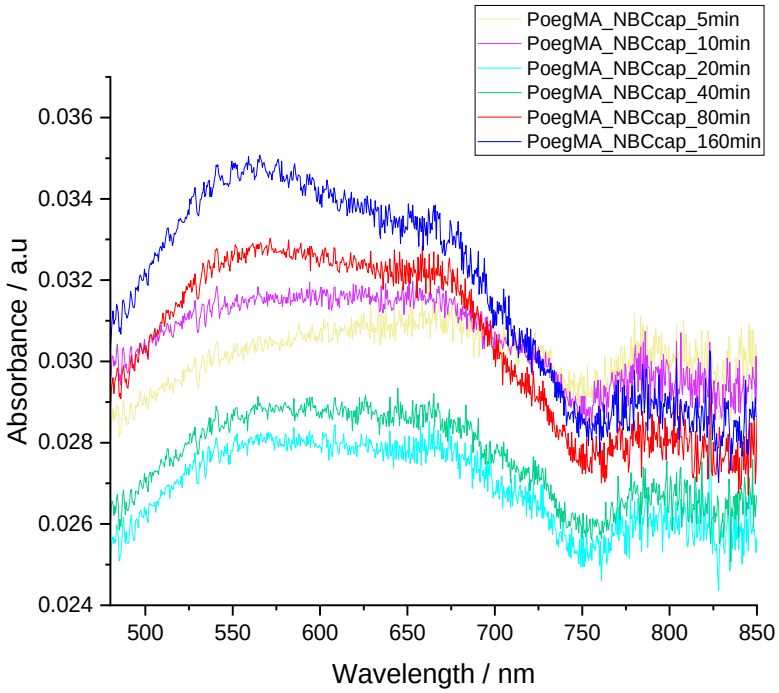

Figure 5-11: Spectral Peaks Showing Absorbance Intensities for POEGMA NBCcapped at Different Polymerization Times

In the spectra in figure 5-11, which represents UV spectral measurements achieved for NBC capped POEGMA brushes. The highest peak intensity of 0.035 a.u at 535 nm was observed for brush grown for 160 min before 15 hours immersion in a solution of 50 mM NBC while the lowest peak intensity of 0.028 a.u at 535 nm was observed for the brush grown for 20 min polymerization.

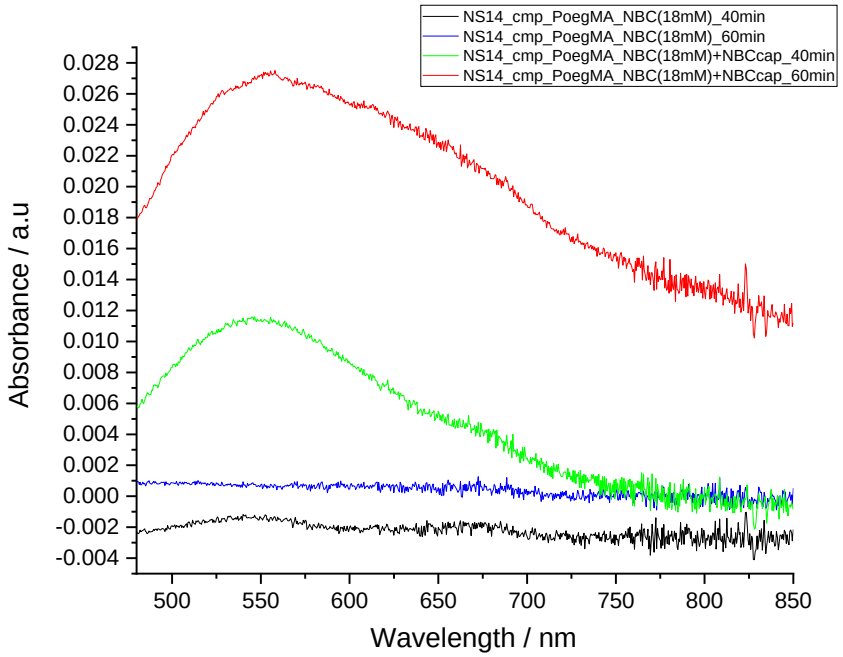

Figure 5-12: Spectral Peaks Showing Absorbance Intensities for POEGMA NBC

The absorption peaks in figure 5-12 above, are those of POEGMA labeled with (18mM) NBC for 40 min and 60 min polymerization, both with intensities of less than 0.001 a.u at about 535 nm. This also included POEGMA labeled with (18mM) NBC for 40 min then capped with NBC solution for 16 hours, showing very prominent absorption intensities of 0.027 a.u and 0.012 a.u at 535 nm respectively.

5.4.6 Effect of pH variation on NBC Solution

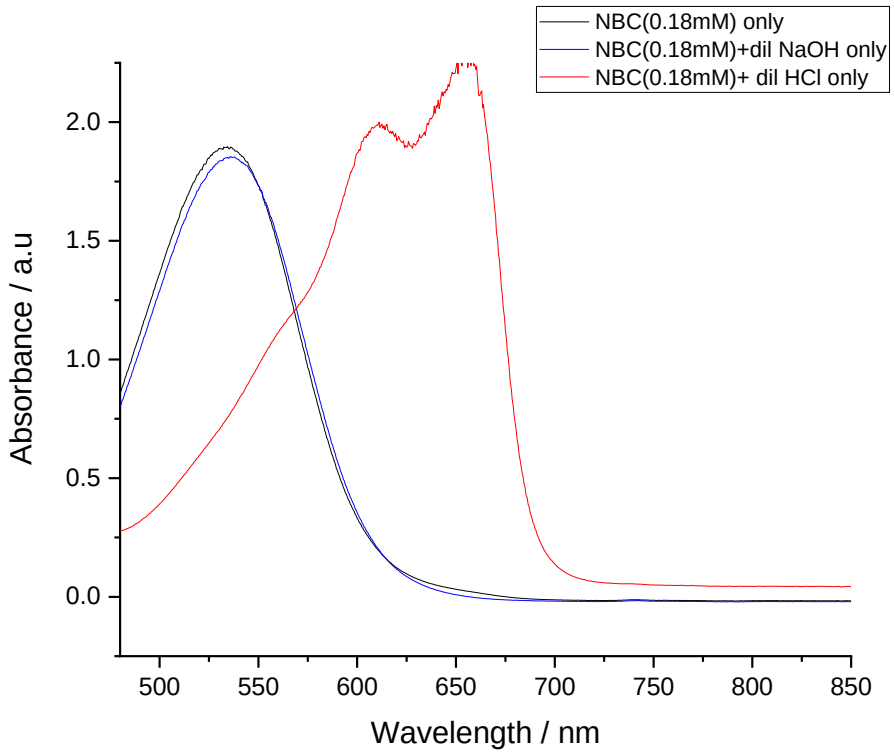

Figure 5-13: Spectral Peaks Showing Wavelength Absorbance for POEGMA NBC in Acidic, Basic and Neutral Media

The spectra in figure 5-13, represent UV spectral measurements achieved for NBC dye in methanol. The absorbance peak for NBC dye in a basic solution was observed at 545 nm, while NBC dye absorbance peak observed from a neutral solution was at 535 nm not too further away. On the contrary, the absorbance peak of NBC dye in an acidic medium, recorded 665 nm. This is a large difference compared to those from a basic and neutral medium. This is expected, as it serves the basis required for pH responsiveness as observed in the work of Madsen et al 2018.

5.4.7 Effect of pH variation on NBC labelled/capped PoegMA brushes

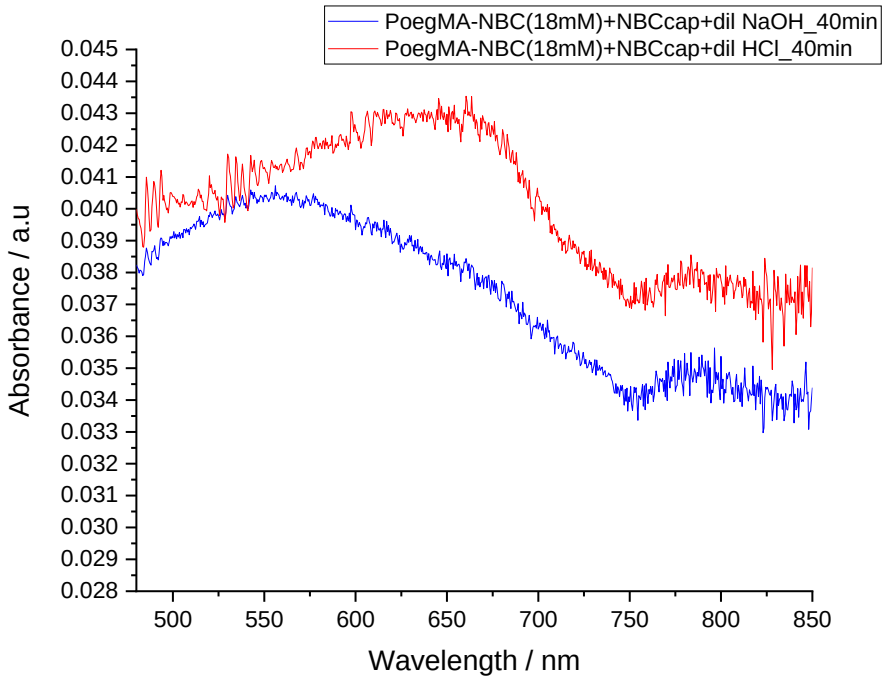

Figure 5-14: Spectral Peaks Showing Wavelength of Absorbance for POEGMA NBC in Acidic and Basic Media

The NBC labelled/capped PoegMA brushes were immersed into solutions of dilute base and dilute acid to produce the absorption peaks shown in figure 5-14. A distinguishing response was observed for the sample measured in dilute acid solution. It shifted towards the longer wavelength of absorption at 650 nm corresponding to a red shift. Thus depicting a positive response to changes in pH as earlier seen in figure 5-13 for NBC solution.

5.5 Influence of ATRP initiator and NBC on polymerization kinetics

5.5.1 S.E Measurments of Brush thickness

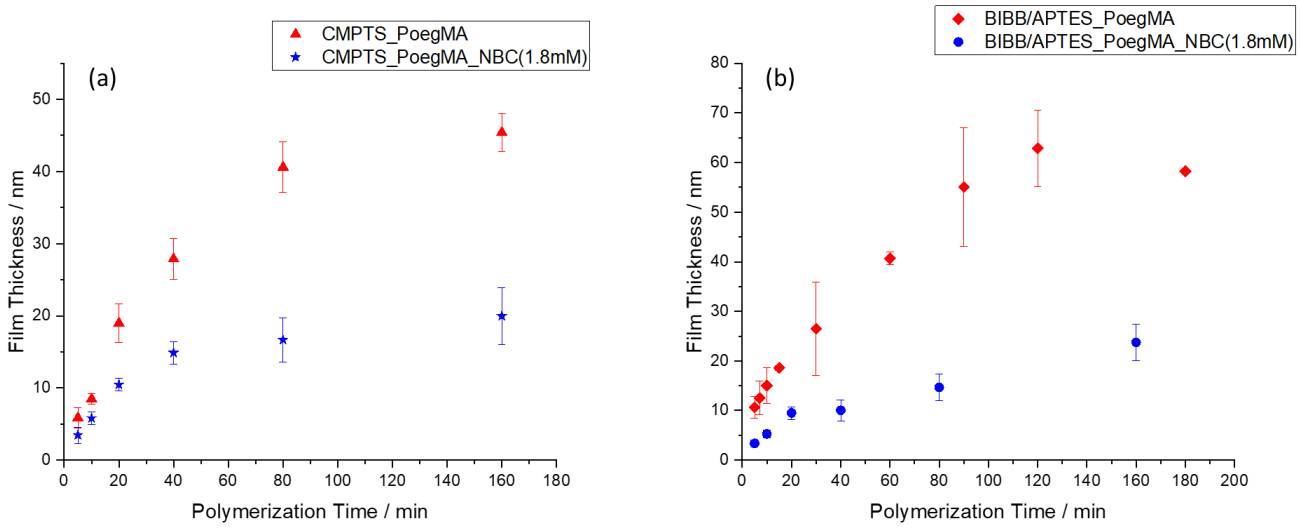

Figure 5-15: S.E Film Thickness Growth Profile for (a) CMPTS POEGMA Brushes with and without NBC Dye and (b BIBB-APTES POEGMA Brushes with and without NBC Dye

In figures 5-15a and 5-15b, the kinetics of growth of POEGMA brushes were compared for two different initiators, Cl and Br (adsorbed films of CMPTS and BIBB-APTES, respectively). For each initiator, polymerisation kinetics were additionally compared in the presence and absence of NBC. Figures 5-15a and 5-15b show the polymer brush dry thickness as a function of the polymerisation time, as determined using spectroscopic ellipsometry.

For Cl initiators, the POEGMA brush thickness increased approximately monotonically for 80 min, reaching a dry thickness of 40 nm after 80 min (Figure 5-15a). Thereafter, the rate of polymerisation slowed dramatically, and the film thickness increased very little at longer times, reaching 42 nm after 160 min.

When NBC was added to the polymerisation reaction mixture at a concentration of 1.8 mM, the rate of growth of the brush layer was found to be significantly reduced. The dry thickness of the polymer film reached only 13 nm in the first 40 min of polymerization, and increased to a maximum value of only 18 nm after 160 min. the difference between the NBC labeled and non labeled CMPTS POEGMA growth kinetics is quite significant as it adds up to an average of 65% gap between each corresponding points as seen in Figure 5-15a.

When Br was used as the initiator, growth in the dry brush thckness was again monotonic, reaching a thickness of 52 nm after 80 min. At each time point, the brush thickness was higher for the films grown from Br initiators, reflecting the expected faster kinetics for Br compared to Cl initiators.[151] At longer polymerisation times, the dry brush thickness increased comparatively little, increasing by only 20 nm when the time was increased to 160 min.

The data in Figure 5-15b show that addition of NBC to the reaction mixture also slowed the polymerisation reaction, with a significntly reduced film thickness being measured at all polymerisation times. The addition of NBC was found to reduce the thickness of the polymer film by ~60%.

These observations provide clear evidence for the inhibitory effect of NBC on the polymerisation reaction. This can be attributed to the reaction inhibition caused by NBC acting as a chain transfer agent, or as an electron trap halting the progress in the growth of the polymer.

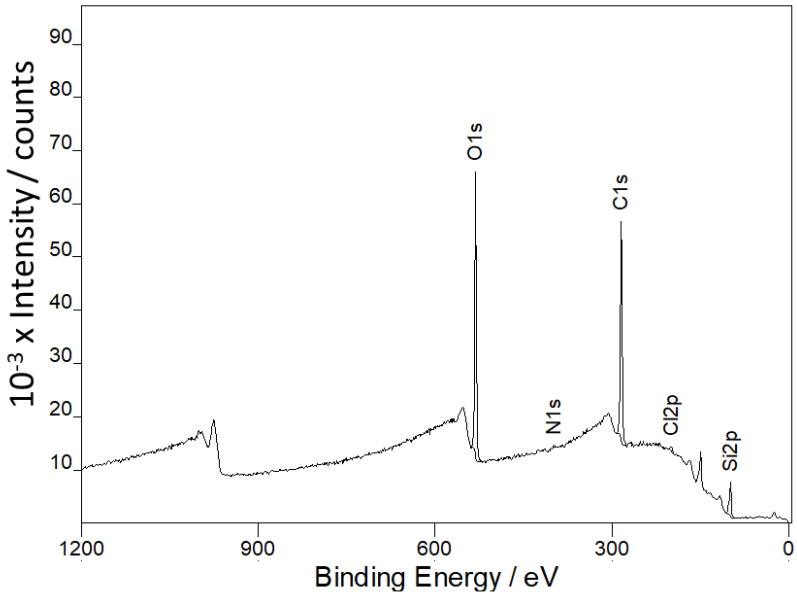

Figure 5-16: XPS Wide Scan for POEGMA Brush with incorporated NBC on glass substrate

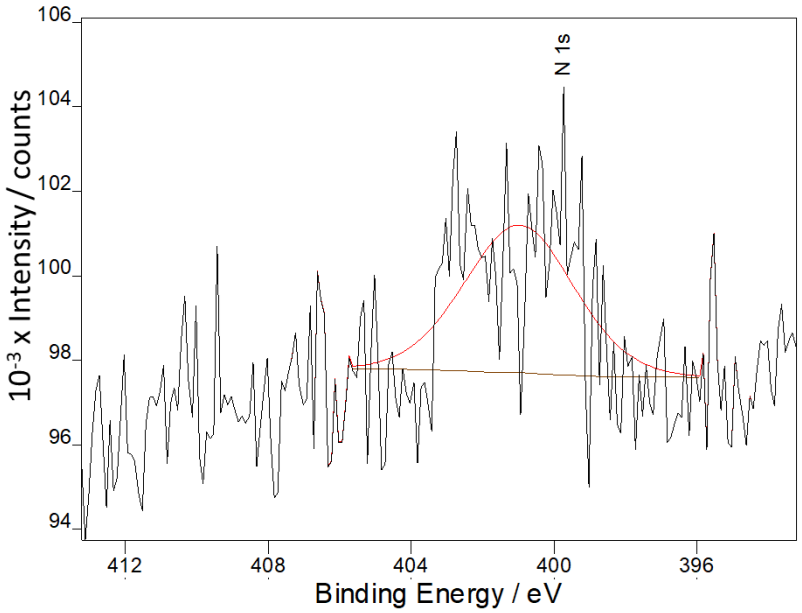

Figure 5-17: XPS High Resolution Scan for POEGMA Brush with incorporated NBC on glass substrate

X-ray Photoelectron Spectroscopy (XPS) wide scan was performed on NBC labeled POEGMA samples and the spectra in figures 5-16 and 5-17 were reported for the chemical environments on the surface. Figure 5-16 revealed a very intense C1s peak at 285 eV which about three quarters of O1s peak, an indication that some layers of polymer exist on the surface. The wide scan spectrum also shows N1s at 402 eV which is about 0.3% of C1s peak intensity. The Si2p peak on the other hand appeared as a sixth of C1s peak . This is an indication that Silicon surface has been covered by some layers of polymer. Similarly, Figure 5-17 shows a high resolution spectrum of N1s at about 402 eV, though the peak appeared less intense, it however is an evidence for the presence of N1s on the sample surface.

5.6 Covalent attachment of Modified Nile Blue to polymer brush scaffolds

To test whether higher degrees of dye binding could be achieved using covalent coupling to pendant amine groups on PCysMA, two different reactions were compared. Both relied upon the modification of the pendant amine groups of the polymer to introduce reactive functional groups that would bind Nile Blue derivatives with amine linkers. Bifunctional linkers (glutarldehyde and DSS); in both cases, one end of the linker coupled to an amine on the polymer, and the other remained free for conjugation to the dye. In these experiments, a fixed polymerisation time of 40 min was used throughout, yielding a polymer brush thickness of 20 nm. This enabled investigation of the kinetics of dye-polymer binding.

The spectra in figure 5-18 below, represents UV spectral measurements achieved for amine-modified Nile Blue disolved in ethanol. Its absorption peak in a basic solution was observed at 530 nm, while in an acidic solution was at 660 nm as depicted in figure 5-18.

This is a large difference and it is expected to serve as the basis required for pH responsiveness.

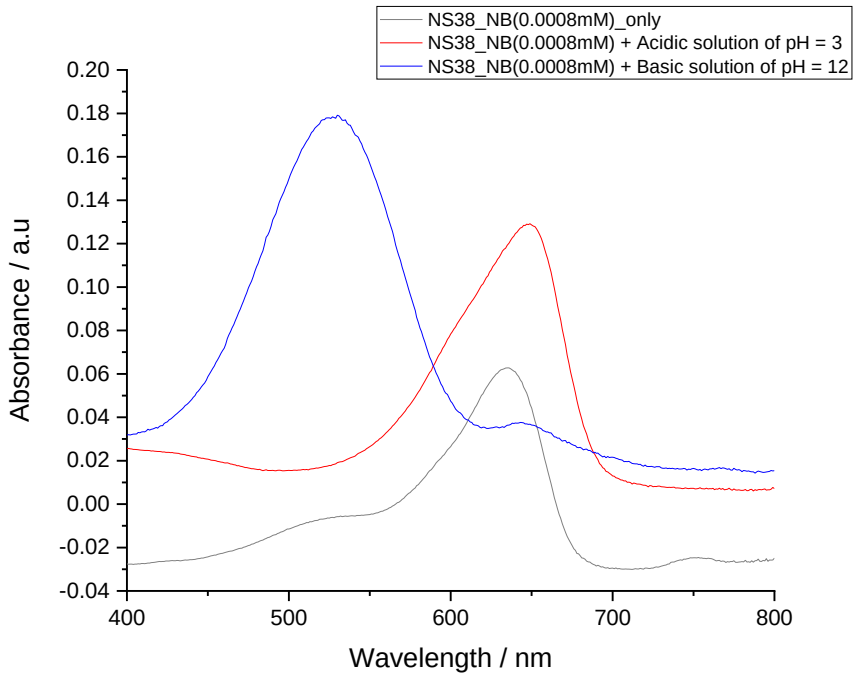

Figure 5-18: Wavelength of Absorbance for Modified Nile Blue in Both acidic and basic media

5.6.1 Conjugation of Nile Blue to PCysMA using DSS

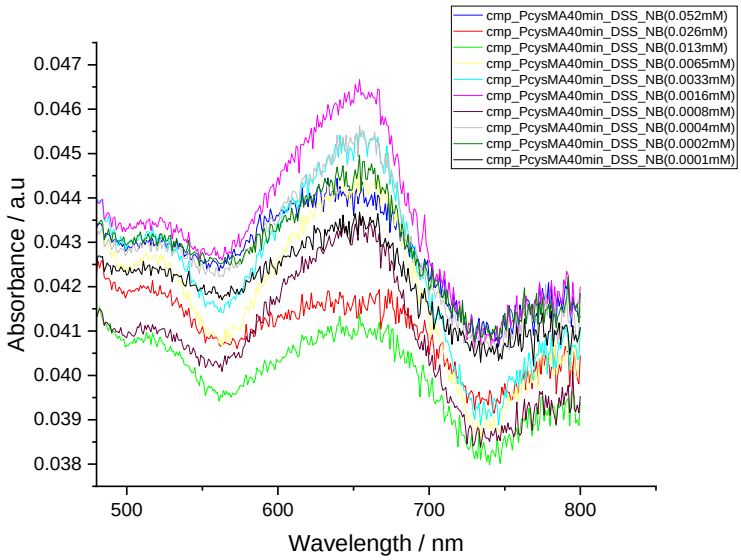

Figure 5-19: Absorption Intensity Peaks for PCysMA DSS-Nile Blue

Polymer brush films were incubated in DSS solutions with a range of concentrations. It is striking that for all of these samples, a strong absorption is observed at 660 nm, in contrast to the behaviour observed for NBC-labelling of POEGMA brushes. Such occurrence could probably be as a result of the dielectric environment of the polymer. PCysMA is zwitterionic, whereas POEGMA is uncharged. Data in figure 5-19, showed the highest peak intensity of 0.0465 a.u at 660 nm was observed for about 15 nm film thickness of CMPTS PCysMA brush that reacted with 0.0016 mM of modified Nile Blue for 24 hours at 50^{o}c, while the lowest of 0.041 a.u intensity at 660 nm was observed for the CMPTS PCysMA brushes that reacted with 0.013 mM of modified Nile blue dye. The CMPTS PCysMA brushes that reacted with lower concentrations of modified Nile blue appeared with much stronger peak intensities compared to those that reacted with a much higher concentrations of the modified Nile blue dye.

5.6.2 Effect of pH variation on Amine-modified Nile Blue Conjugated to PCysMA using DSS

The data in figures 5-20 and 5-21 are UV-vissible spectra observed for pH responsiveness of varying solution concentation of modified Nile blue that reacted with DSS derivatized CMPTS PCysMA brushes. The spectra did not reveal any change in peak positions for all the various modified Nile blue concentrations that reacted and were observed earlier with peaks at 660 nm.

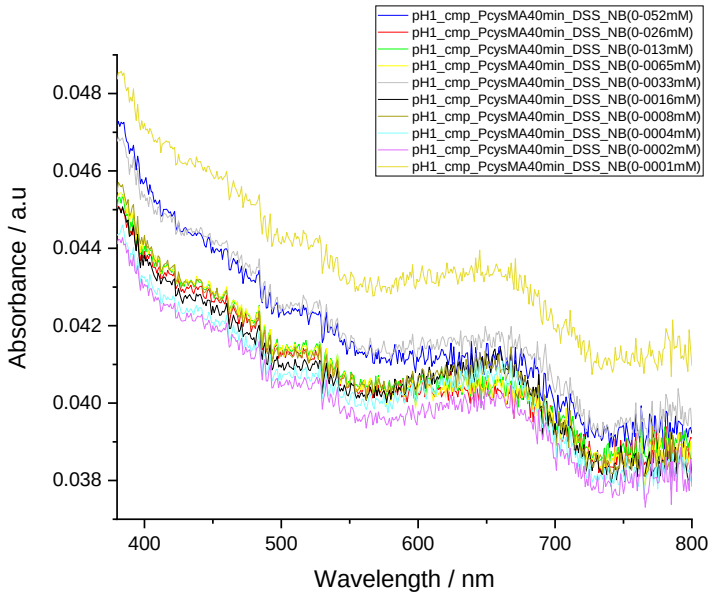

Figure 5-20: Absorption Intensity Peaks for PCysMA DSS for pH Responsiveness at pH 1

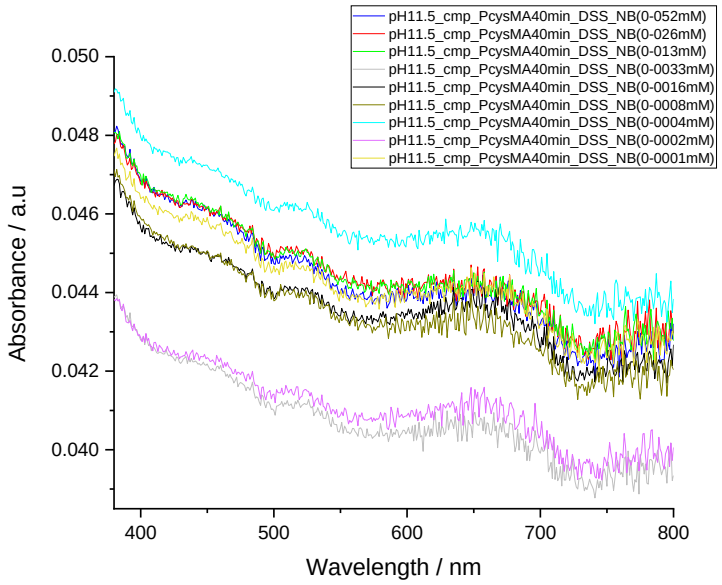

Figure 5-21: Absorbance Intensity Peaks of PCysMA DSS for pH Responsiveness at pH 11.5

5.6.3 Conjugation of Nile Blue to PCysMA using Gluteraldehyde

The data in figure 5-22, showed CMPTS PCysMA brushes that was derivatized with gluteraldehyde before the reaction with varying solution concentrations of modified Nile blue dye as described (see section 5.2.4). The highest peak intensity of about 0.046 a.u at 660 nm was observed for about 15 nm film thickness of CMPTS PCysMA brush that reacted with 0.0008 mM of modified Nile Blue for 24 hours at 50^{o}C, while the lowest of 0.036 a.u intensity at 660 nm was observed. Similar to the CMPTS PCysMA brushes that was derivatized with DSS, the gluteraldehyde derivatized brushes that reacted with lower concentrations of modified Nile blue also appeared with much stronger peak intensities compared to those that reacted with a much higher concentrations of the modified Nile blue dye. This trend suggest that despite being observed as absorption peaks at 660 nm,

the higher solution concentration of modified Nile blue reacting with the derivatized CMPTS PCysMA brushes, do not significantly determine the intensity of the absorption peaks.

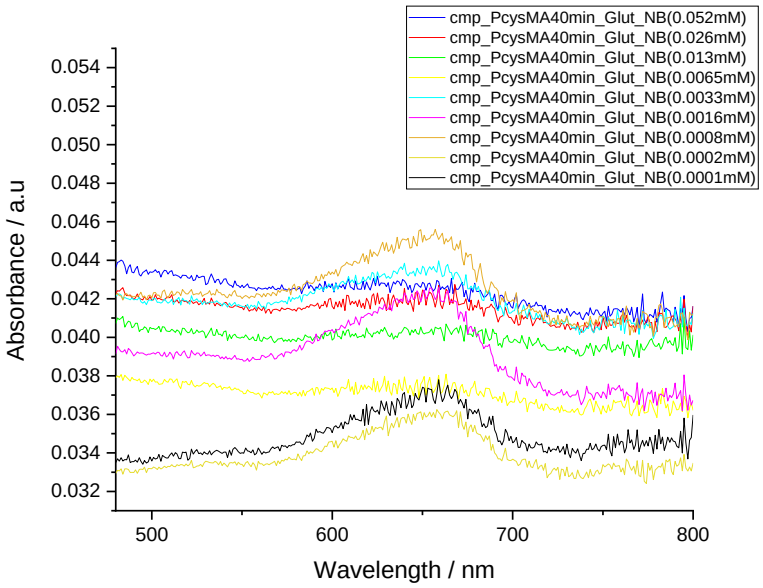

Figure 5-22: Absorbance Intensities Peaks of PCysMA Gluteraldehyde-Nile Blue

5.6.4 Effect of pH variation on Amine-modified Nile Blue Conjugated to PCysMA using Gluteraldehyde

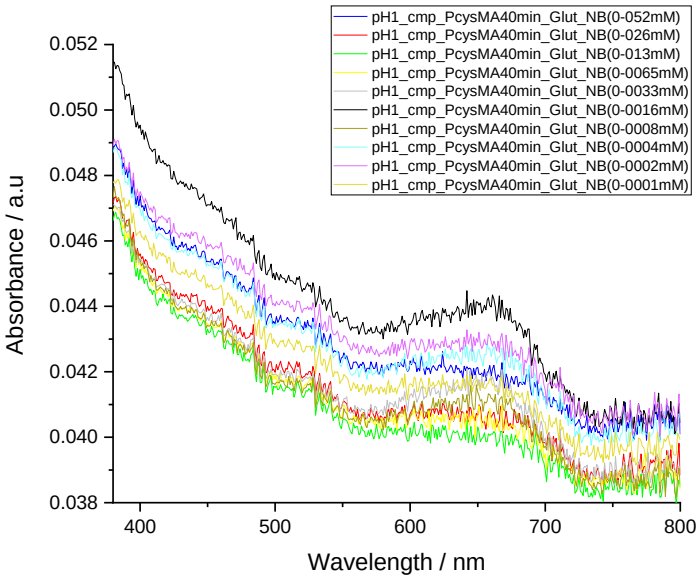

Figure 5-23: Absorbance Intensity Peaks of PCysMA Gluteraldehyde for pH Responsiveness at pH 1

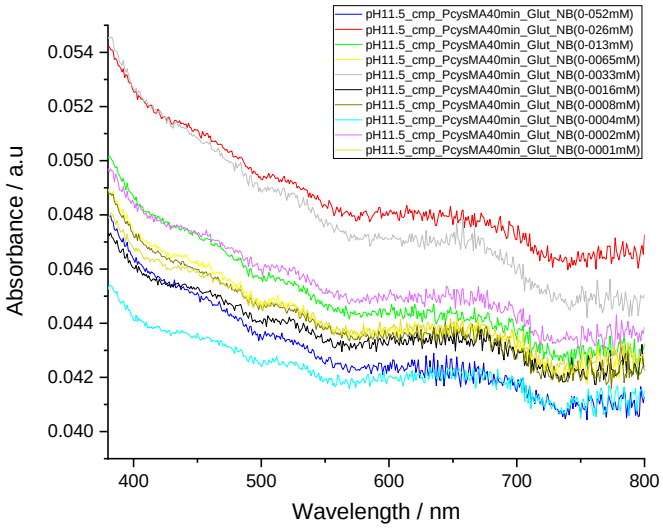

Figure 5-24: Absorbance Intensity Peaks of PCysMA Gluteraldehyde for pH Responsive at pH 11.5

The data in figures 5-23 and 5-24 are UV-visible spectra observed for pH responsiveness of varying solution concentation of modified Nile blue that reacted with gluteraldehyde derivatized CMPTS PCysMA brushes. The spectra did not reveal any change in peak positions for all the various modified Nile blue concentrations that reacted which were originally at 660 nm. This trend was similarly observed for the DSS derivatized CMPTS PCysMA brushes. Since, pH responsiveness was exibited when the solution of modified Nile blue was measured in both basic and acidic media as was presented in figure 5-18 earlier, inactivity for the modified Nile blue functionalized PCysMA, was not expected.

5.6.5 XPS analysis and Depth Profiling

Table 5-1: XPS PCysMA Brushes Nile Blue for Different Polymerization

Sample ID	Cl2p	O1s	N1s	C1s	S2p	Si2p
CMPTS	1.06	58.67	0	13.92	0	25.81
PCysMA 10min + NB	0.31	0	4.19	83.49	2.79	9.21
PCysMA 20min + NB	0.06	0	4.44	88.99	3.89	2.64
PCysMA 40min + NB	0	0	4.4	89.76	3.88	1.94
PCysMA 80min + NB	0.07	0	4.54	89.58	4.13	1.65

The data in Table 5-1 was obtained from high resolution scan of CMPTS PCysMA surface that reacted with the modified Nile blue dye. Table 5-1 provides an overview of its percentatage atomic composition. Cl2p was seen to have decreased hugely from 1.1% to 0.3% at the start of polymerization from CMPTS surface to PCysMA surface respectively, while S2p increased from 0% to about 4%. C1s atomic composition increased remarkably from 14% to about 90% while Si2p decreased sharply from 26% to 2%, providing clear evidence of surface coverage by modified Nile blue CMPTS PCysMA brushes. Although not much can be seen regarding the presence of the modified Nile blue from the data provided in Table 5-1 however, the overlayed wide scan spectra in Figure

5-25 below has provided enough evidence about the presence of nitrogen from the modified Nile blue which clearly is shown by the increasing intensity of the neutral N1s at 399 eV, signifying that more of the modified NB is coupled to brushes with increasing film thickness as the polymerization time progresses.

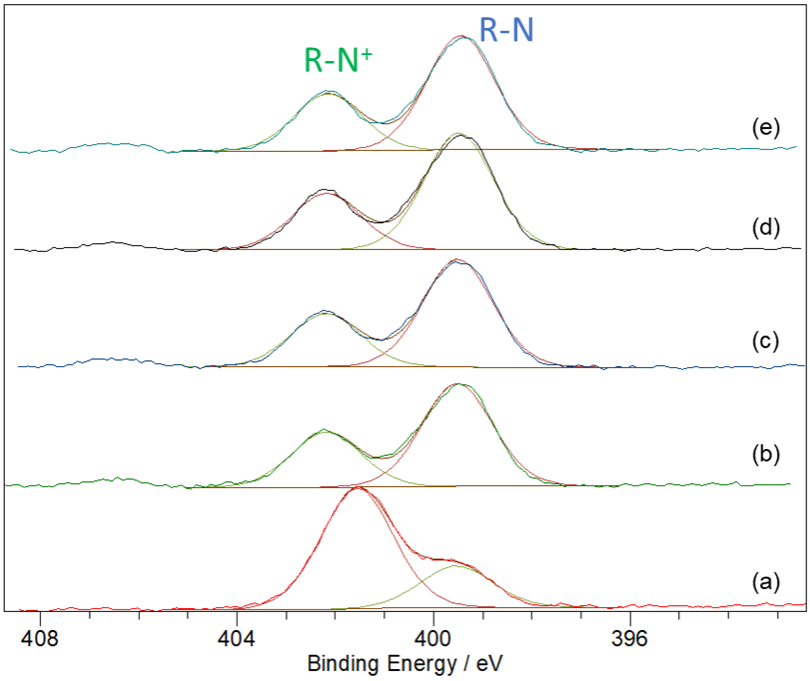

Figure 5-25: XPS PCysMA Brushes at Different Polymerization Time coupled to modified Nile Blue (a) CMPTS PCysMA N1s Peak, (b) N1s peak for 10 min PCysMA Brush Coupled to Modified NB (c) N1s peak for 20 min PCysMA Brush Coupled to Modified NB (d) N1s p

Figure 5-25 show XPS N1s spectra of CMPTS PCysMA surface that reacted with the modified Nile blue dye. The PCysMA sample spectrum is represented as (a) showing a noticeably weak N1s peak at 399 eV. Much stronger intensities of N1s at 399 eV are noticeable in figure 5-25 (b), (c), (d) and (e) with increasing peak intensities corresponding to modified NB coupled PCysMA grown at 10 min, 20 min, 40 min and 80 min respectively.

Thus, giving an indication that the amount of NB coupling to PCysMa brushes increases with increasing brush thickness.

Table 5-2: XPS PCysMA Brushes Nile blue for DSS and Gluteraldehyde

Sample ID	Cl2p	O1s	N1s	C1s	Si2p	F1s
CMPTS	1.06	58.67	0	13.92	25.81	0
PCysMA 40min	0.45	37.13	3.09	52.75	6.84	0
PCysMA + DSS	0.22	37.33	2.98	52.14	7.25	0
PCysMA + DSS +TFEA	0.12	39.68	2.69	47.62	8.67	1.35
PCysMA + DSS + NB	0	36.55	3.11	51.95	8.15	0
PCysMA + Glut +NB	0	28.75	3.09	65.26	2.84	0

Table 5-2 and Figure 5-26 show XPS high resolution spectra data of a number of sample substrates analyzed to ascertain the atomic constituents present. Starting with the CMPTS sample, nitrogen was not found in the spectral representation for CMPTS in figure 5-26, as well as a 0.0% atomic composition on the sample surface as shown in Table 5-2. Thus, confirming the absence of nitrogen from CMPTS sample as expected. For the sample consisting of PCysMA brushes grown for 40 min, there is a significant N1s peak present at 402 eV in figure 5-26. This corresponds to the protonated amine from PCysMA brush layer. Its composition adds up to 3.09% N1s presence in the atomic composition on the sample surface as shown in Table 5-26. Much more intense N1s peaks are shown at 399 eV in figure 5-26 representing nitrogen environment contribution on the surface due to coupling of trifluoroethylamine (TFEA) and disiccinimidyl suberate (DSS) to PCysMA brushes. Furthermore, surfaces functionalized with amine-modified NB couple to PCysMA brushes through glutaradehyde (Glut) and DSS linkers revealed very prominent N1s peaks at 399 eV in figure 5-26, as well as constituting 3.09% and 3.11% of the total surface composition. Thus, confirming the presence of modified NB in the PCysMA brushes.

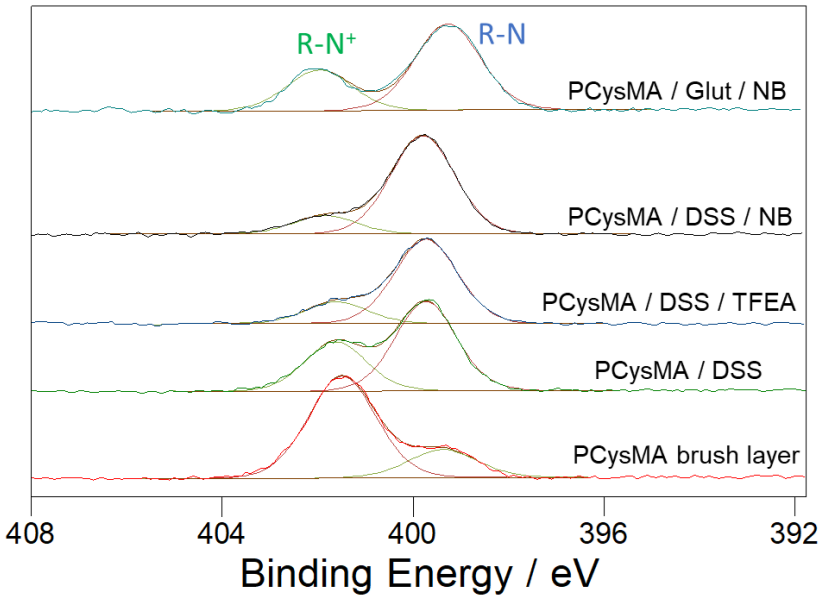

Figure 5-26: XPS N1s Spectra of PCysMA Brushes Coupled to Nile Blue through DSS, Gluteraldehyde and TFEA

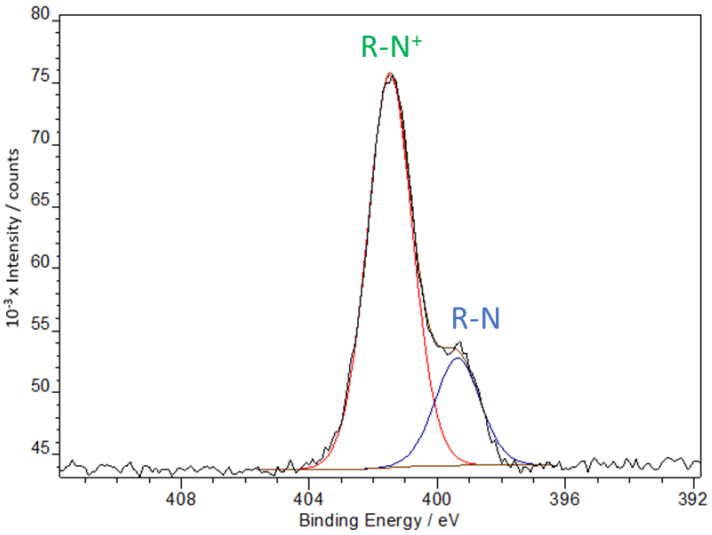

Figure 5-27: XPS N1s spectrum of a PCysMA brush at 40 min polymerization time

The spectral fitting in Figure 5-27 above represents, high resolution spectrum of N1s with two component fittings in the ratio of 3 : 1 corresponding to protonated N1s peak at 402 eV and unprotonated N1s peak at 399 eV in PCysMA.

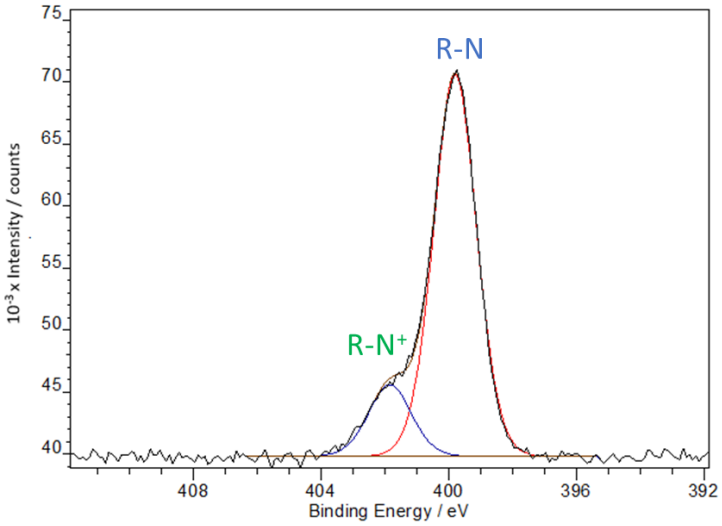

Figure 5-28: XPS N1s spectrum of a PCysMA brush following activation with DSS and coupling to amine functionalized Nile Blue

The spectral fitting in Figure 5-28 above represents, high resolution spectrum of N1s with two component fittings of PCysMA becoming transformed owing to derivatization with DSS and reaction with modified Nile blue resulting in a change in ratio of N1s at 402 eV to N1s at 399 eV from ratio of 3 : 1 to ratio 1 : 4 corresponding to N1s (399 eV) contributions from DSS and modified Nile blue.

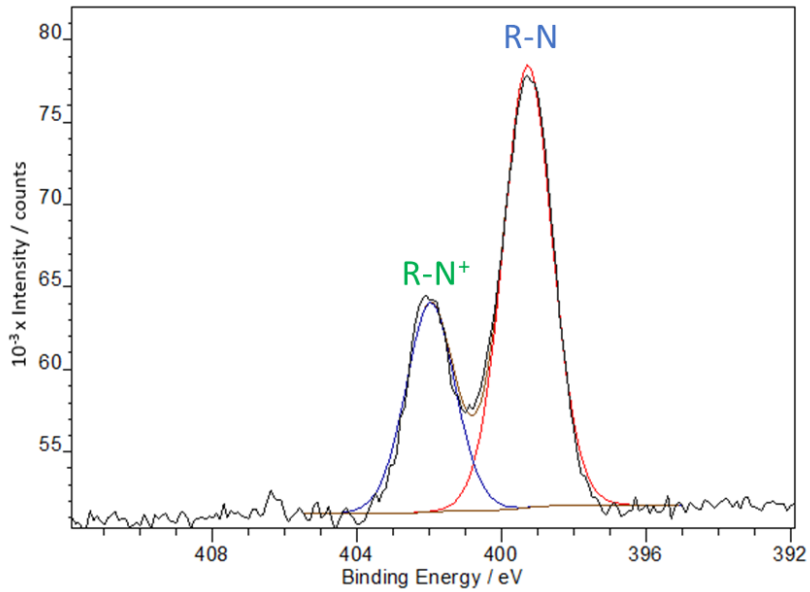

Figure 5-29: XPS N1s spectrum of a PCysMA brush following activation with glutaraldehyde and coupling to amine functionalized Nile Blue

The spectral fitting in Figure 5-29 above represents, high resolution spectrum of N1s with two component fittings of PCysMA becoming transformed owing to derivatization with gluteraldehyde and reaction with modified Nile blue resulting in a change in ratio of N1s at 402 eV to N1s at 399 eV from ratio of 3 : 1 to ratio 1 : 2 corresponding to N1s (399 eV) contribution from modified Nile blue.

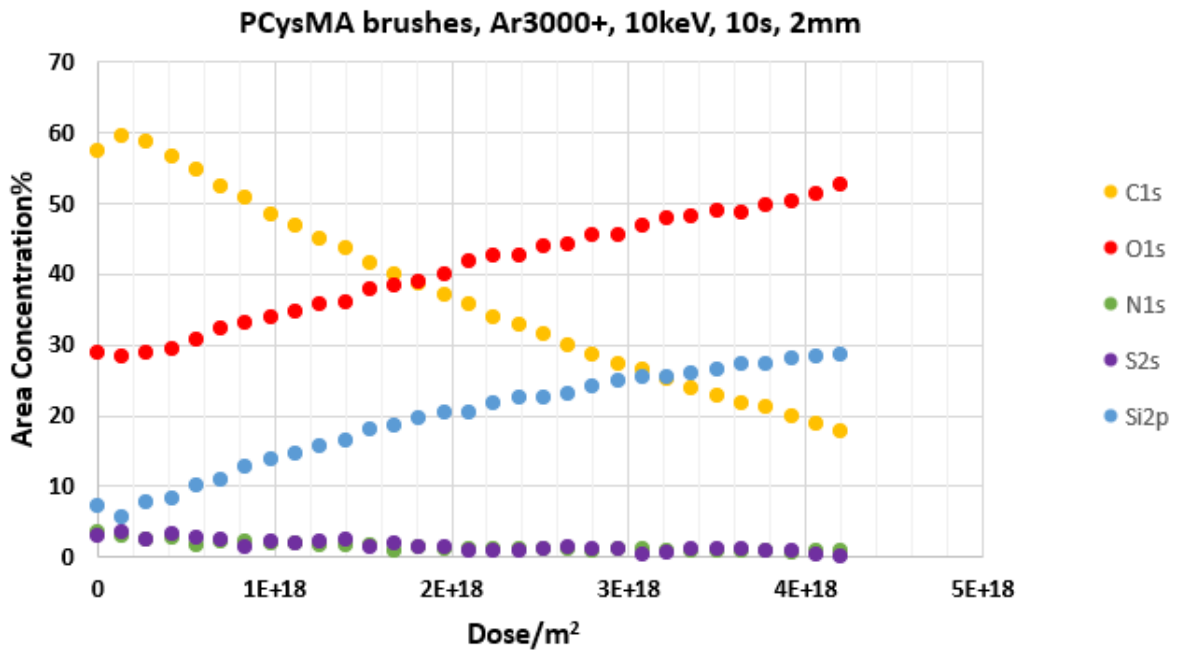

Figure 5-30: XPS Depth Profile Scan for PCysMA Brush Coupled to NB

From the depth profiling information seen in Figure 5-30, a change occurred in the whole polymer brush reaching the interface between polymer and the substrate. This can also be interpreted from elemental composition at the interface were carbon crosses oxygen.

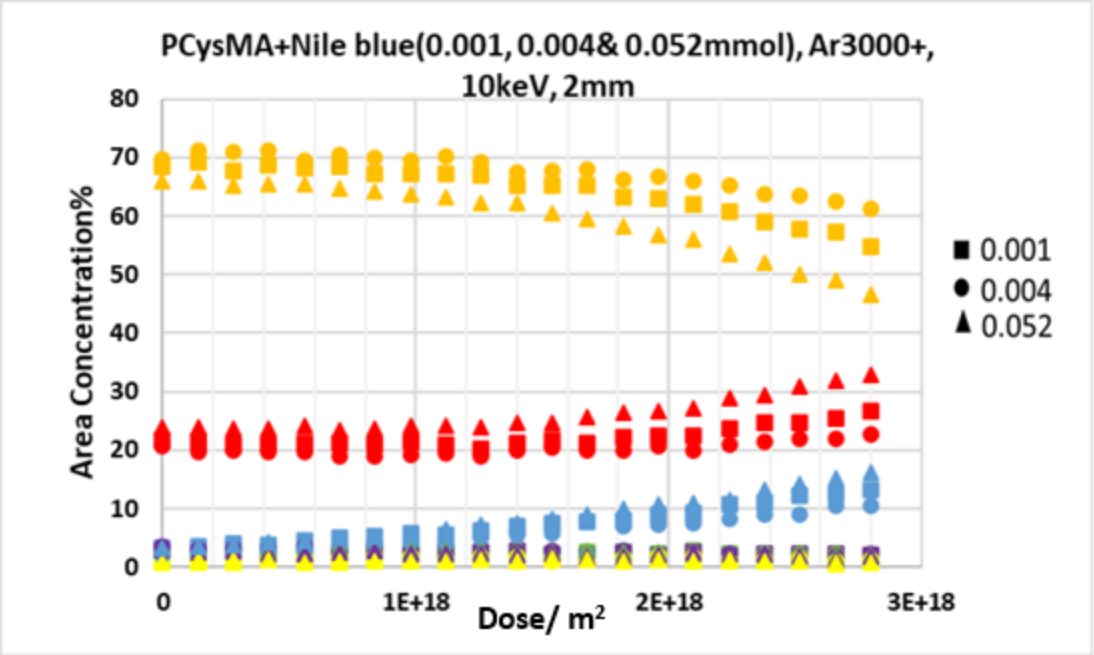

Figure 5-31: XPS Depth Profile Scan for PCysMA Brush NB for Three Samples

From the depth profiling information seen in Figure 5-31, there was no significant difference resulting from the change in concentration of the modified Nile blue from 0.001 mM to 0.052 mM. This was also noticed earlier in Figures 5-19 and 5-22 above.

5.7 Conclussion

74.5% yield corresponding to 0.83g of Nile blue 2-(methacryloyloxy) ethyl carbamate was synthesised and characterised by NMR and mass spectrometry the data obtained correlated with the findings from the work of Madsen et. al, 2018. The three methods for the introduction of Nile blue dye into the polymer brushes were performed. Although they were not all entirely a success. There were however, relative successes in a couple of the methods used. For example, inspite of very weak absorbance intensities seen for NBC dye and of the very low concentrations that acually got labelled and capped in the POEGMA brushes, the brushes successfully showed a positive pH responsiveness when

measured in a basic as well as acidic media. In addititon, data from ellipsometry measurements showed that NBC dye was successfully introduced into the POEGMA brushes as shown from the retardation or inhibited film thickness observed in the growth profile or growth kinetics seen in Figures 5-15a and 5-15b. The XPS wide scan and high resolution spectra in Figure 5-25 and 5-26 also confirmed NBC dye incorporation into the POEGMA brushes. On the other hand, the amine-modified Nile blue dye, showed prominent absorbance peak intensities for Nile blue at 660 nm even at very low concentrations. The successful incorperation of the *ratiomeric* NBC dye into the polymer brush structures, will form the basis for the fabrication of the two component brush regime with pH sensing capability.

CHAPTER 6: COMPARATIVE STUDIES OF SURFACE-GRAFTED POLYMER ON SURFACES WITH VARYING INITIATOR DENSITIES

6.1 Introduction

Polymer brushes provide a powerful method for controlling surface chemistry and interactions. The fabrication of microsystems on surfaces have been actioned via the utilization of the varying properties exhibited by these brushes enabling the construction of multi-component brush regime. The brush structure can take the form of an assembly of charge neutral polymer and a zwitterionic polymer as well as amphoteric polymer brushes on surfaces to enhance the functioning ability of the device.[21,159]

Polymer brushes offer a variety of advantages such as control of brush thickness, capacity for formation of copolymers and the ease of derivatization and coupling to other reactive groups. However, polymer patterning is more complicated, particularly where it is necessary to organize multiple components.[15,16] Compartmentalization is important in biological systems. Cells are contained in membranes, and within cells organelles are also enclosed within membrane systems. Cells represent fundamental functional unit for the existence of all living organisms.[22] The location of important functional components of cells are in membranes.[4] A high fraction of the targets of antibiotics are bound by membrane structures. In recent years microfabrication of miniaturized study platforms or microsystems are being investigated via incorporation of polymer brushes and Supported lipid bilayers (SLBs) for the application of several cellular processes.[7]

To answer many fundamental questions in biology it is necessary to create model systems in which components can be localized at specific regions. In this study, we aim to form patterned surface on initiator films to facilitate the construction of a multi-

component brush system. To measure membrane transport processes, it is additionally necessary to be able to incorporate into the system a means to measure the rates of membrane transport processes such as proton transfer.

The main aim of this chapter is to explore methods for constructing polymer brush microsystems that might ultimately be used as workbenches for studying biological processes. The aim is to build a structure consisting of well-defined corrals that incorporate a pH-responsive reporter. The system will comprise walls formed from biologically inert POEGMA brushes incorporating an integral sensor NBC dye, along with a PCysMA brush platform chosen for the corrals because it supports membrane diffusion – it could be used to contain model supported lipid bilayers.

The main questions are: Can we incorporate dye? How do structures and properties depend on grafting density? What method of dye binding will be employed?

The microsystem is to be designed in such a way that it incorporates reporters for the *in-situ* measurements of membrane transport. Silane films of 3-(2-bromoisobutyramido) propyltriethoxysilane (BIBB-APTES) and 4-(chloromethylphenyl) trichlorosilane (CMPTS) initiator monolayers were deployed to achieve significant functionalization and control of various silicon surface chemistry. The formation of these self-assembled monolayers on surfaces is to usher in a uniform optimal condition for surface modification via polymer brush growth to facilitate the construction of a two-component brush structure.

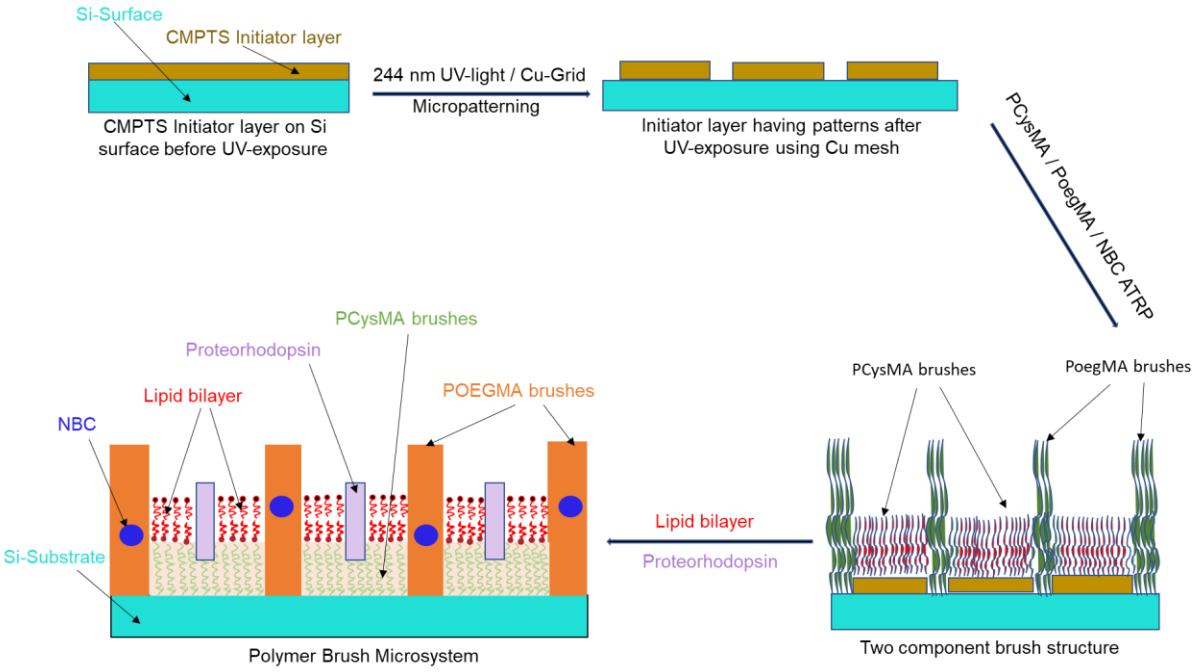

Figure 6-1: Schematic Pathway for the fabrication of Polymer Brush Microsystem

6.2 Experimental

6.2.1 Materials and Methods

Analytical reagent grade 2-bromoisobutyrylbromide (BIBB) 98% purity, triethylamine (TEA) 99% purity, 3-aminopropyltriethoxysilane (APTES) 98% purity, 2,2-bipyridyl 99% purity were supplied by Sigma Aldrich (Gillingham, UK). 4-(chloromethylphenyl)trichlorosilane was supplied by Alfa-Aesar (Lancashire, UK). N,N-dicyclohexylcarbodiimide (DCC) 99% purity and benzoyl bromide (BnB) 97% purity were supplied by Sigma Aldrich (Gillingham, UK). Other HPLC grade chemicals were obtained from Fisher Scientific (Loughborough, UK). These included: ethanol, isopropyl alcohol, dichloromethane, hydrogen peroxide, acetone, toluene, methanol and ethyl acetate. De-ionized water was obtained from an Elgar purification unit (Elgar, pure nanopore 16 MΩ).

BIBB-APTES and CMPTS films were formed on silicon surfaces as described previously in chapter 3, sections 4 and 5 respectively. Polymer brushes were grown from initiator-functionalised surfaces by surface-initiated atom-transfer radical polymerisation as described in chapter 3.

6.2.2 Photo-modification of Surfaces

Photo-modification of samples was carried out using a frequency-doubled argon ion laser emitting at 244 nm (Coherent Innova 300C FreD, Coherent, Ely, UK). The maximum laser power was 100 mW cm^{-2}. To ensure that the laser beam was fully stabilized, it was turned on for 40 min prior to usage. For micro-patterning, the laser beam (diameter ~0.8 mm) was deflected using a mirror placed at 45^{o} to the incident beam and expanded using a divergent lens, enabling irradiation of a region ~1 cm^2 in area.

Sample slides were cut to rectangles with dimensions of 5 mm x 7 mm. After cutting, samples were rinsed with ethanol to remove debris and dried under a stream of nitrogen. Following exposure to the UV laser beam, unpatterned samples were characterized by contact angle measurement, spectroscopic ellipsometry and XPS (see chapter 3 for details).

For micropatterning, the laser beam was focused on to the sample to expose an area of about 2 mm^2. An electron microscope Cu 2000 mesh grid (Agar, Cambridge, UK) was used as a mask (Figure 6-2). The grid that was used consisted 2000 lines per inch forming a pattern of bars at right-angles to each other, resulting into a periodic array of square holes. The pitch of the grid was 12.7 µm. The Cu grid was placed on the sample surface and held in position by a quartz disc during exposure, to prevent warping of the grid. At

the end of the exposure period, the sample was removed and cleaned with ethanol before being dried under a nitrogen gas stream.

The dose at the sample surface is given by the equation:

$$t = \frac{D \cdot \pi \cdot r^2}{LP}, \quad \text{..... (6.1)}$$

where t is the Exposure time [sec], D is the Dose of exposure [J/m^2], r is the sensor radius (0.25 x 10^{-2} m), LP is the Laser power on sample [W], and π = 3.14.

Micropatterned samples were characterized using atomic force microscopy.

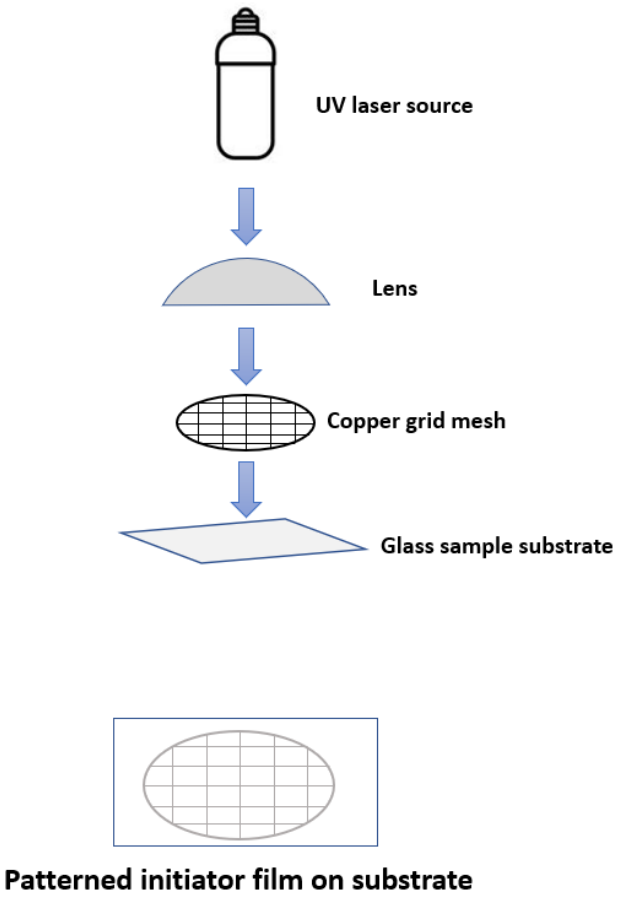

Figure 6-2: Set-up for UV Modification yielding Patterned and Un-patterned Initiator Films

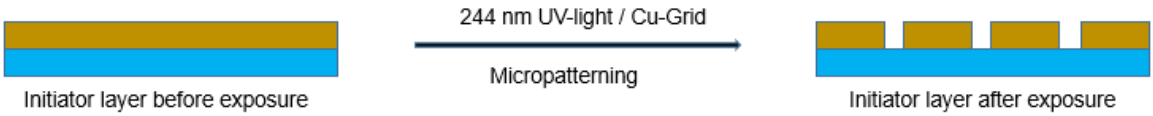

Figure 6-3: Schematics Showing Initiator Films on Substrate before and after UV Modification using a Cu-Grid to achieve a Patterned Substrate

6.2.3 Photo-modification of CMPTS Films

The schematic in figure 6-4 represents the pathway for the photo-catalytic oxidation of benzyl chloride group in CMPTS initiator films by UV-exposure of about 5 Jcm^{-2} through a 2000 copper grid mesh on the CMPTS film surface. The copper mesh protects the unexposed benzyl chloride group directly under the mesh bars from UV-light, as well as allowing UV-oxidation of the C-Cl bond present in the unprotected benzyl chloride to a phenyl radical, before conversion into a benzaldehyde and finally to benzoic acid.

Carbon-halogen bonds are susceptible to photolysis on exposure to UV light.[160] Figure 6-4 shows the mechanism for the photochemical reaction thought to occur when CMPTS is exposed to UV light in the presence of oxygen. C-Cl bond cleavage yields a benzyl radical, which reacts with oxygen to form an aldehyde. Further exposure to UV light leads to further photochemical oxidation to yield a benzoic acid derivative as the final product.

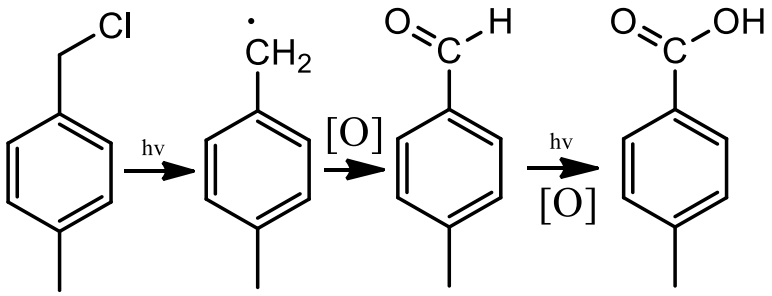

Figure 6-4: Reaction Pathway for the Photo-Catalytic Oxidation C-Cl bond of CMPTS Films to Carboxylic acid Using UV-Exposure Doses

Exposure of initiator-functionalised surfaces to UV light was expected to cause scission of carbon-halogen bonds, leading to a reduced grafting density during ATRP. To examine the effect of the reduced grafting density on the properties of polymers grown by ATRP, two types of measurement were carried out. First, samples were exposed to UV light through a mask, and the height difference between masked and exposed areas was measured as a function of the UV dose using AFM. Second, films with varying initiator densities were prepared by reacting APTES-functionalised substrates in solutions of BIBB and benzoyl bromide.

6.2.3.1 Preparation of two-component polymer brush pattern

CMPTS surfaces were formed as previously described in chapter 3 section 5. Initiator patterned surfaces were generated by a selective exposition of CMPTS functionalized surfaces to 244 nm UV-laser through a Cu-grid mesh. This procedure caused the CMPTS substrates to become de-chlorinated forming benzoic acid terminated surfaces in the square areas of the patterned CMPTS initiator substrates, while maintaining the benzyl chloride UV-laser protected portions in the mesh bars areas of the substrates. This was followed by the immersion of the patterned CMPTS substrates in a solution made up of

10.0 µL glycerol and 0.31g dicyclohexylcarbodiimide (DCC) dissolved in 15.0 mL of dichloromethane (DCM) for 16 h at 20^0C to generate esterified surfaces on the square portions of the patterned CMPTS substrates. The benzyl chloride surfaces in the protected bar areas of the patterned CMPTS substrates were polymerized in a nitrogen atmosphere forming POEGMA brushes as previously outlined in section 4.2.6. Similarly, BIBB surfaces were generated on the esterified square portions of the patterned CMPTS surfaces as outlined earlier in section 4.2.2. Furthermore, PCysMA brushes were formed from the BIBB surfaces generated in the square portions of the CMPTS patterned substrate as outlined previously in section 4.2.5. Consequently, a two-component polymer brush system of POEGMA and PCysMA brushes is formed on the CMPTS substrate as schematically outlined in Figures 6-1 and 6-5.

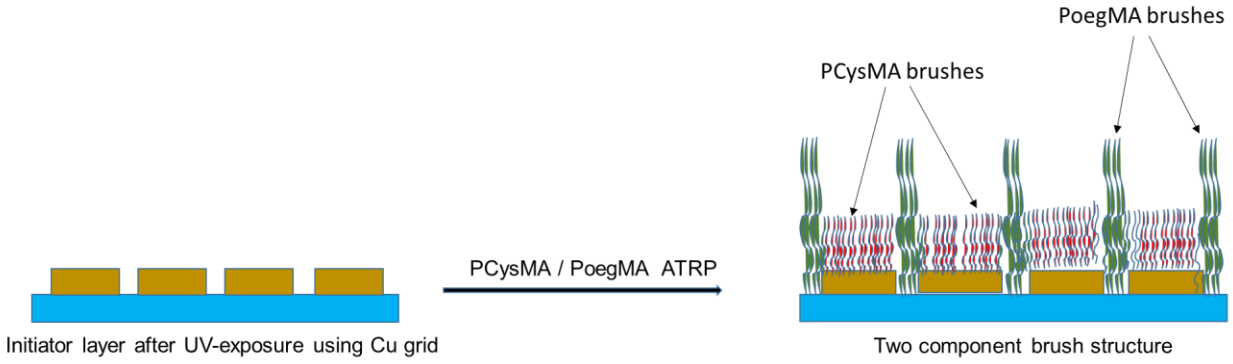

Figure 6-5: Schematics Showing Initiator Film Patterned Substrate before and after POEGMA and PCysMA ATRP to form a Two-Component Brush Structure

6.2.3.2 Preparation of films with varying initiator densities of BIBB and Benzoyl bromide

Piranha cleaned Si-substrates were immersed in a solution of 2% APTES in ethanol for 30 min at 20^{o}C. The APTES coated substrates were retrieved and rinsed with ethanol and dried in a stream of nitrogen gas followed by annealing at 120^{o}C in a vacuum oven for 30 min. Mix initiator densities of BIBB and BnB on APTES surfaces were prepared by the immersion of the annealed APTES substrates in a mixed 0.37 mL solution composed of varying percentage proportions of BIBB and BnB together with 0.41 mL of TEA dissolve in 60 mL of DCM for 30 min at 20^{o}C. For example, substrates composed of 100% BIBB / 0.0% BnB were prepared by the immersion of APTES surfaces in 100% of 0.37 mL BIBB together with 0.41 mL TEA dissolved in 60 mL DCM for 30 min at 20^{0}C before rinsing with DCM and ethanol prior to nitrogen gas drying. Similarly, substrates composed of 70% BIBB / 30% BnB were prepared by the immersion of APTES surfaces in 70% of 0.37 mL BIBB and 30% of 0.37 mL BnB together with 0.41 mL TEA dissolved in 60 mL DCM for 30 min at 20^{o}C before rinsing with DCM and ethanol prior to nitrogen gas drying. In addition, mix initiator density substrates composed of 0.0% BIBB / 100% BnB were prepared by the immersion of APTES surfaces in 100% of 0.37 mL BnB together with 0.41 mL TEA dissolved in 60 mL DCM for 30 min at 20^{o}C before rinsing with DCM and ethanol prior to nitrogen gas drying and characterization.

6.3 Surface Characterization

Advancing water contact angles of the functionalized surfaces were measured using a Rame-Hart model 100-00 goniometer via the sessile drop method. The quoted values are the means of at least three different measurements.

The thickness of the organosilane film was measured by spectroscopic ellipsometry using an M-2000V Ellipsometer (J.A Woollam Co. inc). The Complete Ease software was used to analyse the data. The mean thickness for each sample was determined from at least three different measurements.

Topographic roughness of the surface was measured in triplicate from Tapping Mode AFM images acquired using a Bruker Nanoscope (v) Multimode Atomic Force Microscope (Bruker. Coventry, UK).

X-ray photoelectron spectroscopy was performed using an Axis Ultra/Supra DLD X-ray Photoelectron spectroscopy (Manchester, UK). Data were analysed using Casa XPS software.

6.4 Results and Discussion

6.4.1 Contact Angle Measurements of UV Exposed CMPTS Films

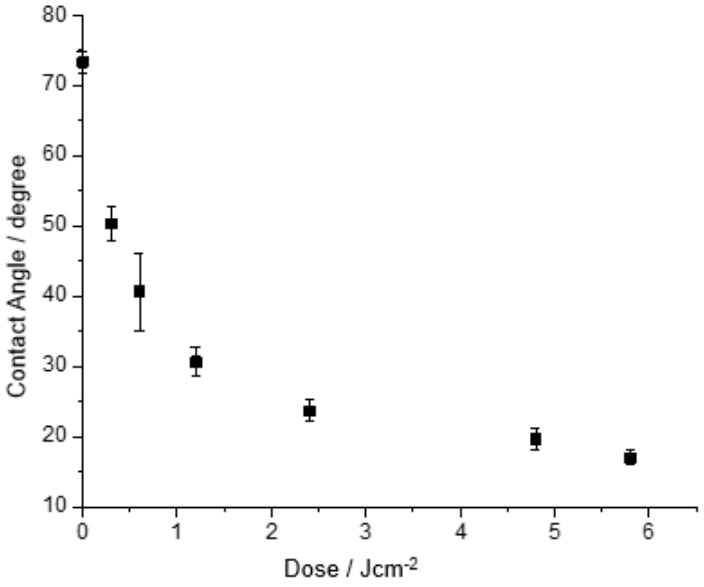

Figure 6-6: Water Contact Angle (degree) of CMPTS as a Function of Increasing UV-Doses

The final product of the photochemical modification of CMPTS films is expected to be a carboxylic acid group. Thus, photomodification of CMPTS films should be accompanied by a change in the water contact angle. Contact angles were measured as a function of UV dose (figure 6-6). The water contact angle of an unmodified CMPTS film is 73^{o}. However, as the UV dose is increased, the contact angle is reduced, reaching a value of 22^{o} at a dose of 2.4 Jcm^{-2}. As the UV-exposure dose increases from 2.4 to 5.8 Jcm^{-2} the contact angles approach a limiting value of 18^{o}.

6.4.2 XPS High Resolution Spectra of Photomodification of CMPTS Films

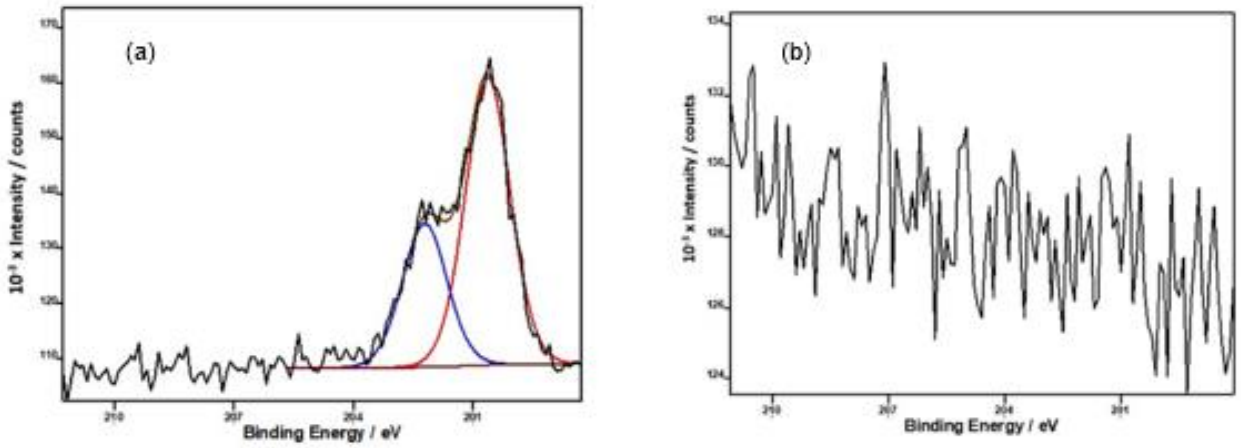

Figure 6-7: XPS High Resolution Spectra of Cl2p at Binding Energy of 201 eV (a) Before UV-Exposure and (b) After UV-Exposure to 4.8 Jcm^{-2} Dose

The XPS data in figure 6-7(a) shows Cl2p peak at 201 eV from CMPTS initiator films before UV-exposure on CMPTS film surface. While figure 6-7(b) showed a post de-chlorination spectrum depicting the disappearance of Cl2p peak at 201 eV from CMPTS surface after UV-exposure dose of about 4.8 Jcm^{-2}.

6.4.3 Growth of POEGMA Brushes from Photomodified CMPTS Films

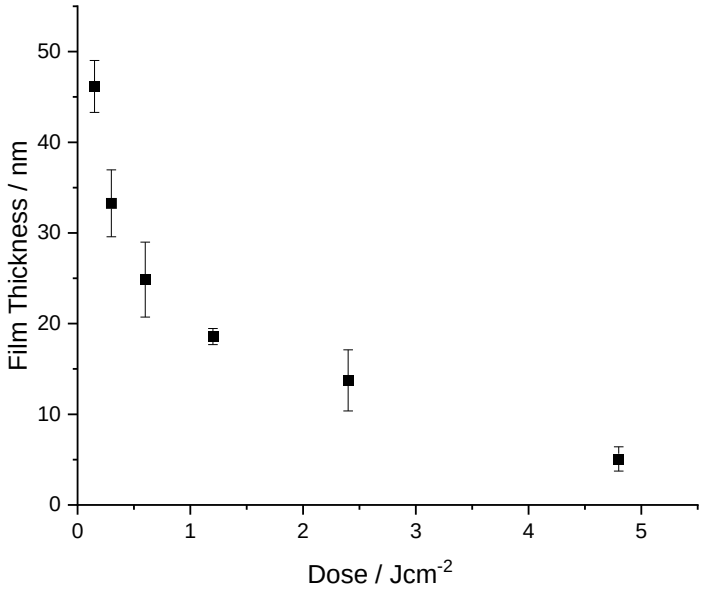

Figure 6-8: Spectroscopic Ellipsometry Measurements of POEGMA Brush Thickness Grown for 160 min from CMPTS UV-Exposed Surfaces as a Function of Increasing UV Doses

UV photolysis of the C-Cl bond leads to a reduction in the density of initiators at the CMPTS surface. To examine the effect of this on the properties of surface-grafted polymer films, spectroscopic ellipsometry was used to measure the mean thickness of POEGMA brushes grown for 160 min each on CMPTS subjected to a range of UV doses (Figure 6-8). The brush thickness can be observed dropping rapidly from 46 nm corresponding to 0.15 Jcm^{-2} to about 25 nm at 0.6 Jcm^{-2}, before slowly reaching a low POEGMA brush thickness of about 5 nm for the 4.8 Jcm^{-2} UV-exposed CMPTS initiator layer.

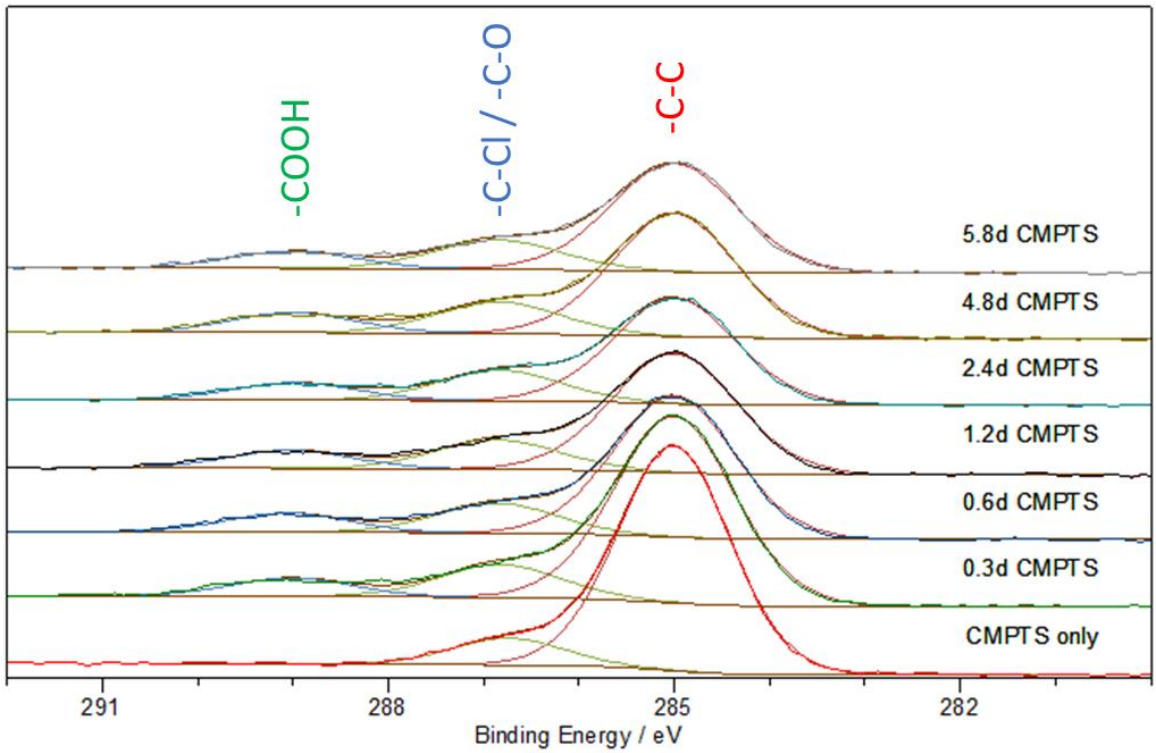

Figure 6-9: Figure 6 9: Overlayed C1s Peaks CMPTS Showing the Evolution of C-Cl Bond at 286 eV into O-C=O at 289 eV, initiated by UV-Exposures Doses, Ranging from 0.0 J/cm2 to 5.8 J/cm2

The XPS high resolution spectral peaks in figure 6-9 represent a progression in the pathway for photo-catalytic oxidation of C-Cl bond from CMPTS initiator films in the presence of oxygen. The benzyl chloride group gets impacted by UV-exposures ranging from 0.3 Jcm^{-2} to 5.8 Jcm^{-2} generating a phenyl radical before conversion to a benzaldehyde and finally to benzoic acid. As can be seen depicted in the spectrum at 289 eV where the carboxylate becomes more prominent with increasing UV doses compared to the C1s component which is at 285 eV.

6.4.4 Formation of Patterned Brushes

Photopatterned PCysMA films were formed by exposure of CMPTS films to UV light (with UV doses ranging from 0.15 up to 4.8 J cm^{-2}) followed by ATRP to achieve polymer brush patterns formed on surfaces using PCysMA and POEGMA.

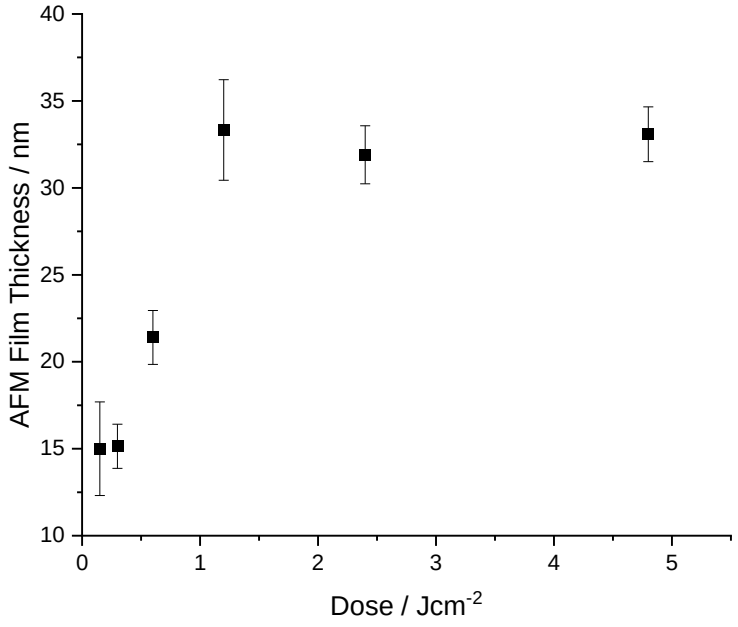

Figure 6-10: AFM Measurements of PCysMA Brush Growth Profile from CMPTS Patterned UV-Exposed Surfaces as a Function of Increasing UV Doses

The growth kinetic in figure 6-10 shows an increase in film thickness of PCysMA brushes polymerized for 160 min, from CMPTS UV-exposed patterned surfaces as the dose raises. The film thickness grew steadily at first, raising from 15 nm at 0.15 Jcm^{-2} reaching a limiting value of about 34 nm at dose 1.2 Jcm^{-2} before levelling to 32 nm at dose 4.8 Jcm^{-2}.

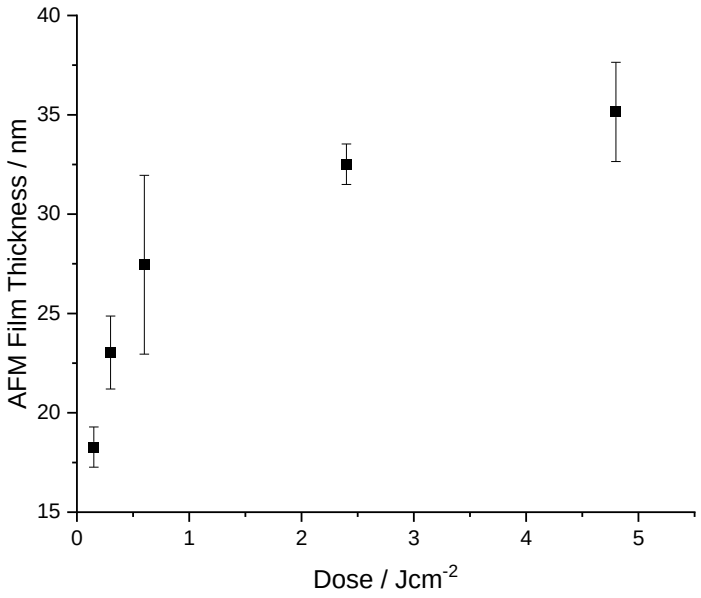

Figure 6-11: AFM Measurements of POEGMA Brush Growth Profile from CMPTS Patterned UV-Exposed Surfaces as a Function of Increasing UV Doses

The growth kinetic in figure 6-11 shows an increase in film thickness of POEGMA brushes grown at 160 min polymerization from CMPTS UV-exposed patterned surfaces with increasing doses. The film thickness initially increased steadily, raising from 18 nm at 0.15 Jcm^{-2} to 27.5 nm at 0.6 Jcm^{-2}, then it slowed down to 32.5 nm at 2.4 Jcm^{-2}, before reaching a limiting value of 34 nm at dose 4.8 Jcm^{-2}.

Comparing the increasing brush thicknesses observed from patterned initiator surfaces as the exposure dose increases which was exhibited in figure 6-11, to the decreasing brush growth trend from unpatterned surfaces made by increasing the UV doses on initiator surfaces as exhibited in figure 6-8, it is apparent that the surface grafting of

polymer brushes can easily be manipulated to achieve a desired density of grafted brushes on the surface.

6.5 Comparative studies of surface-grafted polymer on surfaces with varying initiator densities

Data for photomodified CMPTS surfaces were compared for model systems formed by derivatisation of films of APTES. APTES was reacted with mixtures of bromo (iso butryly bromide) (BIBB) and benzoyl bromide. Reaction of BIBB with APTES yields a surface-bound bromine which acts as an initiator for ATRP, whereas reaction of benzoyl bromide with APTES yields an inert surface. By varying the ratio of BIBB to benzoyl bromide (BnB), it is possible to produce a range of surfaces with systematically varying concentrations of Br initiators.

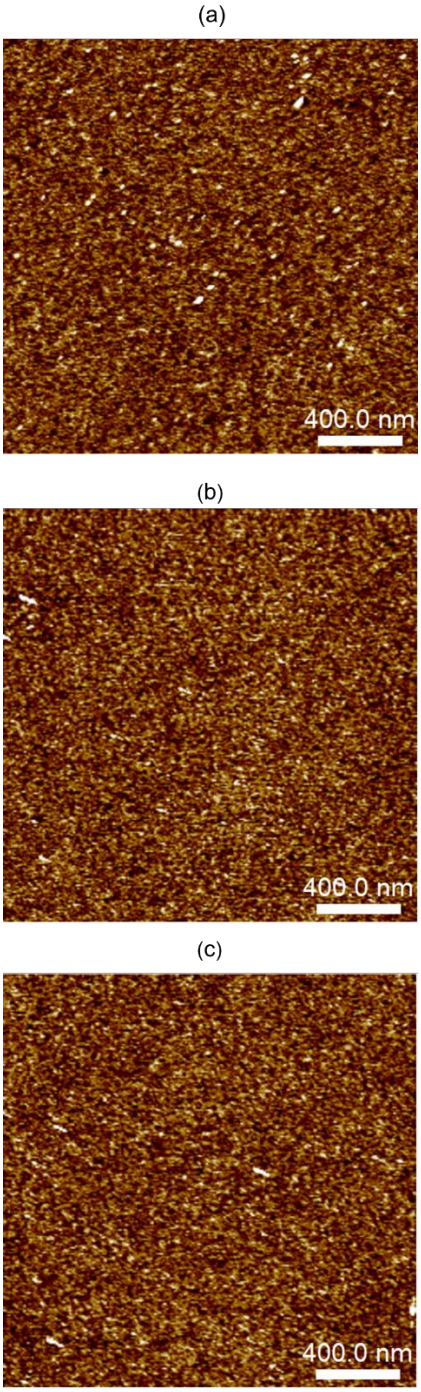

Figure 6-12: AFM Roughness images of Mix initiator Density films of (a) 100/0.0% BIBB/BnB with Roughness = 0.17 nm and ‘’z scale 0 to 1.15 nm‘’ (b) 50/50% BIBB-BnB with Roughness = 0.16 nm and ‘’z scale 0 to 1.09 nm‘’ (c) 0.0/100% BIBB-BnB with Roughness = 0.15 nm and ‘’z scale 0 to 1.06 nm‘’

The surface roughness values in figure 6-12 show a decline in roughness from 0.17 nm for surfaces functionalized by 100% BIBB to 0.15 nm for surfaces made up of 100% Benzoyl bromide.

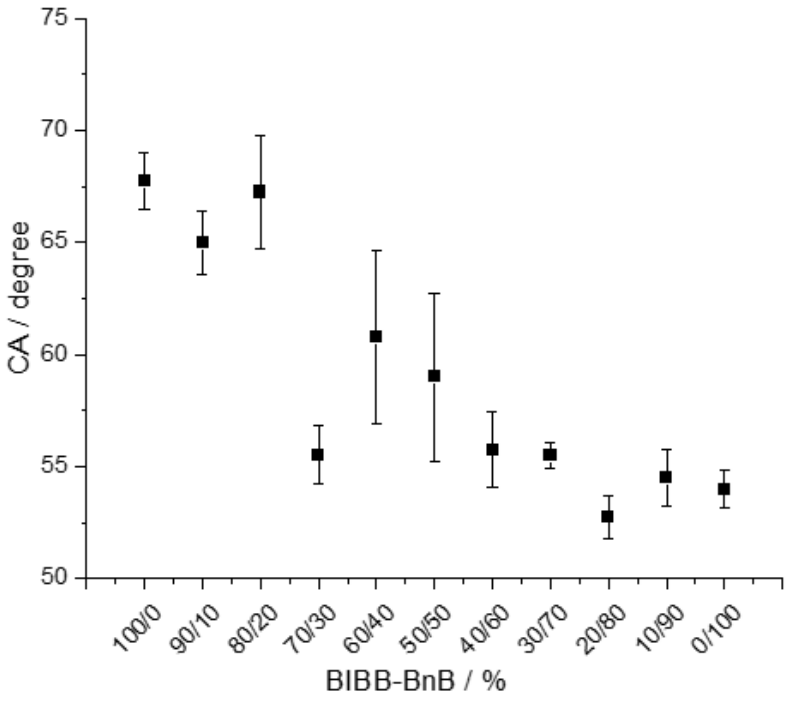

Figure 6-13: Water Contact Angle of BIBB and Benzoyl Bromide (BnB) Mix Grafting Density Initiator Films

Figure 6-13 shows the outcome of contact angle measurements of surfaces made from variations in the grafting density ratios of BIBB and Benzoyl bromide initiators (from 0% - 100%). The trend observed proceeded with a gradual drop in contact angle measured from 67º for 100% BIBB to about 25º for the 80% benzoyl bromide initiator density substrates. The decrease in water contact angle of the surface from 67º to 25º, has

evidenced that, control of hydrophobicity can be achieved through surface modifications caused by varying the grafting densities of BIBB and Benzoyl bromide initiators.

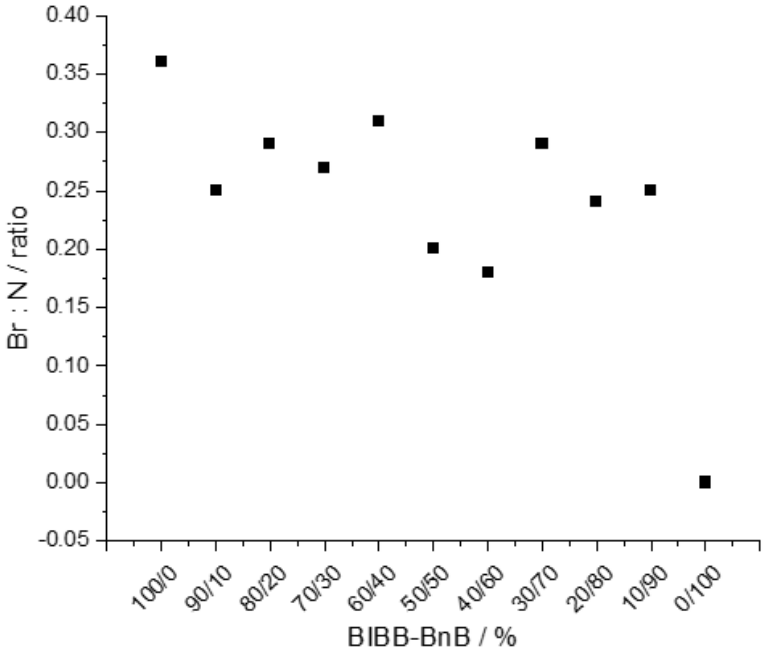

Figure 6-14: XPS Atomic Composition ratio of Br3d to N1s from Mix initiator Density films of BIBB and Benzoyl Bromide plotted against their grafting density percentage composition.

Table 6-1: XPS Percentage Atomic Composition of Mix initiator Densities of BIBB and Benzoyl Bromide (BnB) on APTES layer

Sample ID	Br3d	C1s	N1s	O1s	Br : N
100/00% BIBB/BnB	0.95	23.46	2.66	72.93	0.36
90/10% BIBB/BnB	0.67	23.92	2.63	72.78	0.25
80/20% BIBB/BnB	0.75	23.41	2.58	73.26	0.29
70/30% BIBB/BnB	0.65	23.47	2.44	73.43	0.27
60/40% BIBB/BnB	0.76	23.84	2.44	72.95	0.31

50/50% BIBB/BnB	0.50	24.41	2.54	72.54	0.20
40/60% BIBB/BnB	0.45	23.43	2.51	73.62	0.18
30/70% BIBB/BnB	0.69	23.99	2.39	72.93	0.29
20/80% BIBB/BnB	0.51	24.03	2.12	73.32	0.24
10/90% BIBB/BnB	0.63	23.00	2.53	73.84	0.25
00/100% BIBB/BnB	0.00	26.17	2.68	71.14	0.00

The XPS mix density composition data in figure 6-14 and Table 6-1 show a drop in Br3d to N1s ratio from 0.36 of sample made with 100/0.0% BIBB/BnB to as low as 0.00 belonging to sample composed of 0.0/100% BIBB/BnB. However, the remaining samples ranging from 90% BIBB to 10% BIBB maintained a similar Br : N ratio averaging about 0.25. In addition, the percentage composition of Br3d in Table 6-1 decreases with decreasing grafting percent of BIBB of sample.

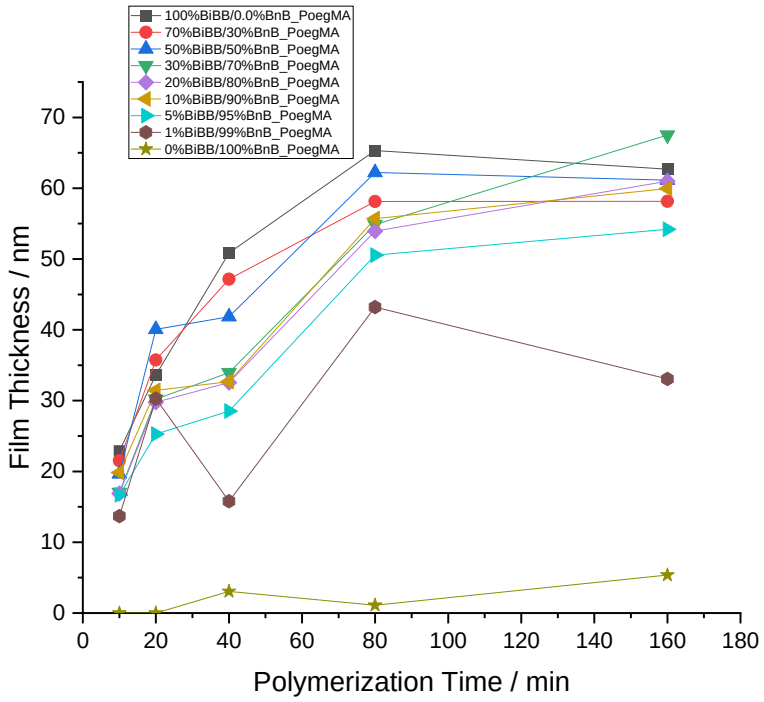

Figure 6-15: Spectroscopic Ellipsometry Measurements of POEGMA Brushes Grown from Films of Mix Initiator Grafting Densities of BIBB and Benzoyl Bromide

Figure 6-15 represents the kinetics showing the ellipsometry film thicknesses of POEGMA brushes grown from surfaces made by variations in the grafting density ratios of BIBB and Benzoyl bromide initiators on APTES surface (from 0% - 100%). From figure 6-15, the kinetics of 100% benzoyl bromide is the least in growth, rarely growing beyond 5 nm film thickness after 160 min polymerization time. On the other hand, 100% BIBB had the highest growth trend, reaching a film thickness of about 62 nm at 80 min, before falling to a limiting value. The remaining mix initiator grafting density brushes, have no very well-defined trend as shown in figure 6-15 above. However, they exhibited film thicknesses above 10 nm from 5 min of polymerization time, staggering all through to between 40 and 58 nm film thickness before reaching a limiting value.

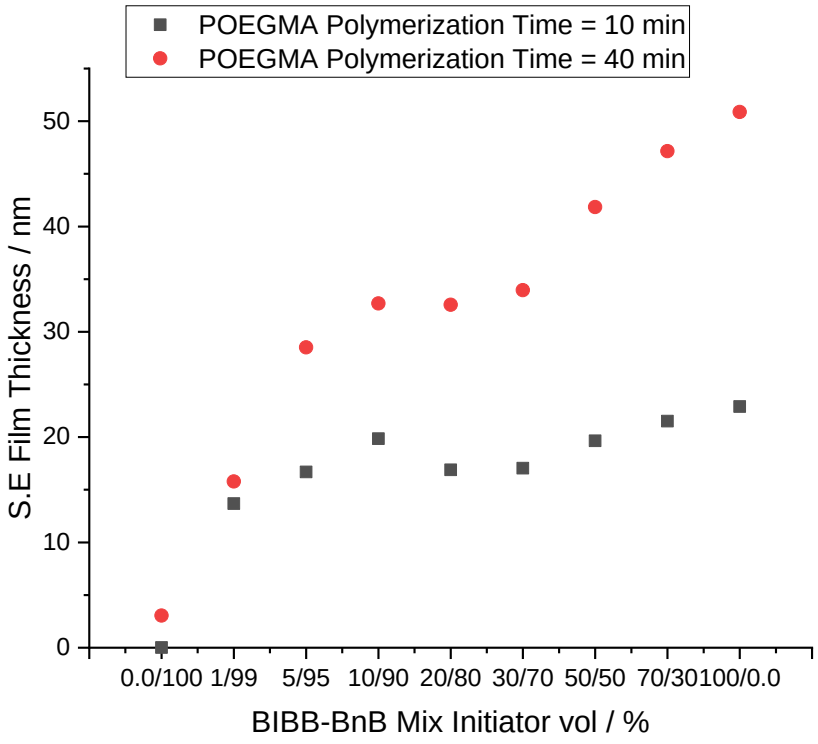

Figure 6-16: A graph of variation in film thickness of POEGMA brushes at polymerization times of 10 min and 40 min as a function of BIBB-BnB mix initiator density percentage

The growth kinetics illustrated in figure 6-16 for both 10 and 40 min polymerization of POEGMA brushes show three different patterns in growth profile which correspond to low, average and full density brushes. As the grafting density ratio of BIBB/BnB mix initiators increases from 0.0 nm to an average of 22 nm brush thickness within the region ranging from 0.0/100% to 5/95% of BIBB/BnB mix initiator layer. The brushes thereafter plateaued averagely in thicknesses through the region between 5/95% to 30/70% of BIBB-BnB mix initiator films before raising steadily to a full density brush regime when the BIBB/BnB ratio reaches 100/0.0%. This depicts a relative level of control in POEGMA brush growth from variation in mix density initiator ratio.

6.6 AFM Measurements

Patterned polymer brushes were formed by exposure of CMPTS and BIBB-APTES films to UV light (with a dose of 4.8 J cm^{-2}) followed by ATRP to achieve brush patterns formed on surfaces using PCysMA and POEGMA.

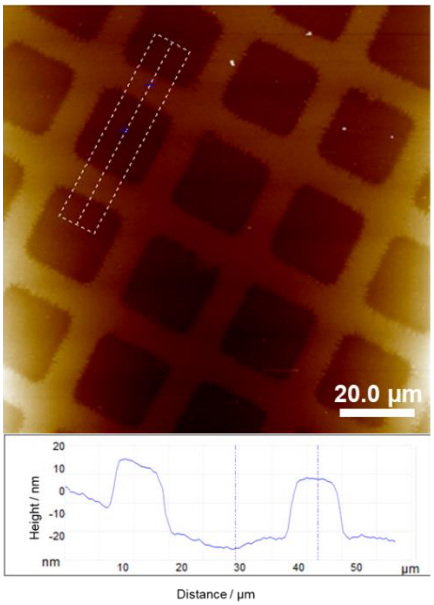

Figure 6-17: Figure 6 17: AFM Height Image of PCysMA Grown on CMPTS Initiator Patterned Surface

Figure 6-17 shows an AFM height image of PCysMA brushes grown from a photopatterned CMPTS film. The thickness of the surface grafted polymer was determined from analysis of a line section through the image. It is assumed that a fully dense brush is grown from the masked regions (bars in figure 6-17). In the exposed areas (squares), the grafting density is reduced in proportion to the UV exposure. At a dose of 4.8 J cm^{-2}, it is expected, based on the data in Figure 6-8, that only a negligible amount of initiator will remain at the surface in the exposed regions; thus, the heights of the bars

correspond, effectively to the thickness of the brush layer. The AFM image in figure 6-17 indicates that the brush thickness is 16.9 ± 0.8 nm after 40 min of polymerization time.

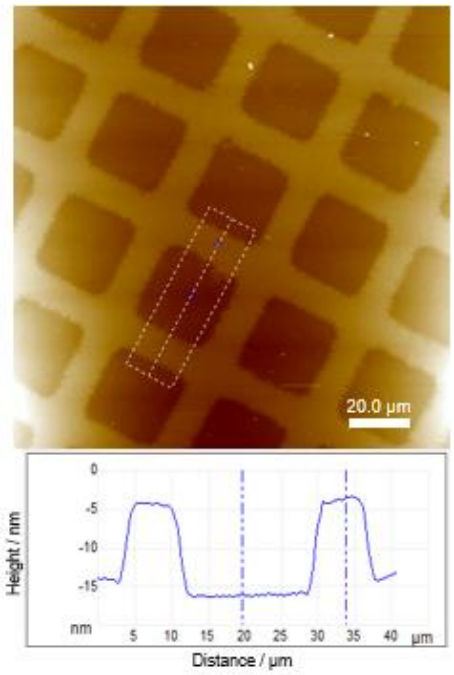

Figure 6-18: AFM Height Image of POEGMA Grown on CMPTS Initiator Patterned Surface

Figure 6-18 shows an AFM height image of POEGMA brushes grown from a photopatterned CMPTS film at 4.8 Jcm^{-2} UV-exposure and esterification of carboxylic acid group formed using excess glycerol with dicyclohexylcarboxylcarbodiimide (DCC) in dichloromethane (DCM), but before re-bromination with BIBB. The thickness of the surface grafted polymer was determined from analysis of a line section through the image. It is assumed that a fully dense brush is grown from the masked regions (bars in figure 6-18). In the exposed areas (squares), the grafting density is reduced in proportion to the UV exposure. At a dose of 4.8 J cm^{-2}, it is expected, based on the data in Figure 6-8, that only a negligible amount of initiator will remain at the surface in the exposed regions; thus,

the heights of the bars correspond, effectively to the thickness of the brush layer. The AFM image in figure 6-18 indicates that the brush thickness is 15.0 ± 0.3 nm after 40 min of polymerization time.

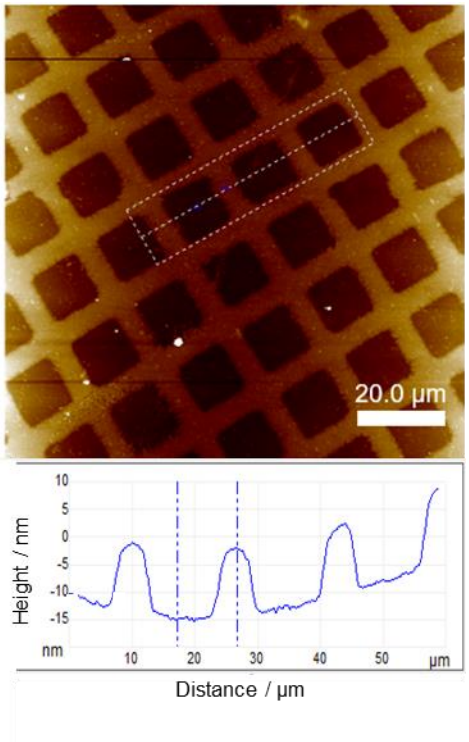

Figure 6-19: Figure 6 19: AFM Height Image of PCysMA Grown on BIBB-APTES Initiator Patterned Surface

Figure 6-19 shows an AFM height image of PCysMA brushes grown from a photopatterned BIBB-APTES film. The thickness of the surface grafted polymer was determined from analysis of a line section through the image. It is assumed that a fully dense brush is grown from the masked regions (bars in figure 6-19). In the exposed areas (squares), the grafting density is reduced in proportion to the UV exposure. At a dose of 4.8 J cm^{-2}, it is expected, based on the data in Figure 6-8, that only a negligible amount of initiator will remain at the surface in the exposed regions; thus, the heights of the bars

correspond, effectively to the thickness of the brush layer. The AFM image in figure 6-19 indicates that the brush thickness is 13.1 ± 0.3 nm after 40 min of polymerization time.

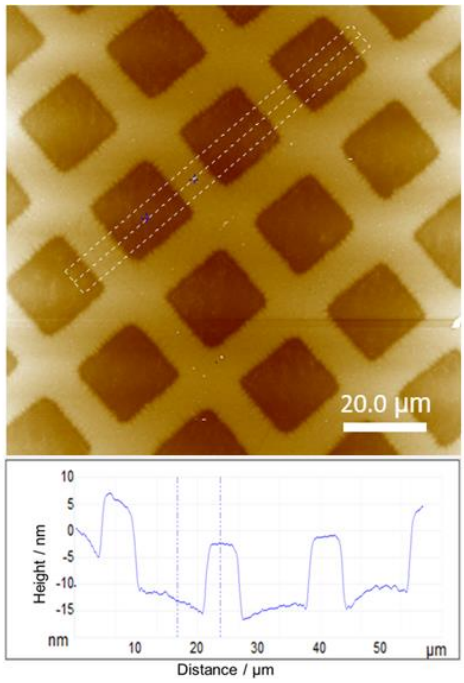

Figure 6-20: Figure 6 20: AFM Height Image of POEGMA Grown on BIBB-APTES Initiator Patterned Surface

Figure 6-20 shows an AFM height image of POEGMA brushes grown from a photopatterned BIBB-APTES film. The thickness of the surface grafted polymer was determined from analysis of a line section through the image. It is assumed that a fully dense brush is grown from the masked regions (bars in figure 6-20). In the exposed areas (squares), the grafting density is reduced in proportion to the UV exposure. At a dose of 4.8 J cm^{-2}, it is expected, based on the data in Figure 6-8, that only a negligible amount of initiator will remain at the surface in the exposed regions; thus, the heights of the bars correspond, effectively to the thickness of the brush layer. The AFM image in figure 6-20 indicates that the brush thickness is 20.1 ± 0.6 nm after 40 min of polymerization time.

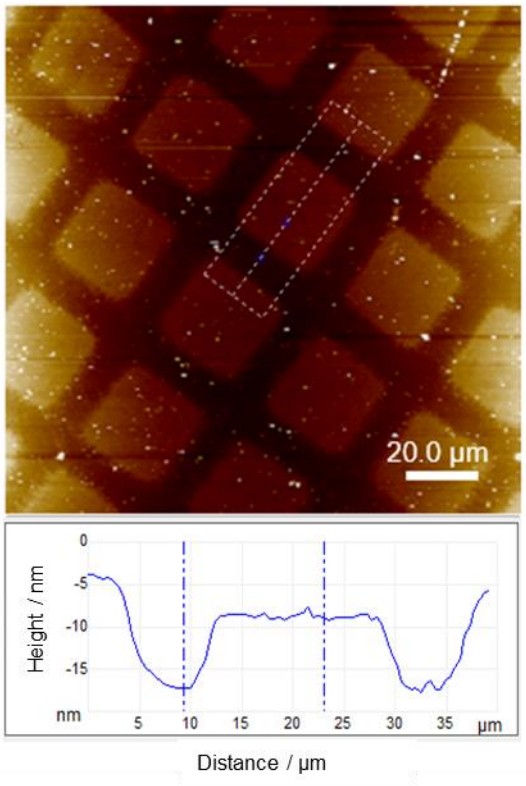

Figure 6-21: Figure 6 21: Two Component Brush Structures made up of POEGMA Bars and PCysMA Squares with NBC and Modified Nile Blue Dye Incorporation

AFM image of patterned CMPTS POEGMA and PCysMA brushes with a final thickness of 12.4 nm after 40 min of polymerization time. The POEGMA and PCysMA two component brush was functionalized by immersion in 0.052 mM solution of modified Nile Blue at 50^{o}C for 24 hours to form a two-component brush system after washing with ethanol and drying in a stream of nitrogen gas.

6.7 Conclusion

In conclusion we have demonstrated that initiator films can be modified with the aid of UV-light exposition to achieve patterned and un-patterned modified surfaces. Surface modification has also been achieved through mixed initiator grafting densities. Polymer

brushes grown from these surfaces tend to have a unique arrangement that confers distinct surface properties and characteristics on the polymer brushes.

The exposure to UV-light caused Cl atoms located at the tip of CMPTS initiator films to cleave with ease as well as selectively, owing to the presence of a Cu-grid mesh which protects as well as expose selected areas of the initiator surface.

Photopatterned CMPTS initiator films on substrates thus obtained, were utilized to fabricate a two-component brush structure comprising of POEGMA serving as wall that incorporated integral reporters, as well as PCysMA platforms capable of accommodating integral proteins on SLBs.

The UV-photopatterning technique deployed in this study has enabled the ease of selective dehalogenation of CMPTS initiator films which provides a convenient pathway for the fabrication of a binary brush architecture that can be further developed to facilitate the construction of a microsystem.

CHAPTER 7: CONCLUSION AND FUTURE WORK

7.1 Conclusion

The growth profile exhibited by the polymer brush structures grown from different surfaces of varying compositions suggest that a form of control has been established in the growth of these polymers and can be repeatedly achieved with ease. From the results of the polymerization kinetics seen of chlorinated and brominated initiator films in figures 4-17, 4-21, 4-26 and 4-30, it showed that brominated initiator films grow thicker brushes compared to the chlorinated films. This was recently observed in the work of Parkatzidis et. al, 2021. They stated that initiator films with chlorinated end group, cause lower activation rates compared to their brominated counterparts under identical conditions.

On the other hand, the amine-modified Nile blue dye showed prominent absorbance peak intensities for Nile blue at 660 nm even at very low concentrations. However, the modified dye could not show a positive pH responsiveness when measured in both basic and acidic solutions. NBC Dye however with very low absorption intensities, showed significant positive response to pH changes in solution. The two-component brush system of POEGMA and PCysMA on patterned CMPTS surfaces was constituted with *ratiomeric* dye incorporation successfully achieved.

7.2 Future Work

Further experimental work should be done to confirm or establish as a fact, the reason for the unresponsiveness of the amine-modified Nile Blue to pH changes.

The two component brushes formed with NBC and NB dye incorporation should be experimented upon along with the incorporation of membrane protein, with a view towards accomplishing the initial goal of this research work.

REFERENCES

1) Cooper, Jonathan. "Grand Challenges in Lab-on-a-Chip Technologies." *Frontiers in Lab on a Chip Technologies*: 1.
2) Groves, Jay T. "Bending mechanics and molecular organization in biological membranes." *Annu. Rev. Phys. Chem.* 58 (2007): 697-717.
3) DeMond, Andrew L., and Jay T. Groves. "Interrogating the T cell synapse with patterned surfaces and photoactivated proteins." *Current opinion in immunology* 19.6 (2007): 722-727.
4) Rabuka, David, et al. "Hierarchical assembly of model cell surfaces: synthesis of mucin mimetic polymers and their display on supported bilayers." *Journal of the American Chemical Society* 129.17 (2007): 5462-5471.
5) Li, Junbo, et al. "Spatial Organization in Proteinaceous Membrane-Stabilized Coacervate Protocells." *Small* 15.36 (2019): 1902893.
6) Wei, Shao-Peng, et al. "Formation and functionalization of membraneless compartments in Escherichia coli." *Nature chemical biology* 16.10 (2020): 1143-1148.
7) Nye, Jeffrey A., and Jay T. Groves. "Kinetic control of histidine-tagged protein surface density on supported lipid bilayers." *Langmuir* 24.8 (2008): 4145-4149.
8) Sackmann, Erich. "Supported membranes: scientific and practical applications." *Science* 271.5245 (1996): 43-48.
9) Kuddannaya, Shreyas, Jingnan Bao, and Yilei Zhang. "Enhanced in vitro biocompatibility of chemically modified poly (dimethylsiloxane) surfaces for stable

adhesion and long-term investigation of brain cerebral cortex cells." *ACS applied materials & interfaces* 7.45 (2015): 25529-25538.

10) Llorente-Garcia, Isabel, et al. "Single-molecule in vivo imaging of bacterial respiratory complexes indicates delocalized oxidative phosphorylation." *Biochimica et Biophysica Acta (BBA)-Bioenergetics* 1837.6 (2014): 811-824.

11) Nelson, Nathan, et al. "The cellular biology of proton-motive force generation by V-ATPases." *Journal of Experimental Biology* 203.1 (2000): 89-95.

12) Breul, Alexander M., Martin D. Hager, and Ulrich S. Schubert. "Fluorescent monomers as building blocks for dye labeled polymers: synthesis and application in energy conversion, biolabeling and sensors." *Chemical Society Reviews* 42.12 (2013): 5366-5407.

13) Baker, Monya. "A living system on a chip." *Nature* 471.7340 (2011): 661-665.

14) Huh, D., et al. "HY HSIN a DE INGBER." *Reconstituting Organ-Level Lung Functions on a Chip. Science [online]* 328.5986 (2010): 1662-1668.

15) Battat, Sarah, David A. Weitz, and George M. Whitesides. "An outlook on microfluidics: the promise and the challenge." *Lab on a Chip* 22.3 (2022): 530-536.

16) DeMond, Andrew L., et al. "T cell receptor microcluster transport through molecular mazes reveals mechanism of translocation." *Biophysical journal* 94.8 (2008): 3286-3292.

17) Jose, Jiney, and Kevin Burgess. "Benzophenoxazine-based fluorescent dyes for labeling biomolecules." *Tetrahedron* 62.48 (2006): 11021-11037.

18) Kamariza, Mireille. *The Power of Solvatochromism: Using Environment-sensitive Trehalose Probes to Detect Mycobacteria with Applications in Research and Medicine*. Stanford University, 2019.

19) Arsov, Zoran, Iztok Urbančič, and Janez Štrancar. "Aggregation-induced emission spectral shift as a measure of local concentration of a pH-activatable rhodamine-based smart probe." *Spectrochimica Acta Part A: Molecular and Biomolecular Spectroscopy* 190 (2018): 486-493.

20) Cao, Xue-Ling, et al. "pH-Induced conformational changes of BSA in fluorescent AuNCs@ BSA and its effects on NCs emission." *Vibrational Spectroscopy* 65 (2013): 186-192.

21) Madsen, J., et al. "Fabrication of microstructured binary polymer brush “corrals” with integral pH sensing for studies of proton transport in model membrane systems." *Chemical science* 9.8 (2018): 2251.

22) Xia, Sijing, et al. "Fabrication of nanometer-and micrometer-scale protein structures by site-specific immobilization of histidine-tagged proteins to aminosiloxane films with photoremovable protein-resistant protecting groups." *Langmuir* 32.7 (2016): 1818-1827.

23) Cheng, N., et al. "Facile formation of highly mobile supported lipid bilayers on surface-quaternized pH-responsive polymer brushes." *Macromolecules* 48.9 (2015): 3095-3103.

24) Simonsson, Lisa, and Fredrik Höök. "Formation and diffusivity characterization of supported lipid bilayers with complex lipid compositions." *Langmuir* 28.28 (2012): 10528-10533.

25) Johnson, Alexander, et al. "Simple, direct routes to polymer brush traps and nanostructures for studies of diffusional transport in supported lipid bilayers." *Langmuir* 33.15 (2017): 3672-367 9.

26) Huh, Dongeun, et al. "Reconstituting organ-level lung functions on a chip." *Science* 328.5986 (2010): 1662-1668.

27) Shin, Michael, et al. "Endothelialized networks with a vascular geometry in microfabricated poly (dimethyl siloxane)." *Biomedical microdevices* 6 (2004): 269-278.

28) Jang, Kihoon, et al. "Development of an osteoblast-based 3D continuous-perfusion microfluidic system for drug screening." *Analytical and bioanalytical chemistry* 390 (2008): 825-832.

29) M. T. Lam, Y. C. Huang, R. K. Birla, S. Takayama, Biomaterials 30, 1150 (2009)

30) D. Huh et al., Proc. Natl. Acad. Sci. U.S.A. 104, 18886 (2007).

31) Wu, Wenshuai, et al. "Direct single-cell antimicrobial susceptibility testing of Escherichia coli in urine using a ready-to-use 3D microwell array chip." *Lab on a Chip* (2023).

32) Inomata, Naoki, et al. "Measurement of cellular thermal properties and their temperature dependence based on frequency spectra via an on-chip-integrated microthermistor." *Lab on a Chip* (2023).

33) Juhng, Seorin, et al. "Fabrication of liraglutide-encapsulated triple layer hyaluronic acid microneedles (TLMs) for the treatment of obesity." *Lab on a Chip* (2023).

34) Shinde, Ashwini, et al. "Metallic micro-ring device for highly efficient large cargo delivery in mammalian cells using infrared light pulses." *Lab on a Chip* (2023).

35) Zeaei, Soroush, et al. "High-DNA integrity sperm selection using rheotaxis and boundary following behavior in a microfluidic chip." *Lab on a Chip* (2023).

36) Watson, Helen. "Biological membranes." *Essays in biochemistry* 59 (2015): 43-69.

37) Kwik, Jeanne, et al. "Membrane cholesterol, lateral mobility, and the phosphatidylinositol 4, 5-bisphosphate-dependent organization of cell actin." *Proceedings of the National Academy of Sciences* 100.24 (2003): 13964-13969.

38) Furukawa, Kazuaki, et al. "Novel “lipid-flow chip” configuration to determine donor-to-acceptor ratio-dependent fluorescence resonance energy transfer efficiency." *Langmuir* 24.3 (2008): 921-926.

39) Cornell, B. A., et al. "The Gramicidin-Based Biosensor: A Functioning Nano-Machine." *Novartis Foundation Symposium 225-Gramicidin and Related Ion Channel-Forming Peptides: Gramicidin and Related Ion Channel-Forming Peptides: Novartis Foundation Symposium 225*. Chichester, UK: John Wiley & Sons, Ltd., 2007.

40) Granéli, Annette, et al. "Formation of supported lipid bilayer membranes on SiO2 from proteoliposomes containing transmembrane proteins." *Langmuir* 19.3 (2003): 842-850.

41) Han, Xiaojun, et al. "Lipid bilayer membrane arrays: fabrication and applications." *Future Trends in Biotechnology* (2012): 121-152.

42) Leney, Aneika C., et al. "Amphipathic polymers enable the study of functional membrane proteins in the gas phase." *Analytical chemistry* 84.22 (2012): 9841-9847.

43) Seddon, Annela M., Paul Curnow, and Paula J. Booth. "Membrane proteins, lipids and detergents: not just a soap opera." *Biochimica et Biophysica Acta (BBA)-Biomembranes* 1666.1-2 (2004): 105-117.

44) Klöpfer, Kai, and Franz Hagn. "Beyond detergent micelles: The advantages and applications of non-micellar and lipid-based membrane mimetics for solution-state NMR." *Progress in Nuclear Magnetic Resonance Spectroscopy* 114 (2019): 271-283.

45) Popot, Jean-Luc. "Amphipols, nanodiscs, and fluorinated surfactants: three nonconventional approaches to studying membrane proteins in aqueous solutions." *Annual review of biochemistry* 79 (2010): 737-775.

46) Sackmann, Erich. "Supported membranes: scientific and practical applications." *Science* 271.5245 (1996): 43-48.

47) Kasemo, Bengt. "Biological surface science." *Surface science* 500.1-3 (2002): 656-677.

48) Diamanti, Eleftheria, et al. "High resistivity lipid bilayers assembled on polyelectrolyte multilayer cushions: an impedance study." *Langmuir* 32.25 (2016): 6263-6271.

49) Katsaras, John, Norbert Kučerka, and Mu-Ping Nieh. "Structure from substrate supported lipid bilayers." *Biointerphases* 3.2 (2008): FB55-FB63.

50) Terrettaz, Samuel, Michael Mayer, and Horst Vogel. "Highly electrically insulating tethered lipid bilayers for probing the function of ion channel proteins." *Langmuir* 19.14 (2003): 5567-5569.

51) Yoshina-Ishii, Chiaki, and Steven G. Boxer. "Arrays of mobile tethered vesicles on supported lipid bilayers." *Journal of the American Chemical Society* 125.13 (2003): 3696-3697.

52) Richter, Ralf P., Josephine Lai Kee Him, and Alain Brisson. "Supported lipid membranes." *Materials today* 6.11 (2003): 32-37.

53) Rozovsky, Sharon, et al. "Single molecule kinetics of ENTH binding to lipid membranes." *The Journal of Physical Chemistry B* 116.17 (2012): 5122-5131.

54) Sych, Taras, et al. "How does liquid-liquid phase separation in model membranes reflect cell membrane heterogeneity?" *Membranes* 11.5 (2021): 323.

55) Devetak, Miha, et al. "Surface structure of Langmuir–Blodgett films of lipophilic guanosine derivatives." *Applied Surface Science* 256.7 (2010): 2038-2043.

56) Shen, William W., et al. "Polymer-supported lipid bilayers on benzophenone-modified substrates." *Biomacromolecules* 2.1 (2001): 70-79.

57) Wang, Lei, et al. "Photosynthetic proteins in supported lipid bilayers: Towards a biokleptic approach for energy capture." *Small* 11.27 (2015): 3306-3318.

58) Kunding, Andreas H., et al. "A fluorescence-based technique to construct size distributions from single-object measurements: application to the extrusion of lipid vesicles." *Biophysical journal* 95.3 (2008): 1176-1188.

59) Titov, Evgenii, et al. "Photoisomerization of an Azobenzene-Containing Surfactant Within a Micelle." *ChemPhotoChem* 5.10 (2021): 926-932.

60) Natan, Amir, et al. "Electrostatic Properties of Ideal and Non-ideal Polar Organic Monolayers: Implications for Electronic Devices." *Advanced Materials* 19.23 (2007): 4103-4117.

61) Love, J. Christopher, et al. "Self-assembled monolayers of thiolates on metals as a form of nanotechnology." *Chemical reviews* 105.4 (2005): 1103-1170.

62) Ulman, Abraham. "Formation and structure of self-assembled monolayers." *Chemical reviews* 96.4 (1996): 1533-1554.

63) Zhang, Chen, et al. "Effects of interface roughness on cohesive strength of self-assembled monolayers." *Applied Surface Science* 397 (2017): 192-198.

64) Senaratne, Wageesha, Luisa Andruzzi, and Christopher K. Ober. "Self-assembled monolayers and polymer brushes in biotechnology: current applications and future perspectives." *Biomacromolecules* 6.5 (2005): 2427-2448.

65) Freemon, Frank R. "American colonial scientists who published in the Philosophical Transactions of the Royal Society." *Notes and Records of the Royal Society of London* 39.2 (1985): 191-206.

66) Schoenbaum, Carolyn A., Daniel K. Schwartz, and J. Will Medlin. "Controlling the surface environment of heterogeneous catalysts using self-assembled monolayers." *Accounts of Chemical Research* 47.4 (2014): 1438-1445.

67) Trabelsi, Siwar, et al. "Semi-fluorinated phosphonic acids form stable nanoscale clusters in Langmuir–Blodgett and self-assembled monolayers." *Soft Matter* 5.4 (2009): 750-758.

68) Ashkenasy, Gonen, et al. "Molecular engineering of semiconductor surfaces and devices." *Accounts of Chemical Research* 35.2 (2002): 121-128.

69) Pei, Xiaowei, et al. "Correlation between the structure and wettability of photoswitchable hydrophilic azobenzene monolayers on silicon." *Langmuir* 27.15 (2011): 9403-9412.

70) Raigoza, Annette F., et al. "One-pot reaction for the preparation of biofunctionalized self-assembled monolayers on gold surfaces." *Applied Surface Science* 394 (2017): 288-296.

71) T.M. Owens, K.T. Nicholson, M.M.B. Holl and S. Suzer. *J. Am. Chem. Soc*., 2002. Vol. 124 (24), 6800-6801.

72) Prakash, Shaurya, M. B. Karacor, and Sanjay Banerjee. "Surface modification in microsystems and nanosystems." *Surface Science Reports* 64.7 (2009): 233-254.

73) McDermott, Mark T., John-Bruce D. Green, and Marc D. Porter. "Scanning force microscopic exploration of the lubrication capabilities of n-alkanethiolate monolayers chemisorbed at gold: structural basis of microscopic friction and wear." *Langmuir* 13.9 (1997): 2504-2510.

74) Ballauff, Matthias, Markus Biesalski, and Axel HE Müller. "Polymer brushes." *Polymer* 100.98 (2016): 387-388.

75) Zou, Lei, et al. "Modification of side chain terminals of PEGylated molecular bottle brushes—A toolbar of molecular nanoobjects." *Polymer* 54.2 (2013): 481-484.

76) Cheng, Guanglou, et al. "Amphiphilic cylindrical core− shell brushes via a “grafting from” process using ATRP." *Macromolecules* 34.20 (2001): 6883-6888.

77) Kolb, Hartmuth C., M. G. Finn, and K. Barry Sharpless. "Click chemistry: diverse chemical function from a few good reactions." *Angewandte Chemie International Edition* 40.11 (2001): 2004-2021.

78) Binder, Wolfgang H., et al. "Reversible and irreversible binding of nanoparticles to polymeric surfaces." *Journal of Nanomaterials* 2009 (2009).

79) Lutz, Jean-François. "1, 3-Dipolar cycloadditions of azides and alkynes: a universal ligation tool in polymer and materials science." *Angewandte Chemie International Edition* 46.7 (2007): 1018-1025.

80) Min, Ke, et al. "High yield synthesis of molecular brushes via ATRP in miniemulsion." *Macromolecules* 40.18 (2007): 6557-6563.

81) Wang, Jin-Shan, and Krzysztof Matyjaszewski. "Controlled/" living" radical polymerization. atom transfer radical polymerization in the presence of transition-metal complexes." *Journal of the American Chemical Society* 117.20 (1995): 5614-5615.

82) Matyjaszewski, Krzysztof, and Jianhui Xia. "Atom transfer radical polymerization." *Chemical reviews* 101.9 (2001): 2921-2990.

83) Yamamoto, Shin-ichi, and Krzysztof Matyjaszewski. "ARGET ATRP synthesis of thermally responsive polymers with oligo (ethylene oxide) units." *Polymer journal* 40.6 (2008): 496-497.

84) Tsarevsky, Nicolay V., Wade A. Braunecker, and Krzysztof Matyjaszewski. "Electron transfer reactions relevant to atom transfer radical polymerization." *Journal of organometallic chemistry* 692.15 (2007): 3212-3222.

85) Zhao, Yulai, et al. "The synthesis of modified polyethylene via coordination polymerization followed by ATRP, RAFT, NMRP or ROP." *Progress in polymer science* 35.10 (2010): 1195-1216.

86) Matyjaszewski, Krzysztof, et al. "Utilizing halide exchange to improve control of atom transfer radical polymerization." *Macromolecules* 31.20 (1998): 6836-6840.

87) Perruchot, C., et al. "Synthesis of well-defined, polymer-grafted silica particles by aqueous ATRP." *Langmuir* 17.15 (2001): 4479-4481.

88) Prucker, O., and Jürgen Rühe. "Mechanism of radical chain polymerizations initiated by azo compounds covalently bound to the surface of spherical particles." *Macromolecules* 31.3 (1998): 602-613.

89) Fan, Xiaowu, et al. "Living anionic surface-initiated polymerization (LASIP) of styrene from clay nanoparticles using surface bound 1, 1-diphenylethylene (DPE) initiators." *Langmuir* 18.11 (2002): 4511-4518.

90) Prucker, O., and Jürgen Rühe. "Synthesis of poly (styrene) monolayers attached to high surface area silica gels through self-assembled monolayers of azo initiators." *Macromolecules* 31.3 (1998): 592-601.

91) Henze, Michael, et al. "“Grafting through”: mechanistic aspects of radical polymerization reactions with surface-attached monomers." *Macromolecules* 47.9 (2014): 2929-2937.

92) Luzinov, Igor, et al. "Epoxy-terminated self-assembled monolayers: molecular glues for polymer layers." *Langmuir* 16.2 (2000): 504-516.

93) Zhou, Qingye, et al. "Living anionic surface-initiated polymerization (LASIP) of a polymer on silica nanoparticles." *Langmuir* 18.8 (2002): 3324-3331.

94) Kang, Chengjun, Rowena M. Crockett, and Nicholas D. Spencer. "Molecular-weight determination of polymer brushes generated by SI-ATRP on flat surfaces." *Macromolecules* 47.1 (2014): 269-275.

95) Yoshikawa, Sachio, Takamitsu Iida, and Norio Tsubokawa. "Grafting of living polymer cations with organic pigments." *Progress in organic coatings* 31.1-2 (1997): 127-131.

96) Tsubokawa, Norio, Kazuhiro Saitoh, and Yukio Shirai. "Surface grafting of polymers onto ultrafine silica: cationic polymerization initiated by benzylium perchlorate groups introduced onto ultrafine silica surface." *Polymer Bulletin* 35.4 (1995): 399-406.

97) Tsubokawa, Norio. "Preparation and properties of polymer-grafted carbon nanotubes and nanofibers." *Polymer Journal* 37.9 (2005): 637-655.

98) Juang, Agnes, et al. "Formation of covalently attached polymer overlayers on Si (111) surfaces using ring-opening metathesis polymerization methods." *Langmuir* 17.5 (2001): 1321-1323.

99) Skaff, Habib, et al. "Preparation of cadmium selenide− Polyolefin composites from functional phosphine oxides and ruthenium-based metathesis." *Journal of the American Chemical Society* 124.20 (2002): 5729-5733.

100) Ingall, Michael DK, et al. "Surface functionalization with polymer and block copolymer films using organometallic initiators." *Journal of the American Chemical Society* 122.32 (2000): 7845-7846.

101) Zong, Guangxi, et al. "Synthesis of polyacrylonitrile-grafted cross-linked N-chlorosulfonamidated polystyrene via surface-initiated ARGET ATRP, and use of the resin in mercury removal after modification." *Journal of hazardous materials* 186.1 (2011): 614-621.

102) Guide to Using WVASE, J.A. Woolam Co., Inc., 2003.

103) Thornton, John. "Scanning Probe Microscopy Training Notebook." *Santa Barbra, Ca: Veeco Metrology Group* (2000): 1-56.

104) Siddiqui, S., et al. "Study of interaction between silicon surfaces in dilute ammonia peroxide mixtures (APM) and their components using atomic force microscope (AFM)." *Microelectronic engineering* 88.12 (2011): 3442-3447.

105) Ambroziak, Robert, et al. "Cubic silver nanoparticles fixed on TiO2 nanotubes as simple and efficient substrates for surface enhanced Raman scattering." *Materials* 12.20 (2019): 3373.

106) Watts, John F., and John Wolstenholme. *An introduction to surface analysis by XPS and AES*. John Wiley & Sons, 2019.

107) Tougaard, Sven. "Practical guide to the use of backgrounds in quantitative XPS." *Journal of Vacuum Science & Technology A: Vacuum, Surfaces, and Films* 39.1 (2021): 011201.

108) Alswieleh, Abdullah M., et al. "Zwitterionic Poly (amino acid methacrylate) Brushes." *Journal of the American Chemical Society* 136.26 (2014): 9404-9413.

109) Alswieleh, Abdullah. *Micro-and Nano-Structure of Polymers and Molecular Materials*. Diss. University of Sheffield, 2014.

110) Al-Jaf, Sirwan. *Natural Modulators of Amyloid formation in Alzheimer's disease*. Diss. University of Sheffield, 2016.

111) Feng, Chun, and Xiaoyu Huang. "Polymer brushes: efficient synthesis and applications." *Accounts of chemical research* 51.9 (2018): 2314-2323.

112) Ayres, Neil. "Polymer brushes: Applications in biomaterials and nanotechnology." *Polymer Chemistry* 1.6 (2010): 769-777.

113) Li, Bin, et al. "Tapping the potential of polymer brushes through synthesis." *Accounts of Chemical Research* 48.2 (2015): 229-237.

114) Diamanti, Steve, et al. "Reactive patterning via post-functionalization of polymer brushes utilizing disuccinimidyl carbonate activation to couple primary amines." *Polymer* 49.17 (2008): 3770-3779.

115) Chen, Meng, et al. "Robust, biomimetic polymer brush layers grown directly from a planar mica surface." *ChemPhysChem* 8.9 (2007): 1303-1306.

116) Nguyen, Ai T., et al. "Stable protein-repellent zwitterionic polymer brushes grafted from silicon nitride." *Langmuir* 27.6 (2011): 2587-2594.

117) Yu, Yunlong, G. Julius Vancso, and Sissi de Beer. "Substantially enhanced stability against degrafting of zwitterionic PMPC brushes by utilizing PGMA-linked initiators." *European polymer journal* 89 (2017): 221-229.

118) Sim, Xuan Ming, et al. "Multistimuli Responsive Reversible Cross-Linking–Decross-Linking of Concentrated Polymer Brushes." *ACS applied materials & interfaces* 12.25 (2020): 28711-28719.

119) Feng, Jianxin, Richard T. Haasch, and Daniel J. Dyer. "Photoinitiated synthesis of mixed polymer brushes of polystyrene and poly (methyl methacrylate)." *Macromolecules* 37.25 (2004): 9525-9537.

120) Lemieux, M., et al. "Reorganization of binary polymer brushes: Reversible switching of surface microstructures and nanomechanical properties." *Macromolecules* 36.19 (2003): 7244-7255.

121) Santer, Svetlana, et al. "Local composition of nanophase-separated mixed polymer brushes." *Macromolecules* 39.8 (2006): 3056-3064.

122) Usov, Denys, et al. "Three-dimensional analysis of switching mechanism of mixed polymer brushes." *Macromolecules* 40.24 (2007): 8774-8783.

123) Gadwal, Ikhlas, et al. "Functionalized molecular bottlebrushes." *Macromolecules* 47.1 (2014): 35-40.

124) Zou, Yuquan, Jayachandran N. Kizhakkedathu, and Donald E. Brooks. "Surface modification of polyvinyl chloride sheets via growth of hydrophilic polymer brushes." *Macromolecules* 42.9 (2009): 3258-3268.

125) Wu, Tao, Kirill Efimenko, and Jan Genzer. "Preparing high-density polymer brushes by mechanically assisted polymer assembly." *Macromolecules* 34.4 (2001): 684-686.

126) Kopyshev, Alexey, et al. "Polymer brushes modified by photosensitive azobenzene containing polyamines." *Polymer* 98 (2016): 421-428.

127) Munirasu, Selvaraj, et al. "Synthesis and morphological study of thick benzyl methacrylate–styrene diblock copolymer brushes." *Langmuir* 27.21 (2011): 13284-13292.

128) Zhao, Bin, and William J. Brittain. "Synthesis, characterization, and properties of tethered polystyrene-b-polyacrylate brushes on flat silicate substrates." *Macromolecules* 33.23 (2000): 8813-8820.

129) Boyes, Stephen G., et al. "Synthesis, characterization, and properties of ABA type triblock copolymer brushes of styrene and methyl acrylate prepared by atom transfer radical polymerization." *Macromolecules* 35.13 (2002): 4960-4967.

130) Sedjo, Randy A., Brian K. Mirous, and William J. Brittain. "Synthesis of polystyrene-block-poly (methyl methacrylate) brushes by reverse atom transfer radical polymerization." *Macromolecules* 33.5 (2000): 1492-1493.

131) Zhao, Bin. "Synthesis of binary mixed homopolymer brushes by combining atom transfer radical polymerization and nitroxide-mediated radical polymerization." *Polymer* 44.15 (2003): 4079-4083.

132) Rowe, Misty D., Brenton AG Hammer, and Stephen G. Boyes. "Synthesis of surface-initiated stimuli-responsive diblock copolymer brushes utilizing a combination of ATRP and RAFT polymerization techniques." *Macromolecules* 41.12 (2008): 4147-4157.

133) Jiang, Xiaoming, et al. "Evolution of phase morphology of mixed poly (tert-butyl acrylate)/polystyrene brushes grafted on silica particles with the change of chain length disparity." *Macromolecules* 43.12 (2010): 5387-5395.

134) Zou, Yuquan, Jayachandran N. Kizhakkedathu, and Donald E. Brooks. "Surface modification of polyvinyl chloride sheets via growth of hydrophilic polymer brushes." *Macromolecules* 42.9 (2009): 3258-3268.

135) Börner, Hans G., et al. "Synthesis of molecular brushes with block copolymer side chains using atom transfer radical polymerization." *Macromolecules* 34.13 (2001): 4375-4383.

136) Zhang, Mingfu, et al. "Amphiphilic cylindrical brushes with poly (acrylic acid) core and poly (n-butyl acrylate) shell and narrow length distribution." *Polymer* 44.5 (2003): 1449-1458.

137) Sedjo, Randy A., Brian K. Mirous, and William J. Brittain. "Synthesis of polystyrene-block-poly (methyl methacrylate) brushes by reverse atom transfer radical polymerization." *Macromolecules* 33.5 (2000): 1492-1493.

138) Sumerlin, Brent S., Dorota Neugebauer, and Krzysztof Matyjaszewski. "Initiation efficiency in the synthesis of molecular brushes by grafting from via atom transfer radical polymerization." *Macromolecules* 38.3 (2005): 702-708.

139) Lee, Hyung-il, et al. "Hetero-grafted block brushes with PCL and PBA side chains." *Macromolecules* 41.16 (2008): 6073-6080.

140) Pyun, Jeffrey, Tomasz Kowalewski, and Krzysztof Matyjaszewski. "Synthesis of polymer brushes using atom transfer radical polymerization." *Macromolecular Rapid Communications* 24.18 (2003): 1043-1059.

141) Nese, Alper, et al. "Synthesis of poly (vinyl acetate) molecular brushes by a combination of atom transfer radical polymerization (ATRP) and reversible addition-fragmentation chain transfer (RAFT) polymerization." *Macromolecules (Print)* 43.9 (2010): 4016-4019.

142) Cheng, Guanglou, et al. "Amphiphilic cylindrical core− shell brushes via a “grafting from” process using ATRP." *Macromolecules* 34.20 (2001): 6883-6888.

143) Lee, Hyung-il, et al. "Molecular brushes with spontaneous gradient by atom transfer radical polymerization." *Macromolecules* 38.20 (2005): 8264-8271.

144) Venkatesh, Rajan, et al. "Novel brush copolymers via controlled radical polymerization." *Macromolecular chemistry and physics* 205.16 (2004): 2161-2168.

145) Börner, Hans G., et al. "Synthesis of molecular brushes with gradient in grafting density by atom transfer polymerization." *Macromolecules* 35.9 (2002): 3387-3394.

146) Boyes, Stephen G., et al. "Synthesis, characterization, and properties of ABA type triblock copolymer brushes of styrene and methyl acrylate prepared by atom transfer radical polymerization." *Macromolecules* 35.13 (2002): 4960-4967.

147) Kim, Jong-Bum, et al. "Synthesis of triblock copolymer brushes by surface-initiated atom transfer radical polymerization." *Macromolecules* 35.14 (2002): 5410-5416.

148) Wu, Tao, Kirill Efimenko, and Jan Genzer. "Preparing high-density polymer brushes by mechanically assisted polymer assembly." *Macromolecules* 34.4 (2001): 684-686.

149) Husseman, Marc, et al. "Controlled synthesis of polymer brushes by “living” free radical polymerization techniques." *Macromolecules* 32.5 (1999): 1424-1431.

150) Matyjaszewski, Krzysztof. "Controlling polymer structures by atom transfer radical polymerization and other controlled/living radical polymerizations." *Macromolecular Symposia*. Vol. 195. No. 1. Weinheim: WILEY-VCH Verlag, 2003.

151) Parkatzidis, Kostas, et al. "Tailoring polymer dispersity by mixing ATRP initiators." *Polymer Chemistry* 12.39 (2021): 5583-5588.

152) Fouz, Munira F., et al. "Bright fluorescent nanotags from bottlebrush polymers with DNA-tipped bristles." *ACS Central Science* 1.8 (2015): 431-438.

153) Kherlopian, Armen R., et al. "A review of imaging techniques for systems biology." *BMC systems biology* 2.1 (2008): 1-18.

154) Korb, Melissa L., et al. "Use of monoclonal antibody–IRDye800CW bioconjugates in the resection of breast cancer." *journal of surgical research* 188.1 (2014): 119-128.

155) Breul, Alexander M., Martin D. Hager, and Ulrich S. Schubert. "Fluorescent monomers as building blocks for dye labeled polymers: synthesis and application in energy conversion, biolabeling and sensors." *Chemical Society Reviews* 42.12 (2013): 5366-5407.

156) Dai, Xiaowen, et al. "Direct visualization of reversible switching of micropatterned polyelectrolyte brushes on gold surfaces using laser scanning confocal microscopy." *Langmuir* 24.22 (2008): 13182-13185.

157) Hollauf, Manuel, Gregor Trimmel, and Astrid-Caroline Knall. "Dye-functionalized polymers via ring opening metathesis polymerization: principal routes and applications." *Monatshefte für Chemie-Chemical Monthly* 146 (2015): 1063-1080.

158) Ionov, Leonid, Vera Bocharova, and Stefan Diez. "Biotemplated synthesis of stimuli-responsive nanopatterned polymer brushes on microtubules." *Soft Matter* 5.1 (2009): 67-71.

159) Rohan, R., Hung, M.K., Yang, Y.F., Hsu, C.W., Yeh, C.K., Chang, Y.L. and Lee, J.T., 2022. Enhancement of the High-Rate Performance of an Organic Radical Thin-Film Battery by Decreasing the Grafting Density of Polymer Brushes. *ACS Applied Polymer Materials*, *4*(4), pp.2365-2372.

160) Sabri, Nadirah Ali, and Shahrul Ainliah Alang Ahmad. "Photo-oxidation Studies of 4-(Chloromethyl) phenyltrichlorosilane on Silicon and Titanium Oxides." *Asian Journal of Chemistry* 28.7 (2016): 1531.